4-26-1989

Discovery of Strong Coupling between Lattice-Band Carriers and Impurity-Band Carriers in Augmented Photoconductivity Measurements on Si:As, Si:Bi, and Si:Al AT 7-16 K

James Edward Heath

DISCOVERY OF STRONG COUPLING BETWEEN LATTICE-BAND CARRIERS AND IMPURITY-BAND CARRIERS IN AUGMENTED PHOTOCONDUCTIVITY MEASUREMENTS ON Si:As, Si:Bi, AND Si:Al AT 7-16 K - HEATH

THE UNIVERSITY OF NEW MEXICO
ALBUQUERQUE, NEW MEXICO 87131

Policy on Use of Theses and Dissertations

Unpublished theses and dissertations accepted for master's and doctor's degrees and deposited in the University of New Mexico Library are open to the public for inspection and reference work. *They are to be used only with due regard to the rights of the authors.* The work of other authors should always be given full credit. Avoid quoting in amounts, over and beyond scholarly needs, such as might impair or destroy the property rights and financial benefits of another author.

To afford reasonable safeguards to authors, and consistent with the above principles, anyone quoting from theses and dissertations must observe the following conditions:

1. Direct quotations during the first two years after completion may be made only with the written permission of the author.

2. After a lapse of two years, theses and dissertations may be quoted without specific prior permission in works of original scholarship provided appropriate credit is given in the case of each quotation.

3. Quotations that are complete units in themselves (e.g., complete chapters or sections) in whatever form they may be reproduced and quotations of whatever length presented as primary material for their own sake (as in anthologies or books of readings) ALWAYS require consent of the authors.

4. The quoting author is responsible for determining "fair use" of material he uses.

This thesis/dissertation by James Edward Heath has been used by the following persons whose signatures attest their acceptance of the above conditions. (A library which borrows this thesis/dissertation for use by its patrons is expected to secure the signature of each user.)

NAME AND ADDRESS	DATE

James Edward Heath

Candidate

Electrical and Computer Engineering

Department

This dissertation is approved, and it is acceptable in quality and form for publication on microfilm:

Approved by the Dissertation Committee:

John K McRae, Chairperson

Kenneth Gingling

D E Newman

Carroll R. Morris

Accepted:

Asst. *Dean, Graduate School*

April 26, 1989

Date

DISCOVERY OF STRONG COUPLING BETWEEN LATTICE-BAND CARRIERS AND IMPURITY-BAND CARRIERS IN AUGMENTED PHOTOCONDUCTIVITY MEASUREMENTS ON Si:As, Si:Bi, AND Si:Al AT 7-16 K

by

James Edward Heath

B.S.E.E., University of Washington, 1979

M.S.E.E., University of New Mexico, 1983

DISSERTATION

Submitted in Partial Fulfillment of the
Requirements for the Degree of
Doctor of Philosophy in Engineering

The University of New Mexico
Albuquerque, New Mexico
May, 1989

DEDICATION

This work is dedicated to

Ok Sook (my best friend, my love, and my wife),

Allison and Jason (my children), and

Paul and Stella (my parents)

whose love and support makes everything possible.

ACKNOWLEDGMENTS

I am indebted to the many individuals who assisted me by providing encouragement, advice, and technical direction throughout this effort. I am extremely grateful to the chairman of my committee, Dr. John McIver, without whom this project would not have been completed, by providing the necessary guidance when the problems seemed insurmountable. Drs. Kenneth Jungling, Donald Neaman, and Carroll Norris provided encouragement and technical support throughout the endeavor.

I appreciate the excellent technical support provided by both Mr. William Kemp and Mr. Mark Altamirano throughout the duration of this project. Their laboratory and technical expertise proved invaluable on countless occasions. Finally, I would like to thank Mrs. Elena Franklin for her superb technical and computer support which permitted a timely completion. I will always be grateful for her unselfish and caring support.

DISCOVERY OF STRONG COUPLING BETWEEN LATTICE-BAND CARRIERS AND IMPURITY-BAND CARRIERS IN AUGMENTED PHOTOCONDUCTIVITY MEASUREMENTS ON Si:As, Si:Bi, AND Si:Al AT 7-16 K

by

James Edward Heath

ABSTRACT OF DISSERTATION

Submitted in Partial Fulfillment of the
Requirements for the Degree of
Doctor of Philosophy in Engineering

The University of New Mexico
Albuquerque, New Mexico
May, 1989

Discovery of Strong Coupling between Lattice-band Carriers and Impurity-band Carriers in Augmented Photoconductivity Measurements on Si:As, Si:Bi, and Si:Al AT 7-16 K

James Edward Heath

B.S.E.E., University of Washington, 1979

M.S.E.E., University of New Mexico, 1983

Ph.D., University of New Mexico, 1989

In this work, low-temperature photoconductivity measurements using excitation in the long-wavelength infrared were performed in conjunction with infrared-blocked band-gap excitation in the first studies of the energy transfer between carriers moving in lattice bands and those associated with an impurity band in a semiconductor. Extrinsic (impurity-band) excitations were produced in Si:As, Si:Bi, and Si:Al detectors by infrared photoexcitation at 29-33.5 μm wavelengths (37-43 meV); this could be augmented by simultaneous intrinsic (band-gap) photoexcitation using infrared-blocked white light to inject lattice-band carriers. Carrier transport was induced by applied electric fields of 35-175 V/cm. The experiments were performed at temperatures of 7-8 K, where thermal ionization of photoexcited impurity-band carriers is unimportant, and also at 16 K, where thermal ionization is more significant. Although simplistic modeling indicates that impurity-band and lattice-band transport should be largely independent under the conditions of our experiments, we observed strong interactions in all cases studied. The presence of very shallow D^- centers associated with the impurity band explains this result, which has important implications for certain proposed infrared detector designs. The effects of white light illumination on the temporal response of the detectors under pulsed

infrared excitation were also investigated in this work. The results can be explained on the basis of a model in which lattice-band carriers interact with D^- centers, in agreement with the conclusions of our spectral studies.

TABLE OF CONTENTS

LIST OF TABLES

LIST OF FIGURES

CHAPTER I

INTRODUCTION AND EXPERIMENT

In this dissertation, the long-wavelength infrared (IR) spectral photoresponse of several impurity-banded extrinsic silicon photodetectors will be investigated at low temperatures with the presence of simultaneous intrinsic photoexcitation. Simplistic modeling suggests that impurity-band and lattice-band transport mechanisms are independent for temperatures below 15 K where thermal ionization occurs in silicon. It will be the purpose of this study to experimentally investigate, for the first time, the existence of coupling mechanisms between impurity-band and lattice-band carriers via their impact on photoconductive response signals for temperatures below thermal ionization. This information will have important implications for infrared detector designs which assume independent transport mechanisms.

Previous studies have concentrated on determining the existence of a second electron weakly bound to shallow impurities in materials such as silicon and germanium. These studies, which will be discussed in detail later, were limited to impurity-band carriers excited by very long wavelength extrinsic radiation well below thermal ionization temperatures. Parallel to these efforts, others began to utilize a new type of photoconductive measurement technique to study shallow impurities in very pure semiconductor materials. These measurement techniques, which will also be discussed later, were performed at higher temperatures to promote the thermal ionization of excited states via phonon coupling. In addition, their experimental samples were very pure materials (principally germanium), not moderately to heavily doped semiconductors as is the current focus.

This study utilized moderately heavily doped samples ($6{\cdot}10^{16}\ cm^{-3}$) for Si:As, Si:Bi, and Si:Al detectors to determine the potential role, if any, weakly bound secondary electrons play as a mechanism for coupling energy between impurity-band

and lattice-band carriers when temperatures are below thermal ionization. Because the role of secondarily bound electrons to shallow impurities is of primary interest, extrinsic illumination (37 - 43 meV) was limited to energies below the isolated ionization energy, yet sufficient to ionize a large percentage of excited states of the shallow impurities which are intimately involved in impurity-band conduction. Therefore, this study attempts to bridge the gap between the previous two classes of studies for the first time by using modified photoconductivity techniques for determining the existence and potential impact of coupling mechanisms between impurity-band and lattice-band conduction mechanisms.

In the following sections we will first give a brief introduction to the field of photoconductivity and the related discipline of photoelectric spectroscopy. The focus is on work in which the optical excitation is in the infrared spectral region. This is the subject of the present dissertation, the primary emphasis in the literature, and also an area of strong practical interest for infrared detector systems. Our introduction first discusses the place of infrared photoconductivity as a research tool for studying energy levels in semiconductors. We then outline the development of photoelectric spectroscopy, a sophisticated subset of the photoconductivity arena which is the technique used in our experiments. After touching on the current practical importance of photoconductivity and related issues, we set the stage for the remainder of this work by describing the details of our experimental apparatus which are germane to the analytical and experimental discussions of subsequent chapters.

I-1 Infrared Photoconductivity as a Research Tool

A number of techniques can be used to investigate the energy levels of an impurity center in a semiconductor crystal. For example, the optical absorption

spectrum can be useful if the impurities have an absorbing transition which yields a distinctive band in a favorable spectral region. Alternatively, the optical emission spectrum under excitation by optical or other means can also be useful in certain circumstances such as identification of impurities. Investigating the effects of photoexcitation on conductivity (a discipline known as photoconductivity), when pursued as a photon-energy spectroscopy at low temperatures, can provide detailed information on energy levels that are effective relative to carrier transport. There are also a number of basically non-spectroscopic techniques in common use to determine energy levels, including measurements of conductivity vs. temperature, or Hall effect vs. temperature, or trapped charge release vs. temperature; these techniques are less informative and will not be discussed further.

Of course, there are limitations associated with all techniques. Optical absorption generally is most useful at fairly high impurity concentrations; for example, in germanium the absorption of groups III and V impurities is difficult to measure even at concentrations of $10^{14} cm^{-3}$. Optical emission can be sensitive at considerably lower impurity concentrations but it is necessary that the impurity of interest have an efficient radiative transition; not all situations of interest fall in this category. Photoconductivity, and photothermal ionization spectroscopy as discussed below, represent some of the most sensitive techniques available for the investigation of transport-related shallow impurity energy levels at low impurity concentrations. This is an important niche for photoconductivity that seems secure for the foreseeable future. It is essential, though, that good low-temperature Ohmic contacts be available in the associated materials technology; fortunately this is the case in silicon, which is the material of the present work.

I-2 Infrared Photoconductivity and Photoelectric Spectroscopy

In a photoconductivity experiment, one measures relative changes in conductivity

$$\triangle \sigma = \triangle N \, e \, \mu \tag{I-1}$$

due to $\triangle N$ carriers of mobility μ, which are photogenerated from a specific energy level[1-3] by photons of a known energy. The photon energy at which an increase of photoconductivity occurs gives the approximate energy separation of the excited impurity levels relative to the nearby band edge.

In 1964 Lifshitz and Nad[4] utilized the photoconductivity method to study materials having relatively low impurity concentrations. They pointed out that the extrinsic photoconductivity signal is proportional to the relative change of the carrier concentration $\triangle N_{ph}/N$ under illumination where N is the concentration of current carriers in the absence of the signal and $\triangle N_{ph}$ is the concentration of current carriers due to illumination. This relationship suggested a potential mechanism for detection and identification of impurities in semiconductors which should remain useful as the impurity concentration N decreases. In contrast, the signal in an optical absorption or emission experiment is proportional to N, and thus becomes small at low impurity concentrations. This is the fundamental reason for the relatively high sensitivity of low-temperature photoconductivity experiments at low impurity concentrations.

Lifshitz and Nad[4] further noted sharp features in photoconductivity spectra at photon energies below the threshold energy of shallow levels in germanium. They explained these distinct features as optical transitions of a bound electron from the ground state to one of the bound excited states, with the electron in the latter state

subsequently being excited into the conduction band by the absorption of lattice phonons at the temperatures of their experiments. This initial interpretation was supported by the temperature dependence of the intensity of photoconductivity peaks[5] and also by theoretical work[6]. Investigations based on this two-step ionization process have become formally known as photothermal ionization spectroscopy or photoelectric spectroscopy, although informally they are accommodated within the discipline of photoconductivity. In Figure I-1, the two-step ionization process is illustrated schematically for the case of a donor. An extensive review of photoelectric spectroscopy techniques has been published[7] to which the reader is referred for further information.

I-3 The Current Importance of Photoconductivity and Related Topics

As alluded to above, infrared photoconductivity developed originally as a largely academic discipline. The use of relatively low temperatures provided a means to obtain physically meaningful data from the very impure semiconductors characteristic of the early days of semiconductor physics, as selectivity in response could be achieved only from a starting point where virtually all carriers were frozen out. As semiconductor material quality has improved, photoconductivity has been important in characterizing impurities present at very low concentrations; the technique is obviously most sensitive to the electrically active impurities of device interest.

The last decade has seen increasing military interest in infrared photoconductivity for long-wavelength detector applications. In principle, little is changed from academic studies, as similar low temperatures and materials are involved in the current generation of state-of-the-art doped silicon detectors. However, there are significant differences in detail, as efforts are made to understand and exploit the

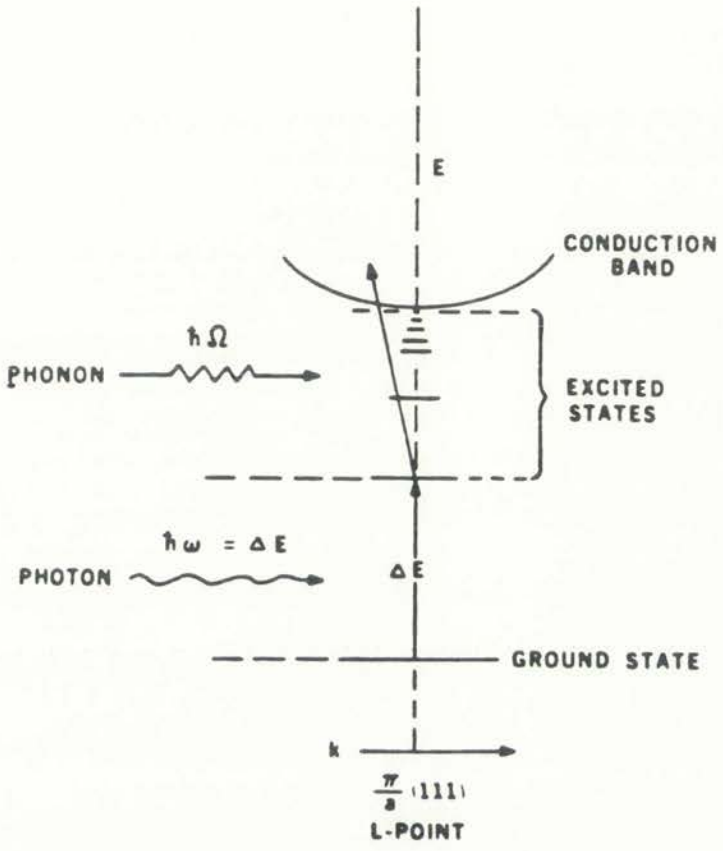

Figure I-1. Schematic illustration of photothermal ionization for n-type material.

physics of these devices to optimize their performance as infrared detectors rather than characterization tools for research. The experimental results and discussion that we will present later have important implications concerning the feasibility of one proposed mode of extrinsic silicon detector operation.

I-4 Experimental Apparatus for Photoelectric Spectroscopy

We conclude this brief introduction to photoelectric spectroscopy with a description of our experimental apparatus (Figures I-2a and b). The apparatus incorporates the standard features expected for photoelectric spectroscopy experiments as well as two important additional features; the standard ones will be discussed first.

The source of the infrared radiation employed for photoexcitation is a commercial blackbody which is operated at a temperature of 1000 K. The infrared radiation reaching the sample is modulated at 10 Hz by a chopper and then spectrally filtered by a double off-axis scanning Czerny-Turner grating monochromator with a spectral resolution of 0.1 micrometer (μm) in the 25 - 35 μm wavelength range. The corresponding energy resolution is 0.129 meV at a photon energy of 40 meV; this resolution is adequate for independent excitation of most of the boron and phosphorus levels in silicon as may be seen from Tables I-1 and I-2. The monochromator calibration was established using a CO_2 laser and the repeatability of the spectral calibration was assured by use of a computer-controlled stepping motor drive. The spectrally resolved IR radiation emerging from the monochromator enters at the side of a liquid-helium Dewar containing the sample under study.

The following precautions and procedures ensured that the radiation incident on the sample did not significantly perturb the sample temperature in our experiments. First, in all cases the samples were bonded against the mounting surface with a

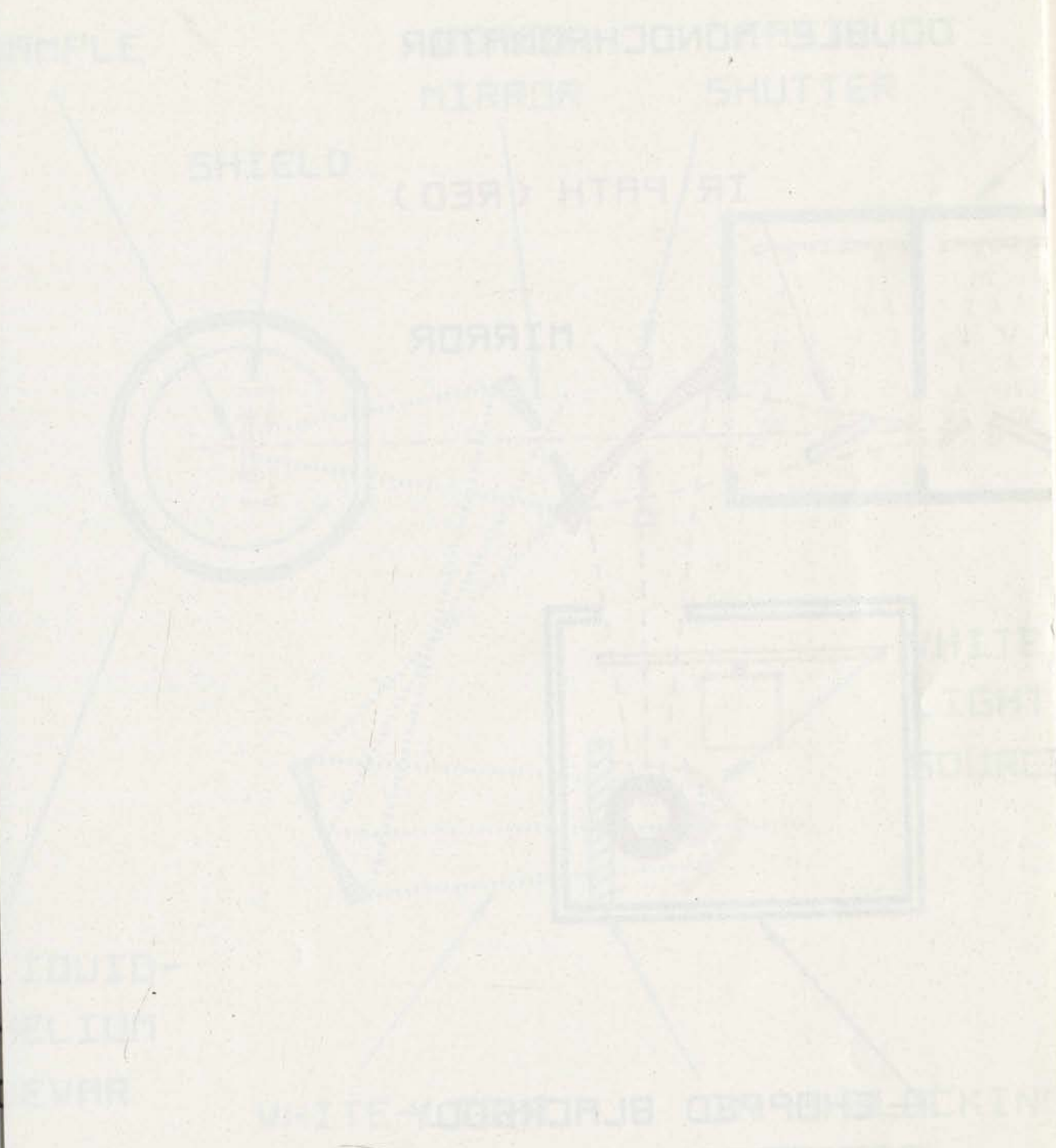

Figure I-2:a. **Experimental Setup: Optical Components and Paths.**

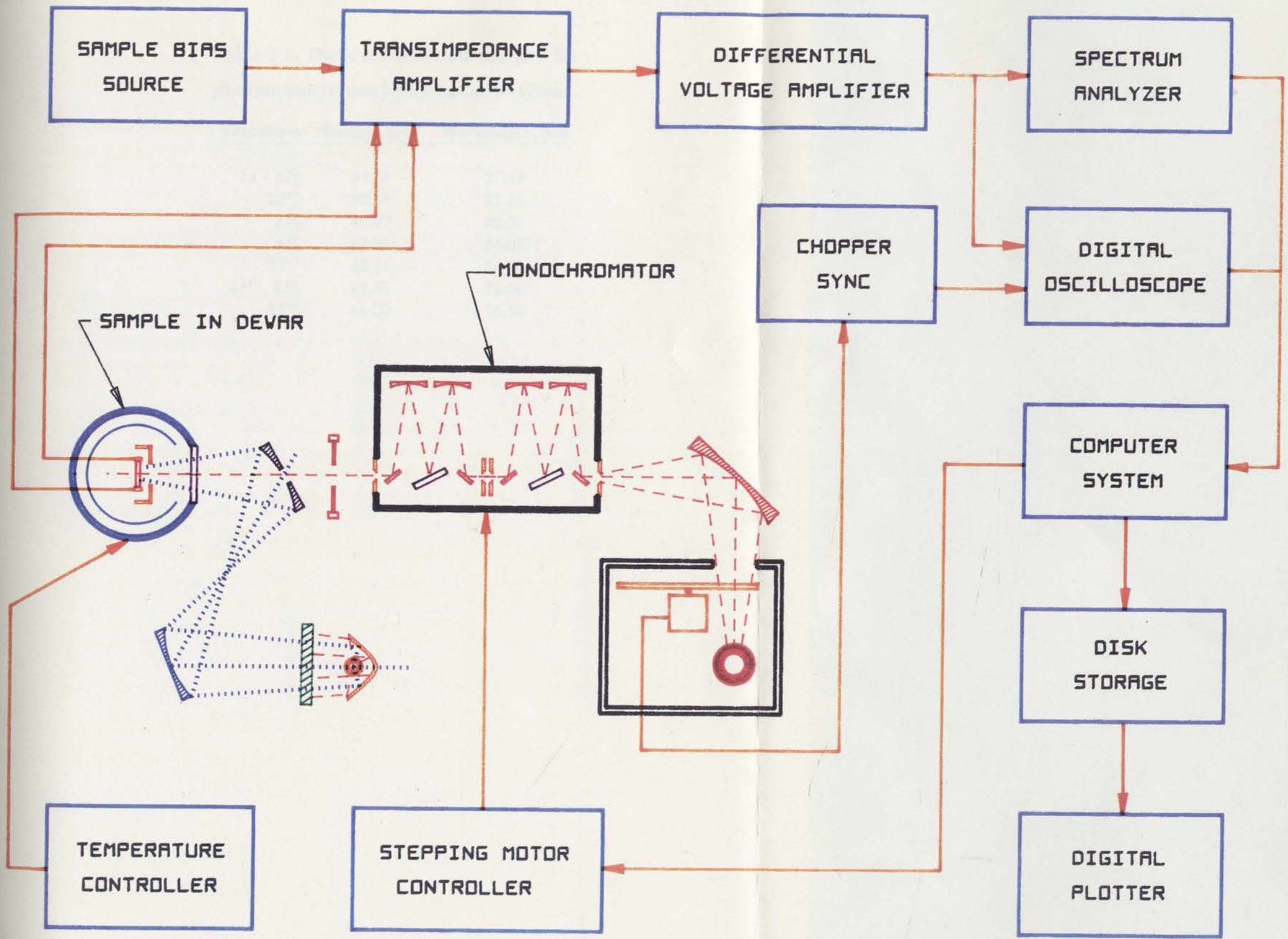

FIGURE I-2(B) - INSTRUMENTATION DIAGRAM

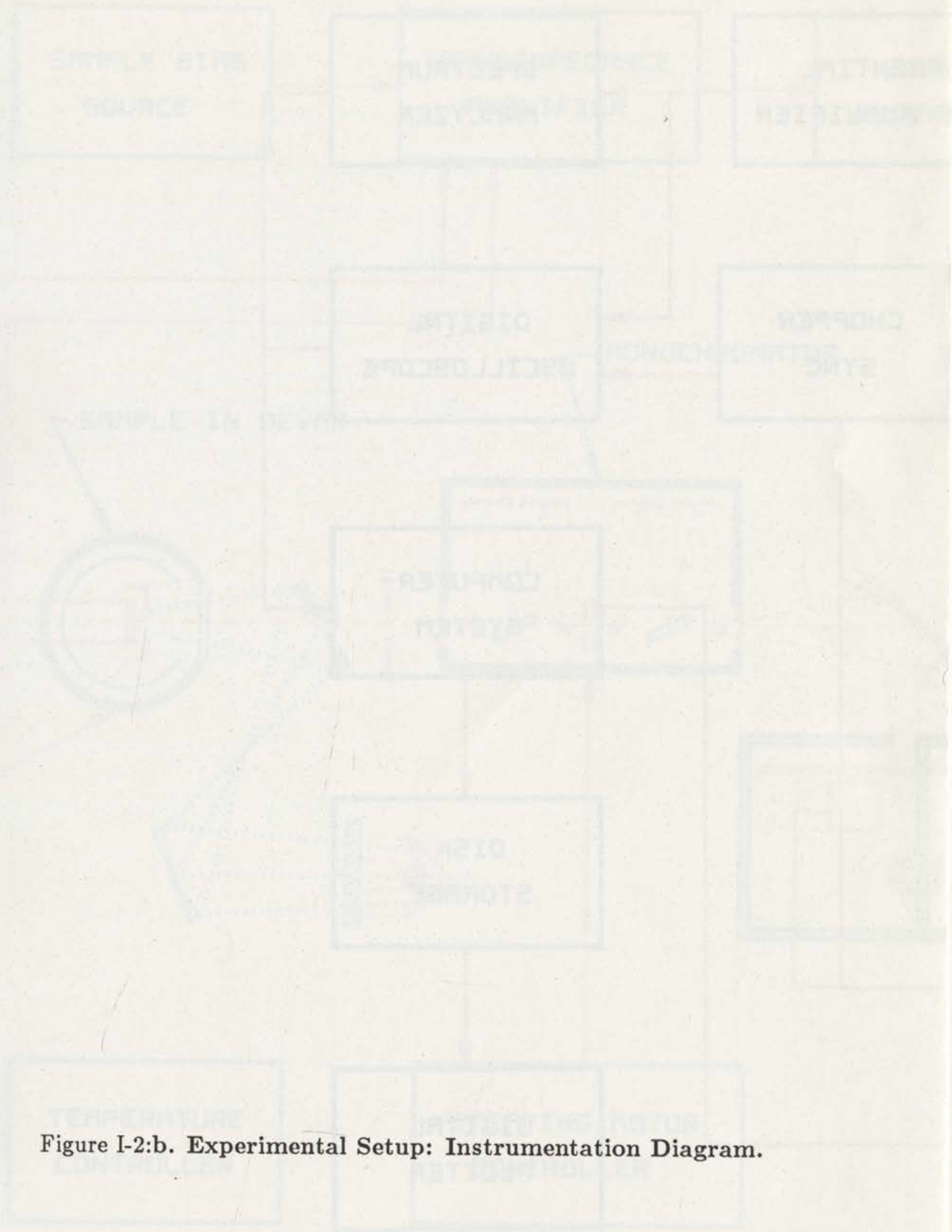

Figure I-2:b. **Experimental Setup: Instrumentation Diagram.**

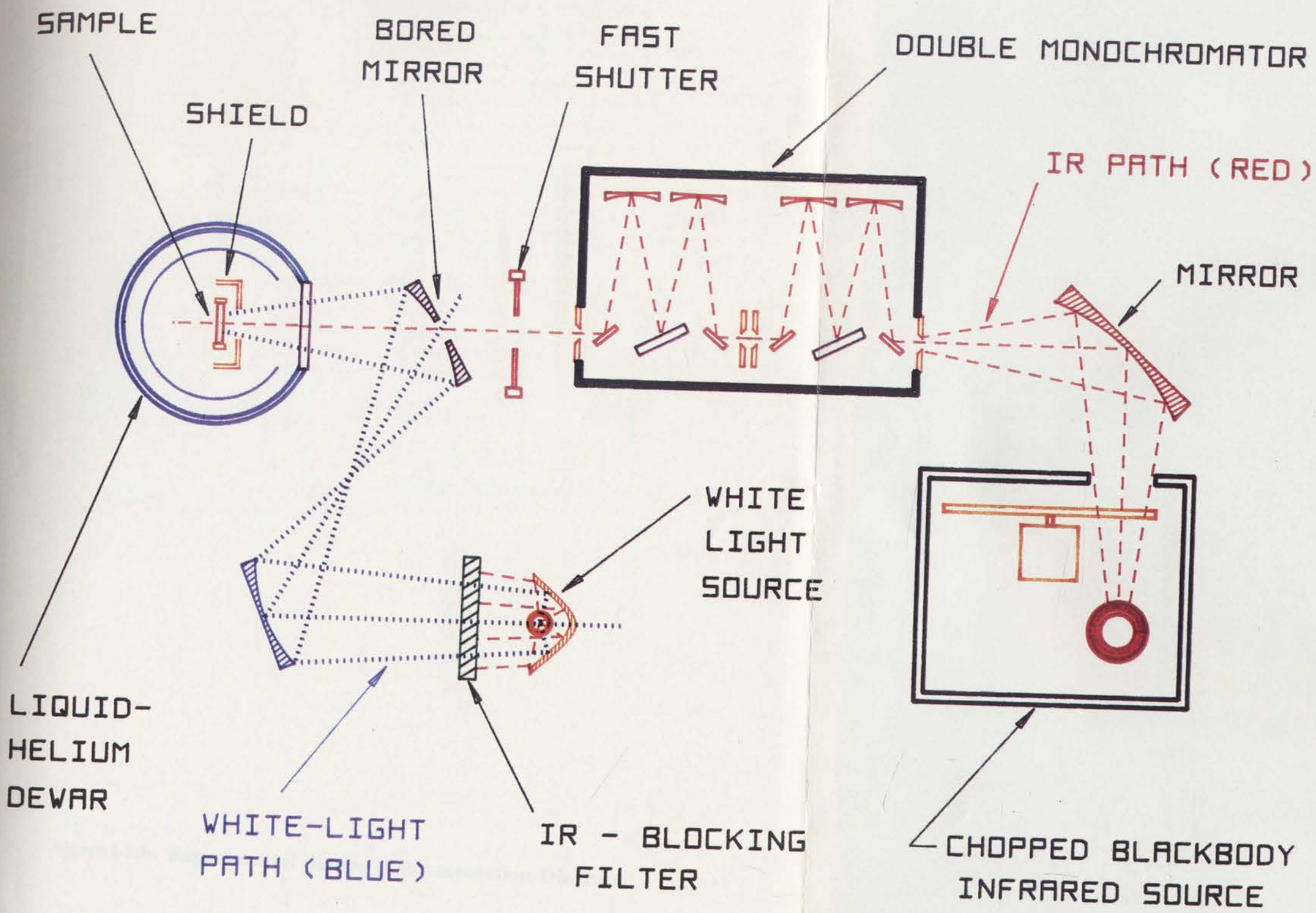

FIGURE I-2(A) - OPTICAL COMPONENTS AND PATHS

Table I-1. Optical transition energies for phosphorus (donor) impurities in silicon.

Transition	Energy, meV	Wavelength, μm
$1s$ - $2P_0$	34.08	27.48
$2P^+$	39.14	31.56
$3P_0$	40.07	32.31
$4P_0$	42.25	34.07
$3P^+$	42.41	34.20
$4P^+$, $5P_0$	43.35	34.96
$5P^+$	44.09	35.56

Table I-2. Optical transition energies for boron (acceptor) impurities in silicon.

Notation in Diagram	Energy, meV	Wavelength, μm
1	30.38	24.50
2	34.53	27.85
3	38.35	30.95
4	39.64	31.96
5	39.91	32.19
6	-	-
7	41.52	33.48
8	42.50	34.27
9	42.79	34.50
10	43.27	34.90
11	43.86	35.37

thermally conductive varnish used commercially to obtain thermal contact at cryogenic temperatures. The mounting surface itself was a thermally conductive ceramic slab which provided electrical isolation of the sample from the Dewar; the ceramic slab was in turn bonded to the cold finger of the Dewar using thermally conductive varnish. Three temperature-sensing silicon diodes, used in conjunction with a Lakeshore Cryogenics temperature monitor, were varnish-bonded in appropriate positions to monitor (1) the temperature of the cold finger, (2) the temperature of the contact shield (discussed later in this chapter), and (3) the temperature of the sample-mounting surface at a distance of 2 mm from the sample center. In the latter case, the temperature sensor was exposed to virtually the same incident radiation as the sample itself. For all samples, we verified both initially and throughout the course of the experiments that the incident radiation affected the monitored temperatures by less than 0.1 K.

The sample was biased at a constant voltage in our photoconductivity measurements. The change in sample current resulting from optical excitation was detected using a modified low-noise transimpedance amplifier which incorporated a sample-biasing capability. To prevent ground loops a differential voltage amplifier was inserted between the transimpedance amplifier and the spectral analyzer which processed the photoconductive signal.

The Dewar window consisted of a KRS-5 window together with an acrylic filter; the measured spectral transmittance of the combination is shown in Figure I-3. Since both the intensity spectrum of the infrared source and the spectral response of the monochromator system were essentially flat over the spectral region of interest, the spectrum of photoexcitation intensity followed closely that of the Dewar window. Correspondingly, the photoconductive response spectra shown in later chapters were

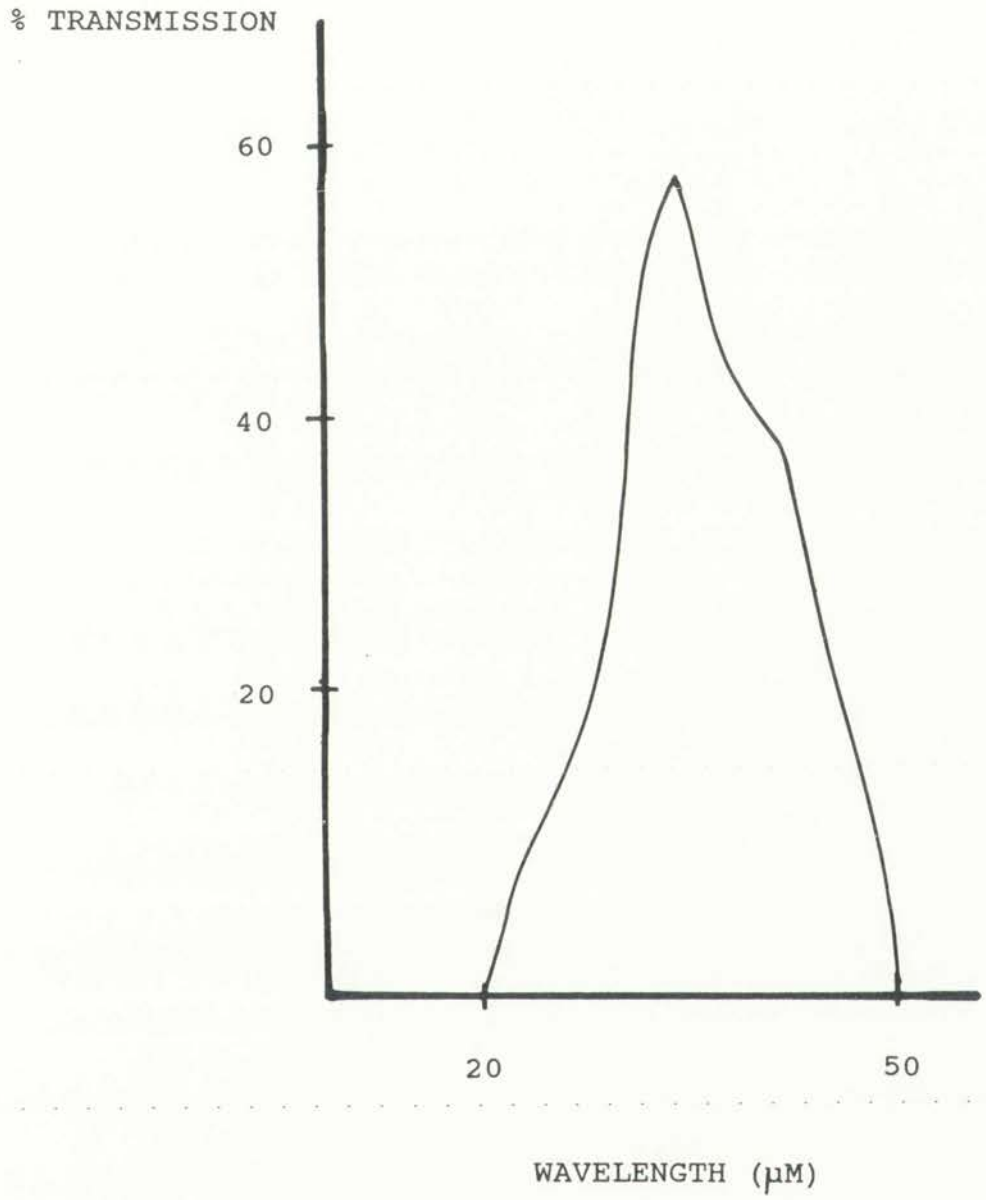

Figure I-3. **Spectral transmittance of a KRS-5 window together with an acrylic filter.**

derived by computer-normalizing the actual photoconductive signal relative to the spectral transmittance of the window. The resulting response spectra were then stored on computer diskettes for subsequent plotting.

One novel feature which proved important in our measurements was the incorporation of a capability to illuminate the sample with white light during the normal photoelectric spectroscopy measurement. This was accomplished (Figure I-2a) using a bored mirror to focus white light into the Dewar without interfering with the infrared beam which passed through a 25-mm-diameter central opening in the mirror. The white light source was a 21-V projection lamp which, without additional filtering, showed the intensity spectra of Figure I-4. It was fortunate that the lamp design incorporated a dichroic mirror which reduced the infrared output relative to a blackbody spectrum. In addition, we placed an optical bandpass filter in front of the lamp to virtually eliminate the infrared output at wavelengths longer than 900 nanometers (nm). The resulting spectrum of our white light illumination is thereby confined to 350-750 nm, as shown in Figure I-5, which incidentally was recorded after passing through the Dewar window. The significance of the low infrared output is that the white light illumination produces negligible sample heating (as verified by our cryogenic thermometer) and also that there is no undesirable additional infrared illumination of the sample when the white light is turned on. In our experiments where white light illumination was employed, we routinely used one of three available white light intensities (as indicated in Figure I-4). From intensity measurements at the sample plane, we determined that the total spectrally integrated power densities in the three cases were $\approx 1\mu W/cm^2$ ("low"), $\approx 3\mu W/cm^2$ ("medium), and $\approx 6\mu W/cm^2$ ("high"). Since the absolute intensities are unimportant in our interpretations, we will subsequently refer to these white light intensities simply by their relative parenthetical designations.

Another important feature of our experimental setup was a fast mechanical (Uniblitz) shutter in the infrared excitation path (Figure I-2). Using this device, a rectangular infrared pulse with a duration from a few milliseconds to one second could be delivered to the sample. The corresponding dynamic effects in the sample response were determined from oscilloscope photographs of the resulting sample current waveform.

Finally, we point out that we were careful to shield the sample contacts from direct illumination, as it is well known that spurious effects may arise from contact illumination if the contacts are not Ohmic. The shield (Figure I-2a) was positioned 1 mm above the photoconductor and exended beyond the end-mounted contacts by 1.5 mm. This arrangement allowed a 3 by 3 mm photoconductive area to be illuminated and eliminated all spurious effects observed without the shield. The shield was maintained at sample temperature by virtue of being securely attached to the cold finger of the Dewar.

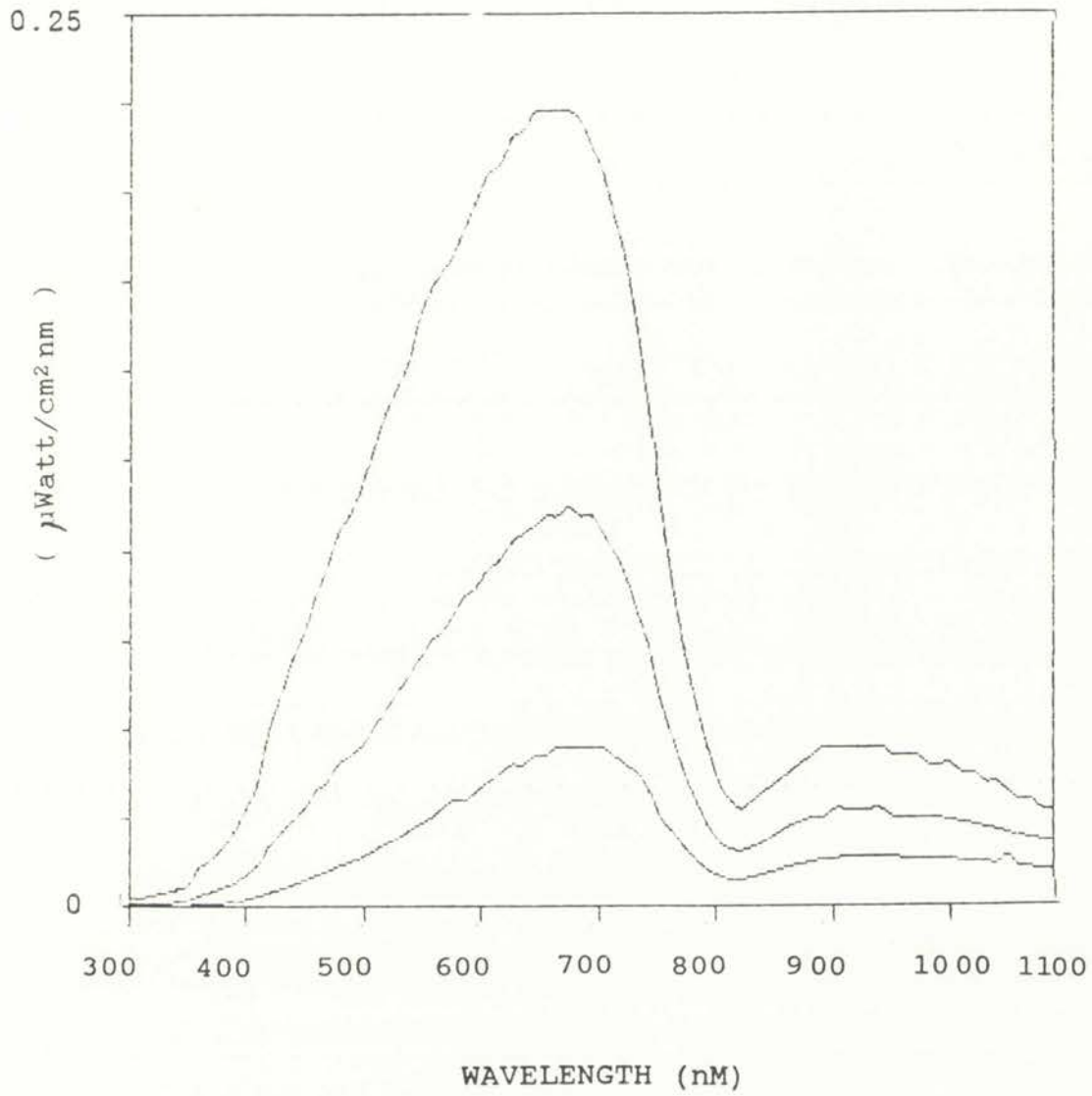

Figure I-4. **Intensity spectra of the white light source incident on Dewar window.**

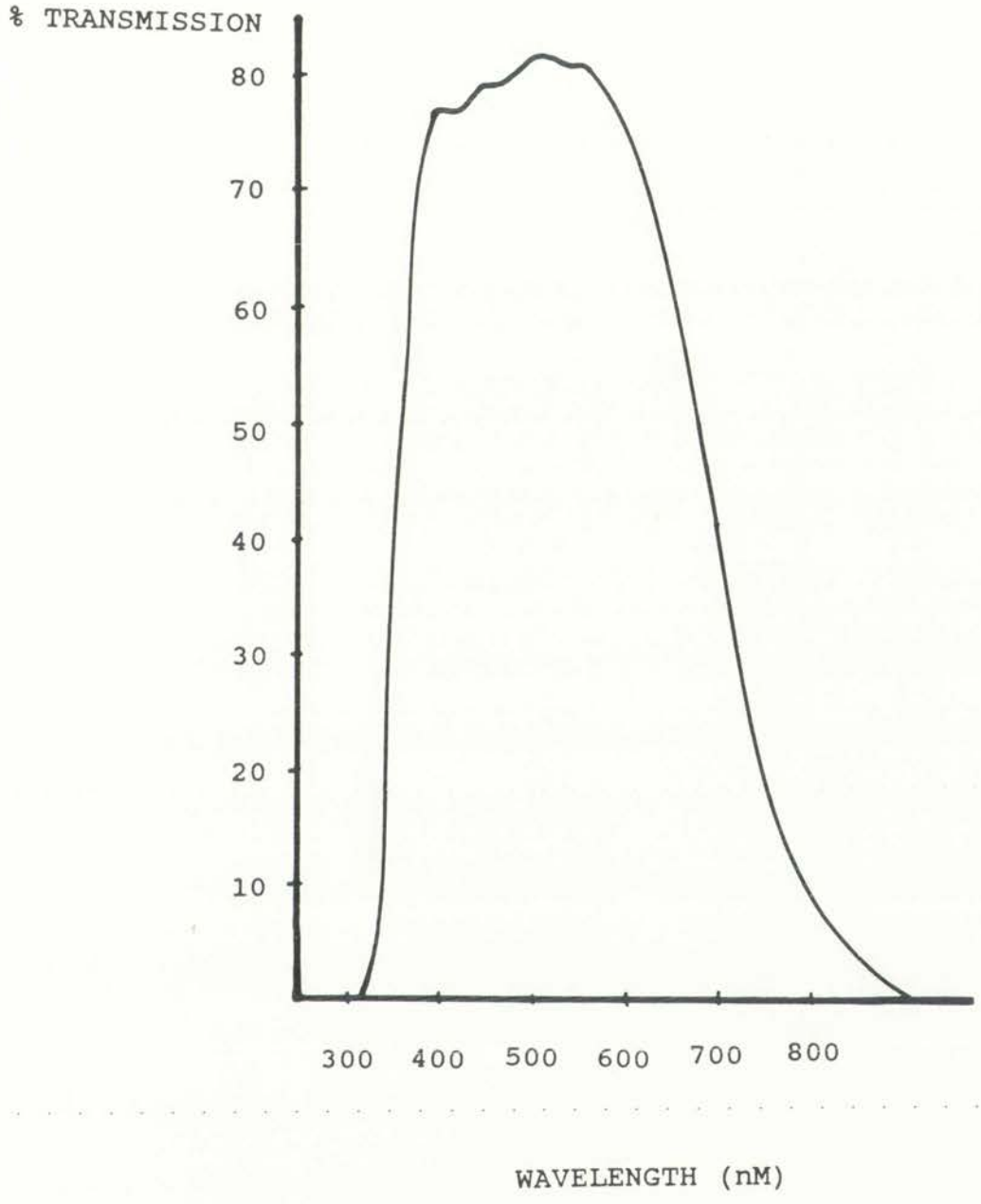

Figure I-5. **Transmission spectrum of the white light source through the Dewar window (KRS-5 + acrylic filter).**

CHAPTER II

FOUNDATIONS OF PHOTOELECTRIC SPECTROSCOPY I

The basic concepts involved in photoconductivity and photoelectric spectroscopy are easily explained in elementary terms - i.e., an electron bound to an impurity energy level at low temperature and unable to participate in conduction is liberated to the conduction band by absorption of a photon of sufficient energy. This simplistic thinking, which assumes isolated, discrete energy levels and focuses on the fate of a single electron, is useful but rarely adequate to explain photoelectric spectroscopy results in detail. It will be clear from our later discussion that such is definitely the case for our data as well. However, pursuit of an understanding sufficiently detailed for interpretation of our spectral and temporal experimental data rapidly leads one to some of the ragged frontiers in semiconductor physics. In this and the following chapter we discuss fundamental issues that are important to our subsequent interpretations, first in the simplest terms and then in more complex contexts.

II-1 The One-Electron Approximation

The one-electron approximation[9-12] has proven to be an important analytical tool of semiconductor physics. It serves also as an useful frame of reference in interpreting experiments, such as will be discussed later, in which collective effects become significant and the one-electron approximation is no longer valid. We next briefly review the basis for the one-electron approximation.

The Hamiltonian for a semiconductor crystal consists of the kinetic energy of all particles in the solid and their interaction energies. The solid is comprised of two groups of electrons - (1) the tightly bound core electrons which are regarded as localized in the vicinity of their respective atomic nuclei, and (2) the more-loosely

bound valence electrons which contribute to chemical bonding and charge transport. The first approximation in developing the Hamiltonian is to consider the valence electrons and lattice ions as independent constituents. Now, the Hamiltonian consists of the kinetic energy of all valence electrons and ions, the energy associated with the interaction of those particles, and the energy associated with external field interactions:

$$H = H_{el} + H_{ion} + H_{el-ion} + H_{ex}. \tag{II-1}$$

Neglecting the last term, the electron part of the Hamiltonian can be written as:

$$H_{el} = H_{el,kin} + H_{el-el} = \sum_{k} \frac{p_k^2}{2\ m} + \frac{1}{8\ \pi\ \epsilon_0} \sum_{kk'}{}' \frac{e^2}{(\vec{r_k} - \vec{r_{k'}})} \tag{II-2}$$

where a Coulomb term for the interaction has been inserted. The sums are for all electron indices except $k = k'$ for the interaction term. The terms p_k, r_k, and m are the momentum, position, and mass of an electron of index k.

The ion portion of the Hamiltonian can be similarly written with the ion parameters designated by capital letters:

$$H_{ion} = H_{ion,kin} + H_{ion-ion} = \sum_{i} \frac{P_i^2}{2\ M_i} + \frac{1}{2} \sum_{ii'}{}' V_{ion}\ (\vec{R_i} - \vec{R_{i'}}). \tag{II-3}$$

The electron-ion interaction can correspondingly be formulated as:

$$H_{el-ion} = \sum_{ki} V_{el-ion}\ (\vec{R_i} - \vec{r_i}). \tag{II-4}$$

Crystal structures in general exhibit a symmetry which results from the periodic arrangement of the ions in the lattice. However, because in reality it is the equilibrium periodicity, rather than their actual positions at any instant, the ion-ion interaction can be divided into two components. One component describes the ion interaction in their equilibrium position, the other corrects for the lattice vibrations. For the latter case the index "*ph*" will be utilized to indicate phonons which describe the vibrations.

$$H_{ion-ion} = H^0_{ion-ion} + H_{ph} \tag{II-5}$$

$$H_{el-ion} = H^0_{el-ion} + H_{el-ph} \tag{II-6}$$

Equations II-1 through II-6 provide the foundation with which to treat most solid-state properties. The next step is changing the Hamiltonian function to the Hamiltonian operator. To further simplify the problem, the adiabatic approximation will be utilized to decouple the Hamiltonian into two components, i.e., the movement of the electrons in a stationary lattice and the movement of the ions in a uniform space charge of electrons. This approximation is based on the fact that the masses for electrons and ions differ by four orders of magnitude or more. As a result, the ions respond only very slowly to electron motion while electrons respond adiabatically to ion position changes.

It is very useful to further simplify the model to the point where it represents basically a one-body problem which includes the electron-electron interaction in the sense of a overall average. Such an approach is provided by the Hartree-Fock approximation. This then results in splitting up the Schrodinger equation for the

many-electron problem into one-electron wave equations. The results of this process is the so-called one-electron approximation which contains the most important parts of the electron-electron interaction.

The development we have just presented leads to the understanding that, in contrast to the distinct and discrete energy levels of isolated atoms before incorporation into a crystal, the stable energy levels of the valence electrons in a crystal fall into distinct continua known as bands which are separated, in the case of semiconductors and insulators, by a gap in which (in a perfect crystal) there are no allowed energy states. In simple semiconductors such as silicon and germanium, the assignment of what were initially the valence electrons of the isolated atoms to the available states in the crystal bands is completed at the point where the last electron has filled the last available state at the top of the so-called valence band of the crystal. With the band gap separating this state from the lowest-energy excited state (the bottom of the conduction band), a minimum energy equal to the band gap is required in order to produce an electronic excitation in the crystal.

The one-electron model developed above further leads to the conclusion that a single electron in an allowed energy band propagates through the crystal in a Bloch wave which is not scattered by the periodic array of ion cores or by the combined averaged potential of the other valence electrons. However, there are several scattering mechanisms which the simplified model is incapable of predicting, which arise from the effect of thermal vibrations on the positions of the ion cores (electron-phonon scattering), from the presence of other electrons which at close range actually do not manifest the assumed averaged potential (electron-electron scattering), and from the presence of potential perturbations arising from crystal defects and impurities.

Scattering mechanisms are important in that they limit the carrier velocity and thus the current that flows in response to an applied electric field. They also tend to maintain thermodynamic equilibrium between the valence electrons and the ion cores of the crystal. Finally, as will be important in subsequent discussions, electron-electron scattering provides a potential energy transfer mechanism between carriers moving in a conduction band and carriers trapped at impurities.

II-2 Effective Mass Theory

We now consider the effects of introducing an impurity in an otherwise perfect crystal that is described within the framework of the one-electron approximation. The resulting effects on the predictions of the electron Schrodinger equation are as follows:[9]

(a) The defect can introduce new energy levels in one of the forbidden energy gaps of the perfect crystal. These are bound or localized states whose wave function is exponentially decreasing away from the defect site.

(b) The defect can scatter electrons whose energies lie within the allowed energy bands of the crystal. The resulting effect can be described as a change in density of states due to the presence of the defect.

The bound states resulting from impurity introduction can be simply described if we further assume that the impurity has one more or one fewer valence electrons in comparison to the atoms of the host crystal. In this case, the impurity will be a "shallow" impurity whose energy levels are relatively close to a band edge.

The effective mass theory[9] is well adapted for the description of shallow levels characteristic of Column V donors or Column III acceptors in silicon. Its main advantage is its simplicity, since it allows the bound state to be described by a Schrodinger hydrogenic equation. Such centers are called hydrogenic because

an electron (or hole) is bound in the Coulomb field of a singly charged donor (or acceptor) as in the case of a hydrogen atom.

Therefore, replacing the mass of the free electron with an appropriately averaged effective mass m^* due to periodic potential influences is required. In addition, the dielectric constant ϵ of the host lattice needs to be used to represent the medium in which the electron is propagating. Incorporating these modifications into the Schrodinger equation results in the energy values obtained for the hydrogen atom, scaled by m^* and ϵ to give

$$E_n = \frac{e^4\ m^*}{8\ \epsilon^2\ h^2} \frac{1}{n^2} \tag{II-7}$$

where e is the charge of the electron and h is Planck's constant. Using the same constants, the Bohr radius r is given by the equation:

$$r_n = \frac{\epsilon\ h^2}{e^2\ m^*} n^2. \tag{II-8}$$

For silicon, the radius of the first Bohr orbit is approximately sixty times larger than the 0.53-Angstrom radius for hydrogen, resulting in an approximate radius of 30 Angstroms. We thus have the important result that the bound electron or hole moves through a volume much larger than that occupied by its parent impurity; this result provides some justification for using the semiconductor dielectric constant ϵ in the Schrodinger equation previously.

Figure I-1 schematically illustrated the discrete energy levels of an assumed hydrogenic shallow impurity, with the energy levels above the first excited state becoming closer and closer as one approaches the continuum of conduction band

states. Many experiments have verified the qualitative correctness of the hydrogenic model for common shallow impurities in semiconductors, although, as one would expect from such a simple model, the quantitative agreement between measured and predicted ionization energies is not precise. According to Kohn[13], ... "it seems surprising that the orbit of a trapped electron or hole winding its way through hundreds of crystal cells can be described at all simply. The theory shows, however, that the larger the orbit the more accurately it can be understood!" Table II-1 illustrates the differences in experimental versus calculated ground-state energy levels for several common impurities in silicon and germanium.

In our later discussion, we will apply or build upon the simple hydrogenic model in several ways. First, note that a carrier bound to a shallow level must receive on the order of seven-tenths of the full ionization energy in order to make the first available transition (Tables I-1 and I-2). Consequently, for impurities of present interest in silicon such as arsenic and bismuth (Table II-1), at least 30 meV of energy must be transferred to the bound carrier before it can reach even the first rung on the ladder of hydrogenic levels leading to its freedom. One important implication of this result, which will be discussed in more detail later, is that carriers trapped in hydrogenic levels will be virtually immune to release from scattering by thermalized band carriers at low temperatures where kT is on the order of 1 meV.

Secondly, it turns out that the concentration of shallow impurity levels in our experimental devices is sufficiently high that nearby levels interact to form a connected band of levels rather than a series of isolated discrete levels. This effect leads to a density of states associated with the resulting impurity band and to band-filling phenomena as well as a variety of complex carrier transport mechanisms

Table II-1. Comparison of experimental and calculated ground-state shallow donor energies for silicon and germanium.[9]

Material:donor	Ionization Energy, eV Experimental	Calculated
Si:P	0.0450	0.0310
Si:As	0.0530	0.0350
Si:Sb	0.0430	0.0390
Si:Bi	0.0690	0.0450
Ge:P	0.0128	0.0089
Ge:As	0.0140	0.0093
Ge:Sb	0.0098	0.0096
Ge:Bi	0.0125	0.0010

within the impurity band.

Thirdly, and by no means of minor importance, is the finding that the qualitative success of the hydrogenic model, which we have noted above, often applies also in regard to the question of binding a second carrier to a shallow impurity level. This phenomenon is analogous to the weak binding of a second electron that is observed in the H^- atom. For our purposes, the importance of this effect lies in the fact that the second bound carrier will have a much lower ionization energy than the first.

II-3 Occupancy of Energy Levels in an Impure Semiconductor

In the following, we will discuss how the valence electrons in a semiconductor are distributed over the available levels in the conduction and valence bands as well as the impurity levels. The electron energy distribution function is the key factor in determining how this process occurs. The appropriate function for the present problem is known as the Fermi distribution, which is developed from the process of assigning interacting particles governed by an exclusion principle and having spin $\pm 1/2$ to available energy states in such a manner that completely filled states have pairs of particles with opposite spins. The Fermi level represents the energy at which the average occupancy of the associated energy level is $1/2$. The Fermi energy distribution function for conduction-band electrons is given by

$$f_n(E) = \frac{1}{1 + e^{(E-E_f)/kT}} \tag{II-9}$$

and the analogous energy distribution function for valence-band holes is

$$f_p(E) = \frac{1}{1 + e^{(E_f - E)/kT}}. \qquad \text{(II-10)}$$

For electrons at energies within approximately kT of the Fermi level and below, the energy distribution is influenced by the occupancy restrictions imposed by the exclusion principle and under these conditions the electron distribution is referred to as degenerate. At higher energies of 2 kT or greater above the Fermi level, these restrictions rapidly become relatively unimportant and the electron energy distribution is to a good approximation

$$f_n(E) \approx e^{-(E - E_f)/kT} \qquad \text{(II-11)}$$

which is analogous to the Maxwellian energy distribution for a gas of non-interacting particles. A similar equation applies, of course, for the approximate hole energy distribution in the non-degenerate case. Figure II-1 shows the Fermi function and illustrates the applicability of the Boltzman approximation.

We now can discuss the thermal excitation of electrons from the valence band continuum into the conduction band. We first assume an idealized intrinsic semiconductor with no impurity levels at a temperature T. The resulting concentration of conduction band electrons is referred to as the intrinsic electron density n_i and correspondingly there will be a concentration of valence band holes p_i which is equal to n_i since they are created and destroyed in pairs for this idealized intrinsic case. These are given by

$$n_i = N_c \; e^{E_f/kT} \qquad \text{(II-12)}$$

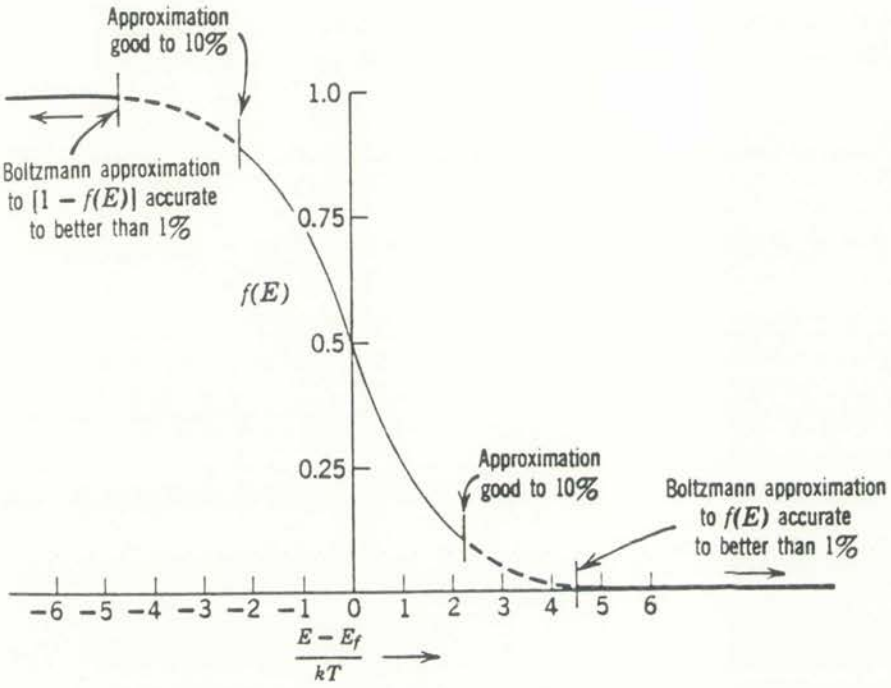

Figure II-1. **The Fermi function utilizing the Boltzman approximation** ($kT = 8.617 \cdot 10^{-5} meV/K$).

and

$$p_i = N_v \; e^{-(E_f - E_g)/kT} \tag{II-13}$$

where N_c and N_v are the effective densities of states for the conduction band and valence band respectively and the semiconductor band gap is E_g. The equations for the effective density of states for silicon are

$$N_c \approx 5.3 \cdot 10^{14} \; T^{1.5} \; cm^{-3} \tag{II-14}$$

and

$$N_v \approx 2 \cdot 10^{14} \; T^{1.5} \; cm^{-3}. \tag{II-15}$$

To find the Fermi level for a pure intrinsic semiconductor one first assumes that all electrons in the conduction band came from the valence band. All electrons in the crystal will then be accounted for if we set the number of electrons in the conduction band equal to the number of holes in the valance band

$$n = p = n_i = p_i \tag{II-16}$$

where n_i and p_i are defined by Equations II-12 and II-13 respectively. Setting Equation II-12 equal to II-13 and solving for the Fermi energy level yields

$$E_f = \frac{E_g}{2} - \frac{kT}{2} \; ln(N_c/N_v). \tag{II-17}$$

We now consider a practical doped or extrinsic semiconductor where carriers will also be made available from impurity levels located within the forbidden gap. While in general the calculations for this case can be sufficiently complex such that numerical solutions are required, it is possible to simplify the mathematics considerably when the Fermi level is within the band gap and no closer than 2 kT to either band edge. This restriction avoids the case of a degenerate electron or hole population, for which the assignment of carriers to available states must include consideration of carrier spin, and makes it possible to use the Maxwellian approximation as discussed previously. Numerically, the approximation neglects "1" with respect to the exponential term in the denominator of Equations II-9 and II-10 for the Fermi energy distribution function. On this basis, the concentration of electrons in the conduction band is still as given by Equation II-12 in the above and can be written as

$$n = N_c \, e^{E_f/kT}. \tag{II-18}$$

However, E_f is no longer given by Equation II-16, but now depends on the impurity concentration N_d as

$$E_f = kT \; ln(N_d/N_c). \tag{II-19}$$

Similarly, if the hole population in the valence band is non-degenerate, one obtains for p, the concentration of holes in the valence band, the following

$$p = N_v \, e^{-(E_g - E_f)/kT} \tag{II-20}$$

Utilizing Equation II-16 to solve for the intrinsic carrier concentration n_i

results in the following equation which is extremely important in solving semiconductor problems

$$n_i^2 = n\ p = N_c\ N_v\ e^{-E_g/kT}. \qquad \text{(II-21)}$$

In comparing the equations for intrinsic and extrinsic conductivity, it may be seen that extrinsic conductivity will dominate at low temperatures, even at very low impurity concentrations. For example, consider a silicon detector at 300 K. Substituting Equations II-14, II-15, and II-17 into Equation II-21 and utilizing the appropriate values for silicon[14] results in 1 $\cdot 10^9$ cm^{-3} electrons available for conduction for the intrinsic silicon case. The extrinsic conduction case can be determined by substituting Equation II-18 into II-17. For a doping concentration N_d of 6 $\cdot 10^{16}$ cm^{-3} results in 1.3 $\cdot 10^{15}$ cm^{-3} electrons available for conduction. Thus intrinsic conductivity competes only weakly with the much stronger extrinsic conductivity mechanisms which arise from the presence of energy levels within the band gap.

The experimental measurements to be discussed in this work were performed at low temperatures (less than 20 K) using crystals with doping densities of 6 $\cdot 10^{16}$ cm^{-3}. As a result, impurity-related conductivity will be considered dominant in the results of our experiments as well as all further discussions.

II-4 Banding Effects Associated with Impurity Levels

In the preceding sections we discussed the structure of electronic states in the vicinity of a single impurity center and outlined the hydrogenic approximation for this case. We now consider how impurity states belonging to nearby centers influence one another in terms of potential charge transfer mechanisms which result in

conduction pathways. One important additional mechanism of conduction becomes possible when the wavefunctions of electrons or holes localized on impurity levels overlap to the point where inter-impurity transitions can occur to an appreciable extent. The occurrence of this effect depends on the radius of the wavefunction on individual impurity centers and on the mean separation of centers. In turn, these factors relate the onset of impurity banding to the depth of the impurity levels and the concentration of impurity centers. In a simplistic approximation, impurity banding occurs when[15]

$$10^{-6} < Na^3 \quad and \quad kT < E_i \tag{II-22}$$

where N is the impurity concentration, a is the characteristic spatial extent of the wavefunction associated with the impurity and E_i is the ionization energy for the impurity.

Our interest in impurity banding is related to the following factors. First of all, at the temperatures of our measurements, even our relatively moderately doped samples will show impurity banding effects. Secondly, at these low temperatures where direct ionization of the impurity levels to the conduction or valence bands is not energetically favored, the dominant conduction mechanism in the absence of photon excitation will be conduction within the impurity band.

In regions of marginal overlap, phenomena which perturb the degree of wave function overlap such as temperature, impurity-band occupancy, or the Fermi level location can show up rather dramatically in degree of changes of macroscopic conductivity. This is one of the more direct manifestations of quantum mechanical effects on the macroscopic properties of semiconductor materials.

CHAPTER III

FOUNDATIONS OF PHOTOELECTRIC SPECTROSCOPY II

In the previous chapter we established the basic origins and characteristics of discrete and banded energy levels in a semiconductor, and also discussed the associated occupancy considerations for these levels. These issues pertain to an essentially static semiconductor with no applied electric field and, thus, no net conduction current. In this chapter we add the relevant dynamic concepts of carrier transport, scattering, and carrier-carrier interactions to complete our foundation for the discussions of subsequent chapters.

III-1 Basic Carrier Transport and Scattering Mechanisms

Here we discuss phenomena related to electrical conduction which apply to free carriers in the conduction and valence bands of a semiconductor.

To begin, we note that bands will exhibit no electrical conduction if they are either completely empty or completely full. Thus an idealized pure semiconductor at $T = 0K$ is an insulator. However, as noted in the previous chapter, the presence of impurities or the effects of thermal excitation will generally result in a concentration of electrons in the conduction band and/or holes in the valence band. These are the so-called "free" carriers (as opposed to carriers that are bound to an impurity) which can move in response to an applied electric field and, thus, conduct current. Intuitive concepts seem to suffice in the case of the electron; for the hole, the collective motion of the valence-band electrons can be described as though a quasiparticle (a positively charged hole) with properties otherwise similar to a free electron were moving in response to an applied field.

The free carriers in the conduction or valence bands will possess thermal energy

by virtue of the various scattering mechanisms that exist which tend to maintain the carriers in thermal equilibrium with the semiconductor lattice. In the absence of an applied electric field, the motion of the carriers will be random and no net current will flow since the average carrier drift velocity is zero. Application of an electric field will perturb the thermal motion of the carriers to yield a net conduction current. In this case, it is commonly found that the average drift velocity of carriers is proportional to the applied field[12], viz

$$v_d(E) = \mu\ E. \tag{III-1}$$

The proportionality factor is the mobility μ; μ is a constant so long as the applied field does not significantly perturb the equilibrium carrier energy distribution by increasing the temperature of the carrier distribution above that of the lattice. Although, as noted earlier, the transport of electrons and holes is conceptually similar, it should be mentioned that the mobilities are generally different for electrons and holes.

In regard to Equation III-1, we note that the motion of "free" carriers in a semiconductor is constrained by scattering processes in such a way that carriers tend to move with constant net average velocity in a constant applied electric field; this is in contrast to the motion of truly free charged particles in vacuum which would exhibit a constant acceleration under a constant applied force.

We next focus on some basic details of the transport and scattering phenomena that are involved in determining the value of the free-carrier mobility at a given temperature. Our discussion uses notation and examples appropriate to conduction-band electrons in n-type silicon; analogous considerations apply also to valence-band

holes in p-type semiconductors.

At a temperature T, conduction-band electrons will have a mean thermal energy of $3/2\ kT$ and, correspondingly, a mean thermal velocity given by[12]

$$v_t = \sqrt{\frac{3\ kT}{m^*}}. \qquad \text{(III-2)}$$

The mean electron velocity is defined between scattering events, which are predominantly the result of scattering from lattice vibrations or phonons, scattering from the potential of ionized impurities, scattering from the lattice disturbance of neutral impurities, and scattering from encounters with other electrons. A brief summary of these four scattering mechanisms for n-type silicon will be discussed in the following paragraphs. A mobility formulation for each case will be presented along with values from the literature for dopant concentrations greater than $1 \cdot 10^{16} cm^{-3}$ at temperatures of 10 K.

Lattice scattering mobility for n-type silicon has been calculated by Long[16] and Norton et. al.[17] based on the general treatment of lattice scattering developed earlier by Herring and Vogt[18] for multivalley semiconductors. Their calculations included contributions from both intravalley acoustical and optical phonon scattering as well as anisotropic scattering effects. The theoretical calculations developed by both Long and Norton agreed well with experimental values. Empirically it has been found for silicon that

$$\mu = 2.1 \cdot 10^9\ T^{-2.5}\ \ \frac{cm^2}{Vs}. \qquad \text{(III-3)}$$

As the dopant density increases or temperature decreases, scattering from im-

purities becomes more important. Theories for ionized impurity scattering have been developed by Brooks[19] and Herring[20], Samoilvich et al.[21], Long[22,23], Li and Thurber[24]. The Brooks-Herring formula is based on the assumption that the Born approximation applies, the relaxation time is a scalar, the energy surfaces are spherical, electron-electron interactions are negligible, and impurity cell effects can be ignored. However, because anisotropy is not accounted for, the resulting mobilities are often overestimated in the Brooks-Herring formula.

For silicon, the anisotropic scattering effect results from the electron mass anisotropy (e.g. $m_t^* = 0.192\ m_o$ and $m_l^* = 0.98\ m_o$ where m_o is the free electron mass, m_t^* is the transverse effective mass, and m_l^* is the longitudinal effective mass) due to its ellipsoidal conduction band structure. Following an extensive study, Long[23] concluded that, if the electron effective mass were used as an adjustable parameter, one would obtain better agreement between theory and experiment. However, Long's modified mobility values were generally too large. To correct this discrepancy, Li and Thurber[24] modified the results of Long[23] and Norton[17] to obtain the following mobility expression for ionized impurity scattering which more closely links theoretical predictions with experimental values.

$$\mu = \frac{7.3 \cdot 10^{17}\ T^{1.5}}{n'\ G(b)} \qquad \text{(III-4)}$$

where

$$G(b) = ln(b+1) - \frac{b}{(b+1)} \qquad \text{(III-5)}$$

with

$$b = \frac{24\ \pi\ m_n^*\ \epsilon\ (kT)^2}{q^2\ h^2\ n'}\ 10^{-6} \qquad \text{(III-6)}$$

and

$$n' = n \left(2 - \frac{n}{N_D}\right) \tag{III-7}$$

where m_n^* is the conductivity effective mass, ϵ is the permittivity of silicon (11.7 ϵ_0), k is Boltzman's constant, T is temperature in degrees Kelvin, q is the electronic charge, h is Planck's constant, n is the electron density, and N_D is the total donor density.

Neutral impurity scattering in the past was generally viewed as contributing less to the scattering than ionized impurities. However, this view is not applicable when temperatures are very low such as 10 K. At these temperatures neutral impurity centers far outnumber the ionized impurities. In order to develop a theoretical formulation of this situation, Erginsoy[25] used the analogy between a neutral donor atom and a hydrogen atom. This approach then permitted the calculation of mobility values through modifying results previously obtained from slow electron scattering off hydrogen atoms. The resulting mobility equation developed by Erginsoy was temperature independent and is given by

$$\mu_E = \frac{2\ \pi^3\ q^3\ m_n^*}{5\ N_N\ \epsilon\ h^3} \cdot 10^{-2} \tag{III-8}$$

where ϵ is the permittivity for silicon, m_n^* is the conductivity effective mass, N_N is the density of neutral impurities, h is Planck's constant, and q is the electronic charge. However, a temperature dependence of neutral impurity scattering mobility exists at low temperatures in silicon.

Erginsoy's formulation was improved upon by Sclar[26] who refined the mobility

equation by including a secondary electron weakly bound to the unionized neutral donor. He concentrated on the "resonant" scattering which would be expected at low energies in connection with the existence of a weakly bound negative ion. In order to modify Erginsoy's formula, Sclar incorporated scattering from a three-dimensional square well to obtain

$$\mu_S = 0.82\ \mu_E \left[\frac{2}{3} \left(\frac{kT}{E_N} \right)^{1/2} + \frac{1}{3} \left(\frac{E_N}{kT} \right)^{1/2} \right] \tag{III-9}$$

with

$$E_N = 1.136 \cdot 10^{-19} \left(\frac{m_n^*}{m_0} \right) \left(\frac{\epsilon_0}{\epsilon} \right)^2 \tag{III-10}$$

where E_N is the scaled binding energy for neutral donors.

McGill and Baron[27] investigated these mobility formulations for the case of low temperatures over three temperature ranges. Their results significantly deviated from the predictions of Erginsoy and of Sclar for temperatures below 2.3 K. However, for temperatures greater than 2.3 K and less than 23 K, good agreement with Sclar's predictions was found. For temperatures above 23 K predictions from all three groups agreed reasonably well. The results of McGill and Baron verify that Equation III-9 is the proper mobility formulation for neutral-impurity scattering over the temperature range of this dissertation's data.

The final scattering mechanism which will be discussed is electron-electron scattering. This component of the total scattering picture becomes vanishingly small at low electron concentrations, but is expected to become important when the concentration of conduction-band electrons becomes large. Li and Thurber[24] have

shown that the presence of significant electron-electron scattering alters the momentum distribution of the conduction-band electrons. Consequently, the effect of electron-electron scattering can be treated through the corresponding changes that are induced in the primary (impurity and lattice) scattering mechanisms as will be indicated below.

The perturbation of the electron momentum distribution induced by electron-electron scattering is the result of a net transfer of momentum from the higher-energy electrons, which dissipate energy more efficiently, to the lower-energy electrons of the distribution. The final result is that the overall rate of momentum transfer to the lattice may be increased somewhat over the rate in the absence of electron-electron scattering. Electron-electron scattering can thus act to reduce the mobility. Li and Thurber[24] point out that the magnitude of this reduction is a function of the energy dependence of the relaxation time. In the case of neutral-impurity scattering, electron-electron scattering has negligible effect on the mobility as here the relaxation time is only a weak function of energy.[24] However, both ionized-impurity scattering and lattice scattering are more significantly affected. For these cases, the calculated maximum effect of electron-electron scattering is to reduce the mobility by 36% and 12%, respectively.[24]

The information in the above can be utilized qualitatively to determine which scattering mechanisms dominate for the studies at hand. Calculations based on Equation III-4 for lattice scattering result in a mobility of $6 \cdot 10^6 cm^2/Vs$. However, values for ionized and neutral impurity scattering are roughly two orders of magnitude lower according to the literature[17,27] and Equations III-8 and III-9. Therefore, for the experimental data to be presented in Chapters IV and V, we can conclude that the principal scattering mechanisms are due to a combination of ionized and

neutral impurities.

In conclusion of this section, we note that scattering is an essential aspect of carrier transport in a semiconductor. In our situation where temperatures are in the vicinity of 10 K, lattice scattering becomes relatively unimportant and other mechanisms (particularly ionized impurity and neutral impurity scattering) become predominant. We remark also that the perspective usually applied to scattering is that it represents a loss mechanism for carrier energy; in the present context, scattering also represents a potential mechanism for the transfer of energy between carriers in different energy states.

III-2 Transport and Energy Levels - Impurities with Discrete Energy Levels

In the previous chapter, we described hydrogenic energy levels at low concentration as well as the banding effects observed at high impurity concentrations. At concentrations intermediate between these two extremes, (1) screening of the fields of ionized impurity levels alters the observed carrier binding energy, and (2) hopping conductivity can transport bound charge between nearby impurity levels. In the next few paragraphs, we briefly discuss energy levels and transport under conditions that may be considered to represent incipient banding in transition to the more general case where unmistakable impurity bands have formed.

It is known that the observed donor ionization energy E_D decreases as the concentration of donors increases. Many interpretations can be found to explain this effect. However, the results of Neumark[28] were found by Norton[17] to give reasonable agreement with experimental results on D^- centers.

In Neumark's interpretation the donor charge is screened by free carriers and

ionized impurities, resulting in a decreased binding energy for the donor electron. She obtained

$$\frac{E_D'}{E_D} = 1 - 1.25 \cdot 10^{-8}\left(\frac{n_1}{T} + \frac{N_I}{T_m}\right)^{1/2} + 3.88 \cdot 10^{-17}\left(\frac{n_1}{T} + \frac{N_I}{T_m}\right) \qquad \text{(III-11)}$$

where T_m is an effective screening temperature for the ionized impurities, n_1 is the density of charge carriers, N_I is the total density of ionized impurities and E_D is the donor ionization energy. Norton has treated the case where it is assumed that $T_M \longrightarrow \infty$.

Thus, we see that the energy levels of shallow impurities may depart significantly from the hydrogenic values at impurity concentrations where banding has not yet occurred. We next discuss carrier transport in this concentration regime.

Consider, for example, an n-doped semiconductor in which compensating acceptors attract donor electrons resulting in an ionized donor concentration N_D^+. Photoexcitation, which will be discussed later, could also have the same effect. There now exists a conduction mechanism which allows electron hopping from a neutral donor to an ionized donor. This was first suggested by Mott[29], by Conwell[30], and by Fritzsche[31]. However, before examining the various hopping conductivity mechanisms, impurity-band conduction concepts will be presented. This will illustrate how charge transfer among impurity levels provides a powerful method for probing the nature of conduction when later coupled with photoconductivity measurements.

It has been found empirically that the temperature dependence of the conductivity $\sigma(T)$ of an extrinsic semiconductor can be represented as[11,12,15]

$$\sigma(T) = \sum_{i=1}^{3} \sigma_i \, e^{(-\epsilon_i/kT)} + \sigma_4 \, e^{(-constant/T^{1/4})}. \qquad \text{(III-12)}$$

Each of the four terms in this expression represents a different conduction process:

(1) The first term dominates at high temperatures and low doping concentrations and results from thermal impurity ionization with activation energy ϵ_1.

(2) The second term begins to become important at lower temperatures and doping levels greater than $3 \cdot 10^{15} cm^{-3}$ in silicon. This conduction process results from electrons with activation energy ϵ_2 from the donor levels to an impurity band called the D^- band or upper Hubbard band.

(3) The third term represents ionized donor charge transport due to nearest neighbor hopping requiring activation energy ϵ_3.

(4) The fourth term results from variable range hopping. This process is important in amorphous semiconductors but, according to Fritzsche[31] and Mott[35], requires temperatures below 4.2 K in silicon. This process should thus be unimportant at the 7 K temperatures of our experimental results.

In general, it is assumed that each contribution to the photoconductivity represented by Equation III-2 can occur also, but with modified parameters in the case of impurity banding, which is discussed next.

III-3 Transport and Energy Levels - Impurities with Banded Energy Levels

In the following, a nonrigorous intuitive description of the formation of the D^- and D^+ impurity bands will be presented. These are also referred to respectively as the upper and lower Hubbard bands. The reader is referred to Hubbard's original papers[32-34] as well as others[15] for further details.

Consider an array of hydrogenic impurities, as we have previously discussed. When the impurities are spaced sufficiently far apart that there is virtually no

wavefunction overlap, the array will show insulating behavior. However, as the wavefunction separation is decreased, metallic conduction can occur as Mott originally indicated[29,35,36] . Hubbard[32-34] and Mott[29,35,36] both explained the insulating behavior as resulting from electron correlation. That is, in order to move an electron from one neutral impurity to another requires an energy (the second term in the above conductivity model for impurity banding)

$$\epsilon_2 = E_i - E_n \qquad \text{(III-13)}$$

where E_i is the ionization energy of a neutral impurity and E_n is the binding energy for a second electron on an impurity. As the concentration of impurity atoms increases, ϵ_2 decreases as wavefunctions increasingly overlap. When ϵ_2 vanishes the transition from insulator to metal occurs. Figure III-1 illustrates the relationship of the density of states as a function of energy and the relationship of the upper and lower Hubbard bands with the energy ϵ_2 and the conduction band.

An additional complication is introduced by the random distribution of donor and acceptor impurities which results in each donor experiencing a slightly different potential than its neighbors. This leads to the appearance of localized states instead of the extended or band-like states in the tail of the upper Hubbard band. An electron can then move only by thermally activated hopping, which will be discussed later.

The mechanisms for impurity-band conduction at concentrations below the metal-insulator transition are as follows. When the temperature is sufficiently low such that no electrons are thermally ionized into either the conduction or upper Hubbard band, N_D-N_A electrons are available to occupy the "N_D" states in the

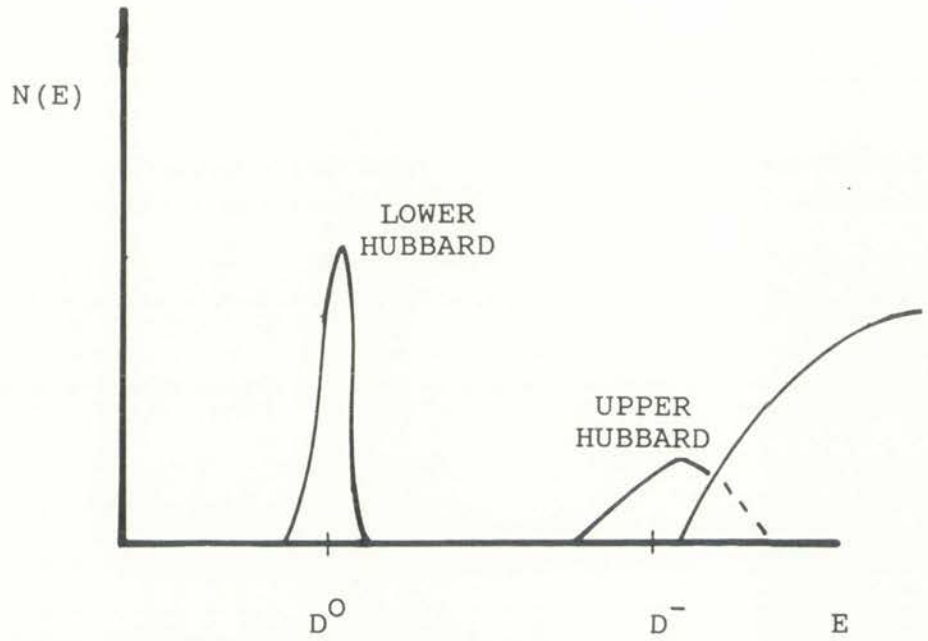

Figure III-1. **Density of states as a function of energy and the relationship of the upper and lower Hubbard bands.**

lower Hubbard band. This then leaves "N_A" empty states in the lower Hubbard band. For low compensation (small N_A), these N_A empty states (which can be thought of as holes) are referred to as D^+ charges, which create a Coulomb potential. This potential results in the formation of localized states within the gap between the Hubbard bands, with the potential for dramatically affecting photoconductivity mechanisms.

The third term in the conductivity model refers to a regime in which conductivity is the result of carriers hopping from occupied to unoccupied impurity sites. This type of conductivity is therefore very sensitive to any perturbations which modulate the small but finite overlap of the wave functions. This type of conductivity is characterized by a much slower time response as compared to impurity-band conduction mechanisms.

In the hopping regime the probability P for carrier hopping is given by[37]

$$P = R_{ph}\, e^{(-2aR - W/kT)} \qquad \text{(III-14)}$$

where R_{ph} is a factor which depends on the phonon frequency. The first term, $2aR$ depends upon the overlap of the wave functions, where a^{-1} determines the spatial extent of the wave function and R is the hopping distance. The second term depends upon the energy difference W between the states through which the carriers hop.

For hopping in the nearest-neighbor regime, there is strong localization ($aR >> 1$) and small dispersion in energy ($W << kT$). Therefore, the probability P that hopping occurs is maximum when the hopping distance R is a minimum. When this situation exists and carriers hop from one site to the closest nearby site, the resulting conductivity is characterized by a constant activation energy ϵ_3 which

is the energy necessary for a carrier to hop from one site to a neighboring unoccupied site. This energy has been calculated by Miller and Abrahams[38] and by Shklovskii and Efros[39]. Their calculations illustrate that the change in ϵ_3 is proportional to the change in N_A.

From the foregoing, it is apparent that the mechanisms of carrier transport in banded impurity levels can be very slow in comparison to the drift of lattice-band carriers in an applied electric field, a topic which will be covered in the following section.

III-4 Energy Distributions and Interactions of Lattice-band Carriers and Impurity-band Carriers

In this concluding section we discuss the energies and velocities of carriers moving in the conduction or valence bands (termed lattice-band carriers) under the conditions of our experiments. We deal with two questions which will be important in our subsequent interpretations: (1) whether lattice-band carriers are likely to impact-ionize impurity-band carriers associated with energy levels that are situated many kT from the conduction-band edge; and (2) whether lattice-band carriers injected by band-to-band absorption are likely to become trapped in impurity bands (thus changing their occupancy) before being swept out of the sample by an applied electric field. These matters are fundamental to understanding the extent to which impurity-band conduction and lattice-band conduction can proceed independently.

We now estimate the relative magnitudes of the electron drift velocity and the mean thermal velocity for parameters relevant to our experiments. Electron mobilities in semiconductors can become quite high at low temperatures owing to the reduction of lattice scattering as temperature is reduced (Equation III-4 or III-9, for example). Mobilities are also dependent on impurity concentration, compensation,

and lattice defects at low temperatures to the point where experiments yield the most reliable values for device calculations.

Experimental data for Si:As have been published[40] which indicate that an electron mobility of approximately 6000 cm^2/V is appropriate for an As concentration of $5.9{\cdot}10^{16} cm^{-3}$ and temperatures of 7-30 K. With an applied electric field of 105 V/cm, from Equation III-1 the carrier drift velocity will be

$$v_d(E) \;=\; \mu\, E \;=\; 6.3 \cdot 10^5 \;\frac{cm}{s}. \qquad \text{(III-15)}$$

In comparison, the mean thermal velocity from Equation III-2 will be

$$v_t \;=\; \sqrt{\frac{3\;kT}{m^*}} \;=\; 2.6 \cdot 10^6 \;\frac{cm}{s}. \qquad \text{(III-16)}$$

From the foregoing we see that the drift velocity is on the order of 25% of the mean thermal velocity for the assumed conditions. Correspondingly, it is still a reasonable approximation to use the thermal-equilibrium Fermi energy distribution for rough estimates that will be adequate for present purposes. On this basis, we can estimate the probability of finding a conduction-band electron with a kinetic energy of 40 meV (sufficient for impact ionization of a donor-band state) as

$$P \;=\; e^{-(E-E_f)/kT} \;\approx\; 1.4 \cdot 10^{-29}. \qquad \text{(III-17)}$$

Thus we conclude that carriers in the impurity band itself are unlikely to be affected by scattering from the lattice-band electrons for the conditions of our experiments.

However, such is not the case for carriers in the D^- band, where ionization energies in the range of 1-10 meV are expected. If a D^- center has an ionization energy of 3 meV, then probability of finding a conduction bands with sufficient energy to ionize a D^- center is

$$P = e^{-(E-E_f)/kT} \approx 6.9 \cdot 10^{-3}. \qquad \text{(III-18)}$$

Lattice-band carriers thus will couple far more strongly to carriers in the very shallow D^- band than to carriers in the deeper banded shallow impurity levels.

Finally, we discuss the possibility of direct capture of lattice-band carriers in impurity levels. This process, which can be regarded as a precursor to recombination across the full band gap, can occur readily under low-field conditions at low temperatures. However, in our experiments, the relatively large sweeping field applied to the samples severely limits the possibility of carrier capture. The reason for this is that the sweeping field will drift injected electrons completely across the 5mm width of our samples in a time given approximately by for ionization is

$$t = \frac{width}{v_d} \approx 0.8\ \mu s \qquad \text{(III-19)}$$

whereas the carrier lifetime in samples such as ours is in the range of hundreds of microseconds or greater. Thus the probability of lattice-band carrier capture by any mechanism, including capture in a shallow impurity level, is small in our experiments.

It may be concluded that the sweeping fields routinely used in our experiments represent a reasonable compromise between (1) the desire to drift lattice-band car-

riers rapidly through the sample to avoid significant changes in impurity-band population by carrier capture and (2) the intent not to enhance the collisional energy transfer to impurity-band carriers by increasing the mean lattice-band carrier energy significantly above the thermal equilibrium value.

Previously it was explained (Figure III-1) how a Coulomb potential brings about the formation of localized states within the Hubbard band gap. It is the transition of electrons (holes) from these states into the conduction (valence) band that accounts for the photoconductivity observed in numerous publications.[57,61–66] Before discussing the formation and properties associated with H^--like centers in more detail, some relevant points should be made. First, H^--like centers and the associated impurity complexes can dramatically affect photoconductivity mechanisms under non-equilibrium conditions resulting from either extrinsic or intrinsic illumination. In order to determine the number of the extra carriers in states with different binding energies, one needs to understand the mechanisms responsible for the formation and destruction of H^--like centers and complexes. However, detailed theoretical interpretation of experimental data encounters considerable difficulties. Secondly these problems become even more pronounced when one considers the molecular impurity complexes of the H_2^- or H^--H^+ type.[63]

In order to simplify the matter, consider H^--like centers and complexes to act as traps. Therefore, in this regime Shockley-Read theory of recombination[67] can be utilized for evaluating the statistics associated with the occupation of second-carrier trapping levels. This will then be utilized to examine potential processes occurring under both intrinsic and extrinsic illumination conditions for low temperatures.

Consider the four fundamental processes involved in recombination through traps and illustrated in Figure III-2. These traps will enhance electron-hole recombi-

nation by capturing electrons from the conduction band and ultimately transferring them to the valence band whenever a hole appears near the trap to recombine with the trapped electron. The net effect is to do away with an electron-hole pair, the trapping level being returned in the end to its original state.

For the above circumstances, the rate at which electrons from the conduction band are captured by the traps will clearly be proportional to the number of electrons in the conduction band and to the number of empty traps available to receive them. This simplified version of the Shockley-Read recombination theory[67,68] begins with the expression

$$R_{cn} = C_n \, N_t \, [1 - f(E_t)] \, n \qquad \text{(III-20)}$$

where C_n is a constant, N_t is the total concentration of trapping centers in the crystal, n is the number of electrons in the conduction band and the Fermi level which coincides with the trap level E_t is given by

$$f(E_t) = \frac{1}{1 + e^{(E_t - E_f)/kT}} \qquad \text{(III-21)}$$

Likewise, the rate at which electrons are emitted from filled traps to the conduction band will be proportional to the number of filled traps, and can thus be expressed as

$$R_{en} = E_n \, N_t \, f(E_t) \qquad \text{(III-22)}$$

where E_n is another proportionality constant. Under equilibrium conditions, the

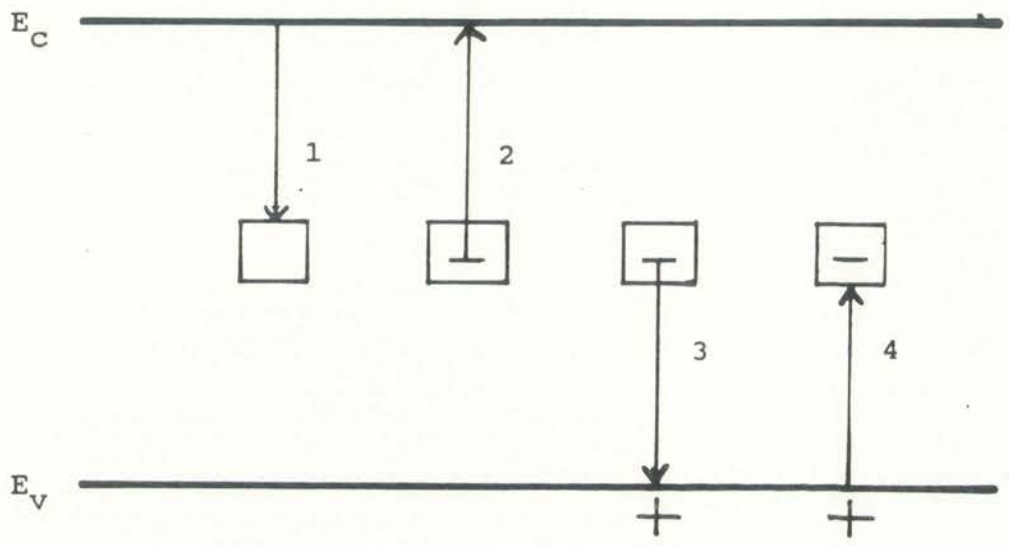

Figure III-2. **Four fundamental processes involved in recombination through traps; (1) capture of a conduction-band electron by an empty trap (2) emission of an electron from the trap to the conduction band (3) capture of a hole from the valence band by a trap containing an electron and (4) promotion of a valence electron into an initially empty trap.**

principle of detailed balancing implies that these two rates must be equal, whereby

$$E_n = n_o \, C_n \left[\frac{1 - f(E_t)}{f(E_t)}\right] \tag{III-23}$$

with n_o as the total number of electrons per unit volume in the conduction band. An expression for n_o is found to be

$$n_o = U_c \, e^{-(E_c - E_f)/kT} \tag{III-24}$$

where

$$U_c = 2\left(\frac{2 \, \pi \, m_n^* \, kT}{h^2}\right)^{3/2}. \tag{III-25}$$

By substituting the explicit value of the Fermi function f_{E_t} from Equation IV-5 the following simple relationship may be obtained

$$E_n = n_o \, C_n \, e^{(E_t - E_f)/kT}. \tag{III-26}$$

Substituting the value given by Equation III-24 for n_o; E_n may finally be written as

$$E_n = n_1 \, C_n \tag{III-27}$$

where

$$n_1 = U_c \, e^{-(E_c - E_t)/kT}. \tag{III-28}$$

In the same way, the rate at which holes are captured from the valence band must be proportional to the concentration of holes and to the number of traps which may receive holes hence

$$R_{cp} = C_p \; N_t \; f(E_t) \; p. \tag{III-29}$$

The rate at which holes are emitted to the valence band from trapping centers is proportional to the number of traps occupied by holes (i.e. empty), from which

$$R_{ep} = E_p \; N_t \; [1 - f(E_t)]. \tag{III-30}$$

For the equilibrium state, R_{cp} must be equal to R_{ep} and by the same reasoning utilized in the above for deriving Equation III-27, one can show that

$$E_p = p_1 \; C_p \tag{III-31}$$

where

$$p_1 = U_v \; e^{-(E_t - E_v)/kT}. \tag{III-32}$$

Figures III-3 and III-4 illustrate the impurity levels and their charge states for the Si:As material in thermal equilibrium. From the above, one can readily assume that the following transitions schematically illustrated in Figures III-5 and III-6 exist within the Si:As samples. Conceptually, Figure III-5 illustrates how intrinsic illumination can act as a mechanism to repopulate shallow neutral impurity centers and H^--like impurities and complexes.

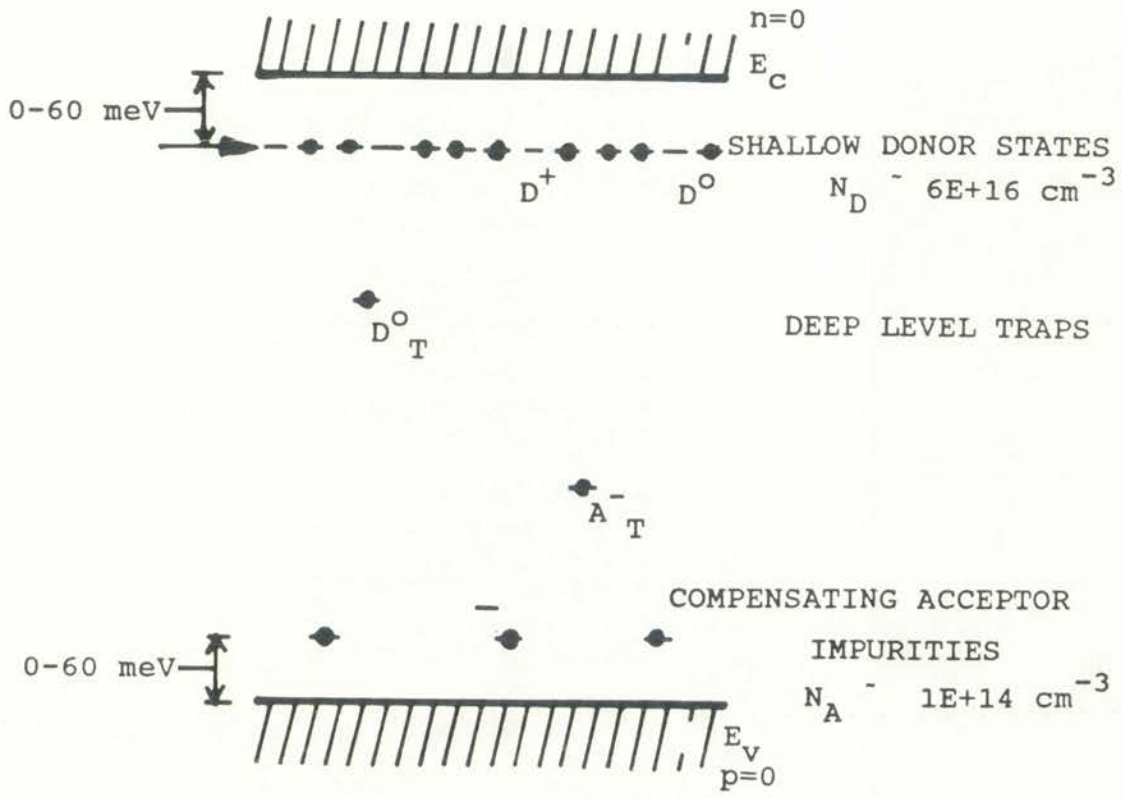

Figure III-3. **Impurity levels and their charge state for the Si:As detector in thermal equilibrium for temperatures below 15 K. Thermal ionization is negligible for these temperatures since $kT < E_i$.**

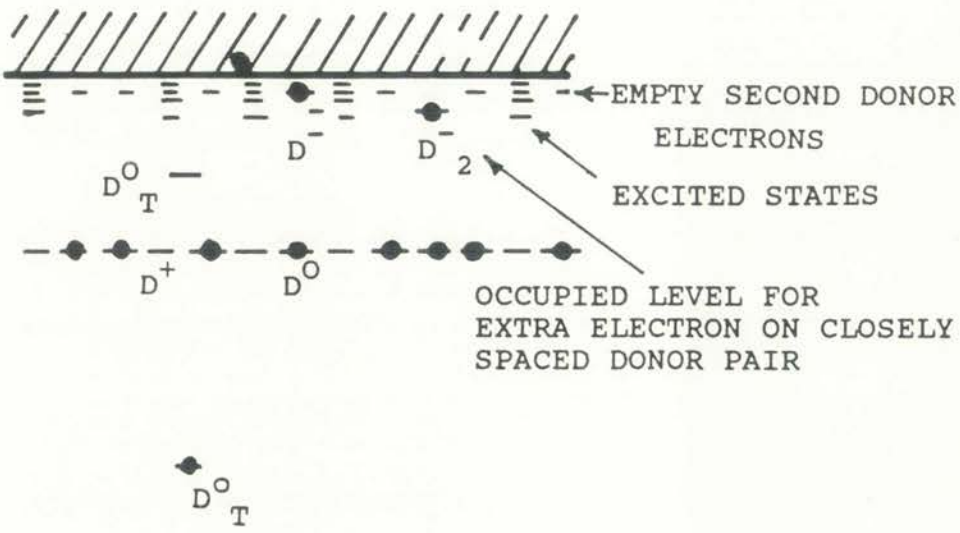

Figure III-4. **Energy levels and their charge state for the shallow impurities of the detector material under extrinsic illumination.**

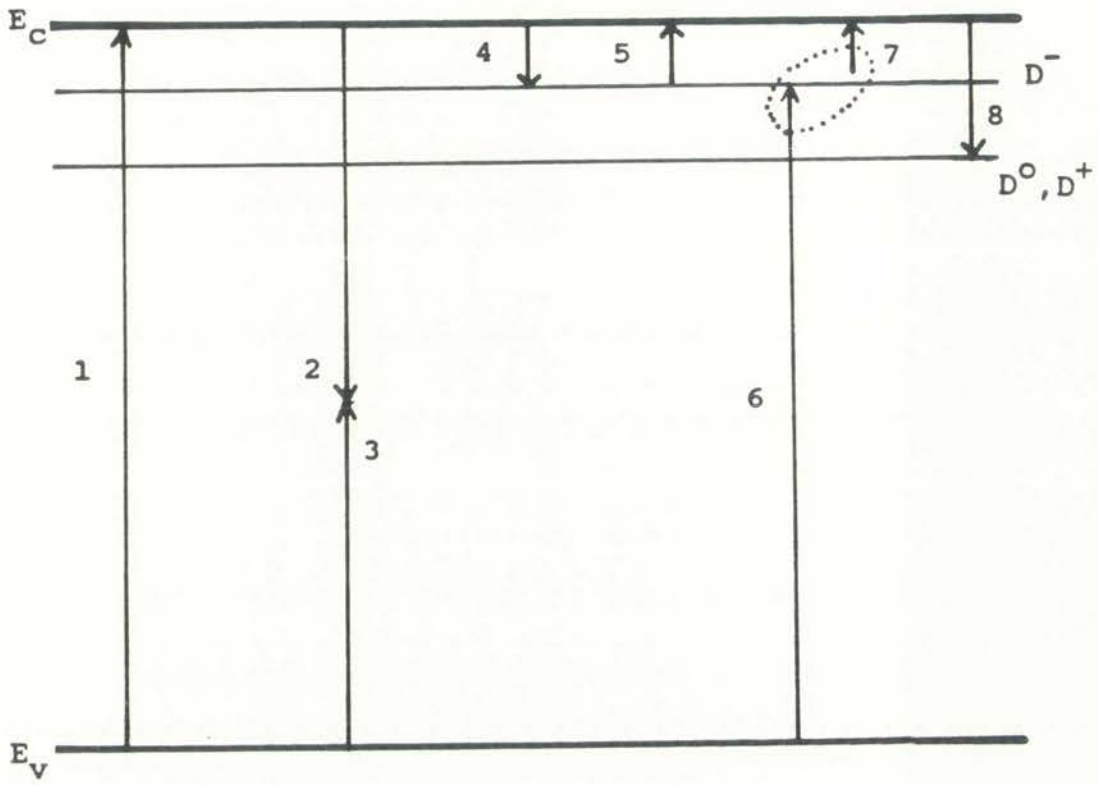

Figure III-5. Repopulation model of shallow neutral impurity centers, D^- centers and associated D center complexes, by intrinsic radiation. (1) band-gap generation of carriers (2,3) Capture of electrons and holes by deep centers (E_T) (4,5) Capture and re-emission of electrons by the neutral donors (6,7) Capture of holes by the D centers and emission of electrons (8) Capture of electrons by ionized donors.

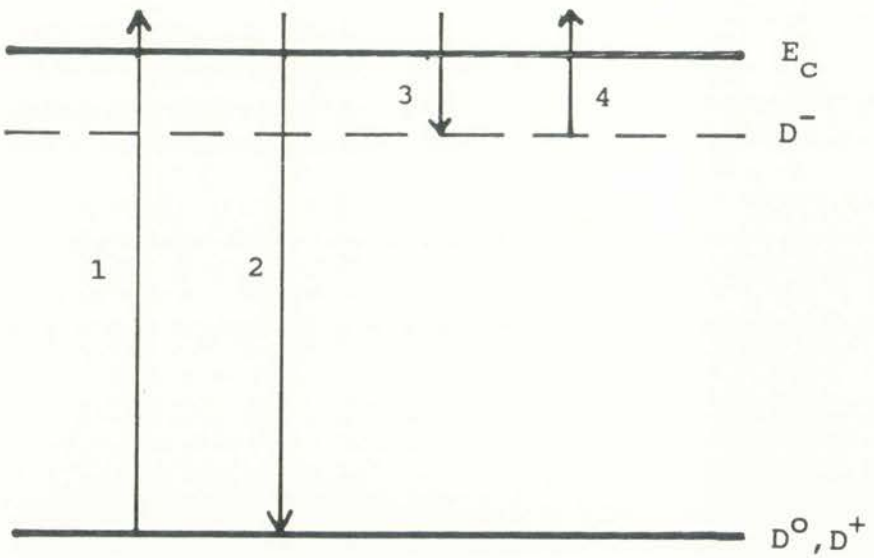

Figure III-6. **Energy transition scheme for D^- centers under extrinsic IR illumination. (1) Electrons emitted from neutral donors and recombine at either (2) ionized donors D^+ or (3) captured by neutral donors D_o producing D^- centers. (4) Thermal emission of captured electrons from D centers for $kT > E_i$.**

However, before any conclusions can be reached, an examination of the importance of extrinsic excitation which transfers electrons from neutral donors into the conduction band (transition 1, Figure III-6) will be made. Free electrons can then recombine at ionized donors (transition 2, Figure III-6) with the rate $n\alpha^+N^+$, where n, N^+ are the concentrations of free carriers and ionized donors, respectively, and α^+ is the coefficient of capture by an attractive center. Transition 3 is the capture of free electrons by neutral impurities with the rate $\alpha^o N^o n$ where α^o is the capture coefficient for a neutral center and N^o is the concentration of neutral donors. The net result of transition 3 is the formation of D^- centers. At high temperatures ($kT > E_i$) the concentration of negatively charged centers D^- is small due to a strong thermal remission of the trapped electrons resulting in transition 4. Transition 4 defines the remission process which can occur from a variety of potential mechanisms, such as scattering or thermal remission and is the concentration of negative charged centers D^- multiplied by the probability for the process occurring, W. The probability of this process occurring can be derived from the detailed balance equation for the D^o state as was shown for Shockley-Read recombination. This probability is

$$W = \alpha^o \; N_D \; e^{(-E_i/kT)} \qquad \text{(III-33)}$$

where N_d is the number of states within an interval kT in the conduction band and E_i is the ionization energy of a D^- center. The distribution of activation energies associated with D^- states have been shown to range from 1 to 10 meV.[69]

CHAPTER IV

SPECTRAL EXPERIMENTAL DATA AND DISCUSSION

In this chapter we will present the results of our spectral experimental data which were obtained for both Si:As and Si:Bi photoconductors. In order to examine the experimental data and optically induced charge transfer mechanisms, the generally accepted models[1-3] for extrinsic photoconductivity will first be reviewed. This will then be followed by the measured spectral photoconductive data for the extrinsic detectors. The extrinsic photon energy was chosen to span the primary energy regime where interaction between conduction or valence-band carriers and the excited states of the shallow silicon impurities such as phosphorus, boron, arsenic, and bismuth could be examined. The energy regime for the extrinsic illumination source was experimentally limited to 5% (43 meV) to 20% (37 meV) below the isolated ionization energies. However, this encompassed a majority of the excited states of interest.

IV-1 Extrinsic Detectors

For an extrinsic detector excited by photons at a wavelength λ, the response current can be expressed as

$$I = \Phi \; A_d \; \eta(\lambda) \; e \; G \qquad \text{(IV-1)}$$

where Φ is the photon flux, A_d the detector area exposed to the flux, $\eta(\lambda)$ the quantum efficiency and e is the electronic charge. G is the photoconductive gain, defined as the average number of electrons flowing in the detector circuit per photogenerated carrier in the detector. Since all experimental data presented utilized detectors with Ohmic contacts, the steady-state gain of the detector is given by

$$G = \frac{\mu \tau E}{d} \qquad \text{(IV-2)}$$

where μ is the carrier mobility, τ the recombination lifetime of the carriers, E the electric field, and d is the interelectrode distance. The gain of Equation IV-2 is independent of frequency since it is assumed that transient space-charge effects are unimportant. Our experimental interpretations of photoconductivity data, as well as most of those in the literature, are based on the assumption that Equation IV-2 is valid. In the next several paragraphs we will demonstrate that this is the case for our experimental conditions.

From Equation IV-2 we can conclude that the photoconductivity should increase linearly with the applied voltage. This makes the assumption that neither the lifetime nor the mobility are voltage dependent. Equation IV-2 also leads one to believe that the photoconductive gain could be made indefinitely large either by increasing the voltage or by decreasing the electrode spacing. However, our simplifying assumptions no longer hold when the voltage reaches a limiting value defined by space-charge equilibrium. This effect is known as "gain saturation" and, as we will demonstrate below, can be neglected at the relatively low bias fields and low signal levels utilized in the present experiments. The gain saturation phenomenon has been observed in a variety of silicon detector configurations[41,42] including various geometries, contact processes, and dopants.

To demonstrate the absence of gain-saturation effects in our photoconductivity measurements, we initally performed photoconductivity experiments on our samples using various values of applied electric field, varying the field both above and below the "typical" value of 100 V/cm used in the majority of our subsequent experiments.

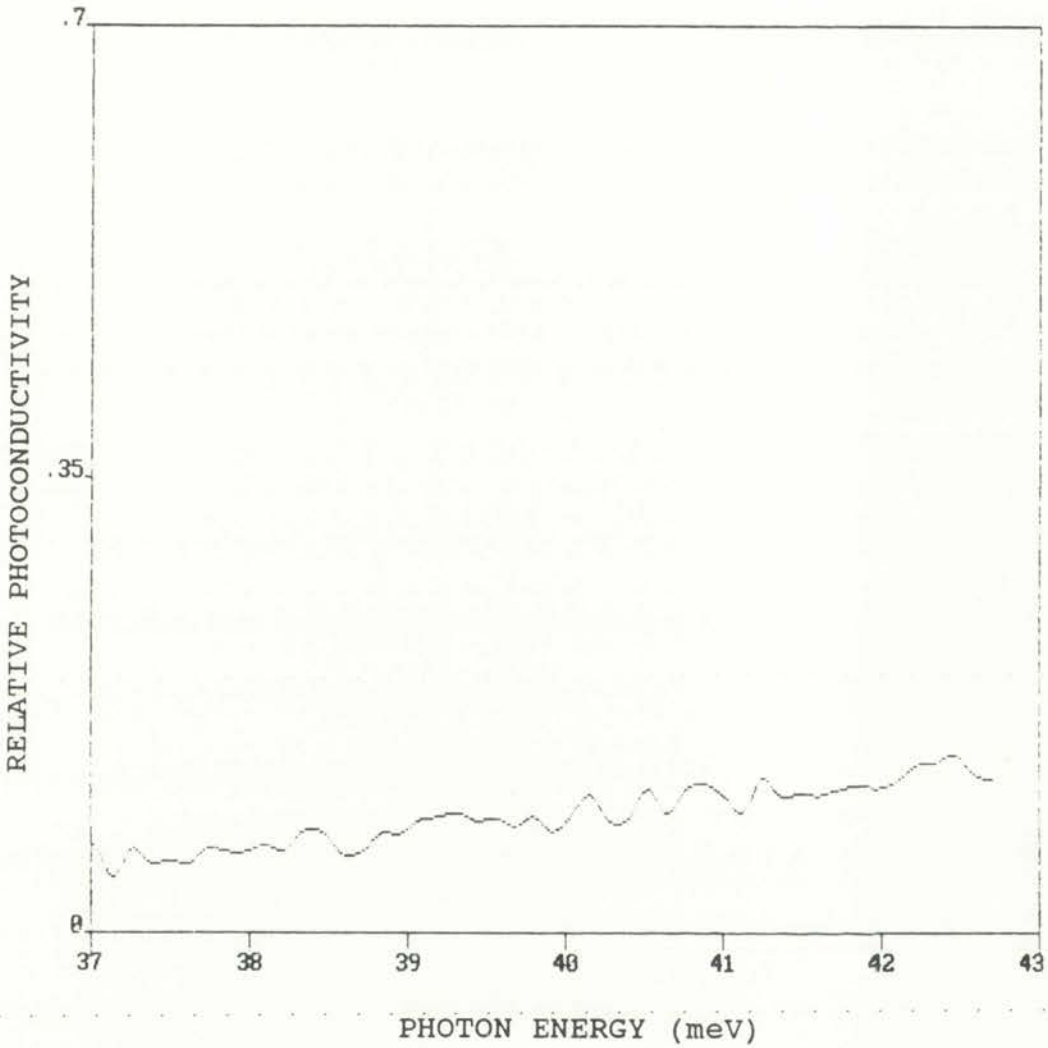

Figure IV-1. **Si:As detector relative photoconductivity response with only IR illumination. Temperature = 7 K, Bias = 35 V/cm.**

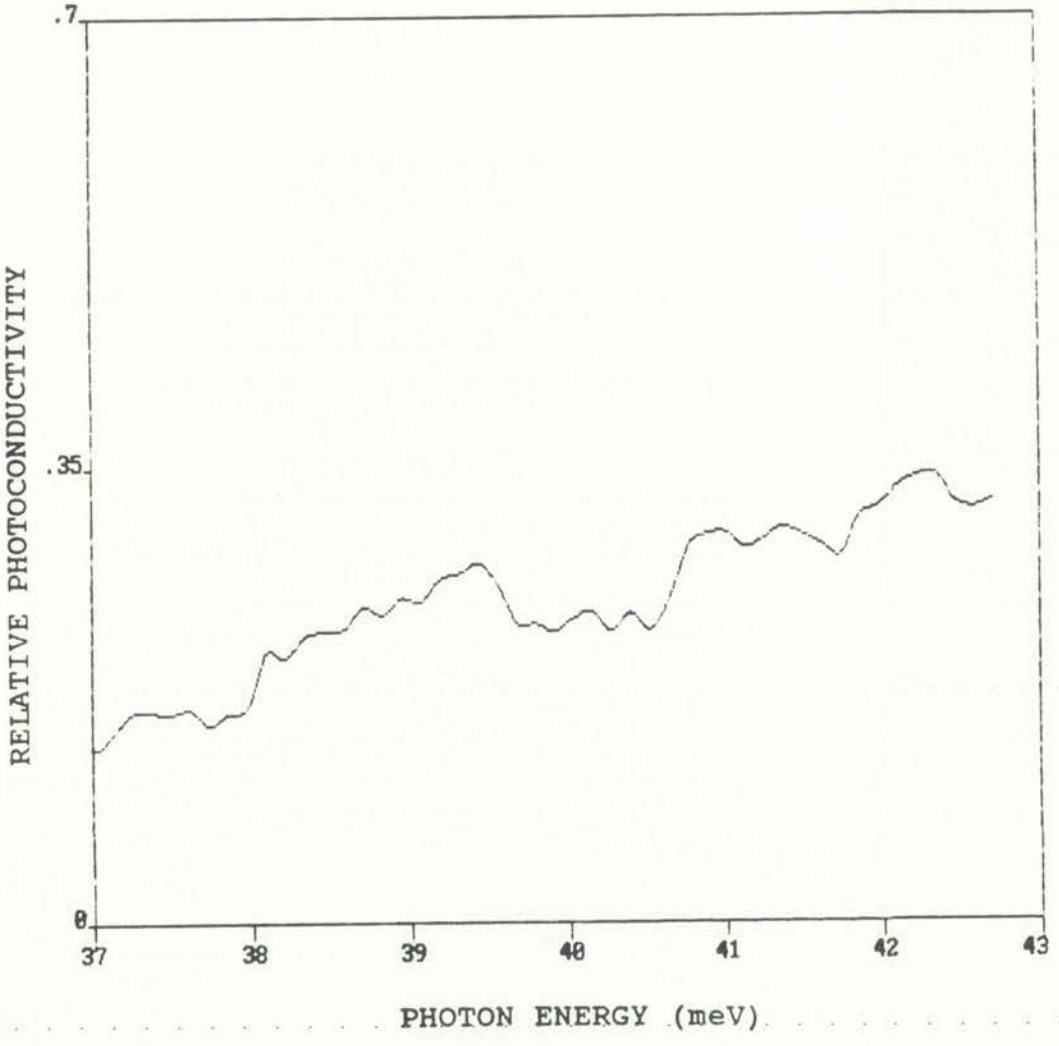

Figure IV-2. **Si:As detector relative photoconductivity response with only IR illumination. Temperature = 7 K, Bias = 105 V/cm.**

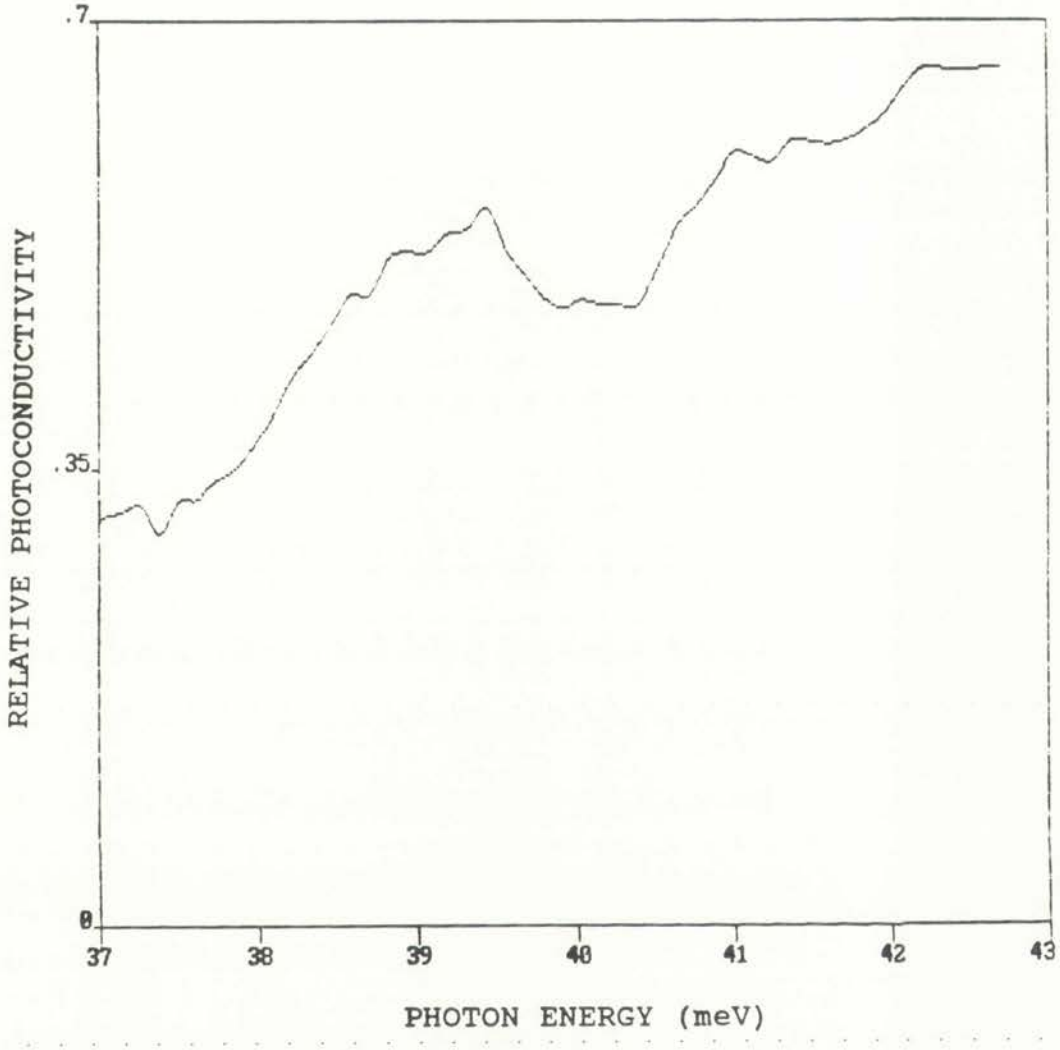

Figure IV-3. **Si:As detector relative photoconductivity response with only IR illumination. Temperature = 7 K, Bias = 175 V/cm.**

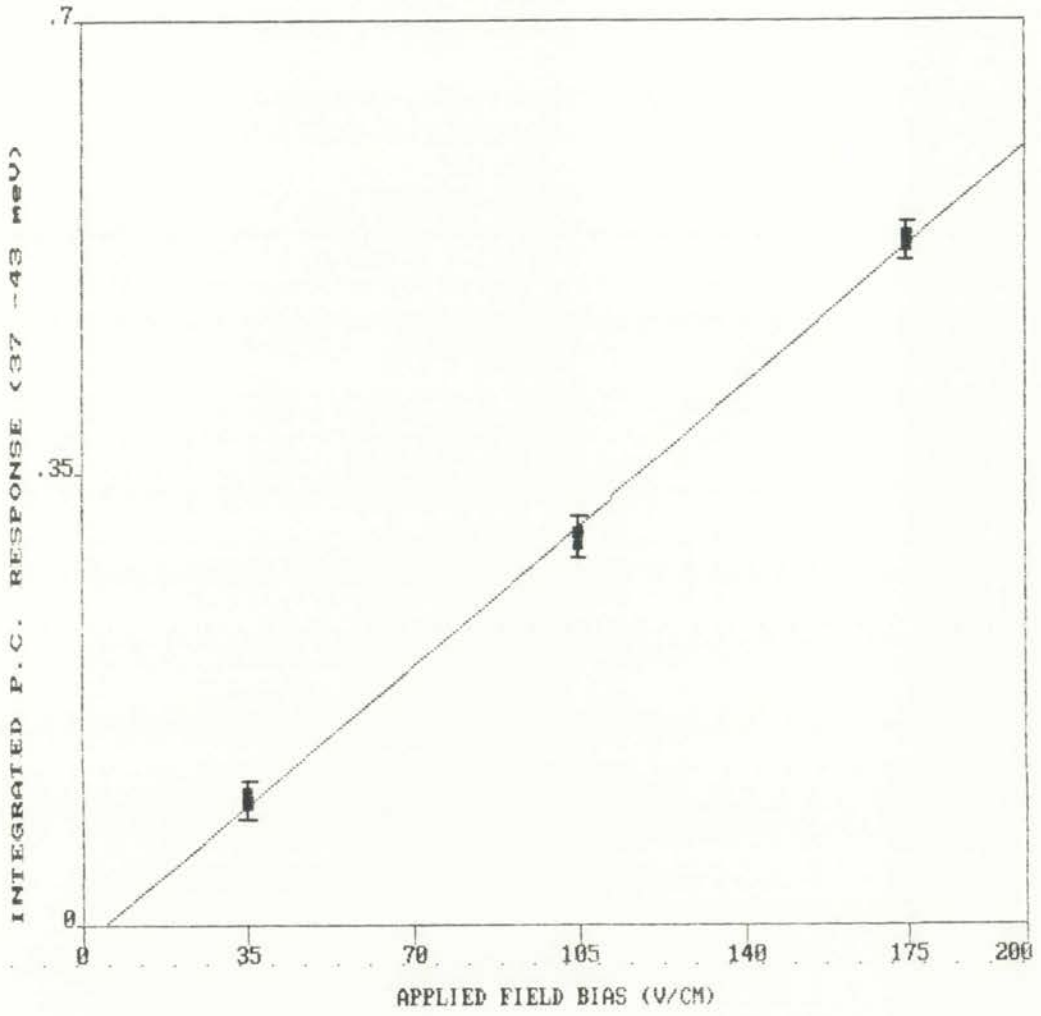

Figure IV-4. **A straight line fit determined by the method of least squares to the average value of the integrated photoconductive response of Figures IV-1 to IV-3 versus the applied field bias for Si:As across the 37-43** *meV* **energy regime.**

A typical result is shown in Figures IV-1 to IV-3 which illustrate how a Si:As detector responds for different bias fields at 7 K. Figure IV-1 shows the photoconductivity spectrum for the lowest bias field of 35 V/cm. Figures IV-2 and IV-3 shows photoconductivity spectra on the same coordinates as in Figure IV-1, but for higher bias fields of 105 and 175 V/cm respectively. For these figures the shape of the photoconductivity spectrum remains similar and the signal increases with increasing electric field in qualitative agreement with Equation IV-2. Quantitatively, Figure IV-4 shows how the spectrally-integrated photoconductive response varies with applied electric field for the data of Figures IV-1 through IV-3. Figure IV-4 shows good agreement with the linear electric field dependence of Equation IV-2. In addition, the fact that the integrated response extrapolates to zero for an applied field near zero demonstrates that contact potential offsets from non-Ohmicity in our sample contacts are negligible for the conditions of our experiments. Similar behavior was observed for all our samples, which included Si:As, Si:Bi, and Si:Al. Therefore, the assumption that our samples are representative of extrinsic detectors where gain saturation can be neglected is valid for our experimental conditions.

Another point that must be verified relative to Equation IV-2 is that the photoconductive gain of our samples is not significantly affected by transient space-charge effects. In cases where this does occur, the response of the detector to modulated IR fluxes will involve the characteristic time associated with establishing space-charge equilibrium. This is called the dielectric relaxation time τ_d which is given by[43]

$$\tau_d = \frac{\epsilon_s \, \epsilon_o}{\sigma} \qquad \text{(IV-3)}$$

where ϵ_S is the relative dielectric constant of the semiconductor material, ϵ_o is the permittivity of free space and σ is the conductivity of the detector material under

operating conditions. Equation IV-2 is valid only for modulation frequencies much lower than $1/\tau_d$. The gain will drop off at higher frequencies and is a function of frequency, dielectric relaxation time, and carrier lifetime.[44] For our measurements, the modulation frequency was typically maintained at 10 Hz. We looked for the presence of transient space-charge effects in our samples by varying the IR chopping frequency over the range of 3 to 20 Hz while monitoring changes in the photoconductive gain. The fact that we observed virtually constant gain over this frequency range allows us to conclude that our subsequent measurements at 10 Hz are performed within the assumptions of Equation IV-2.

Illuminating a semiconductor with above band-gap light affects not only the concentration of current carriers in the bands, but may also affect the concentration of carriers trapped in shallow impurity levels. This implies that the charge of impurity centers can change via a variety of potential charge transfer mechanisms. A better understanding of these phenomena is important for developing infrared detectors required to operate in space environments where it is desired that the detectors discriminate between extrinsic photoconductive signals and signals due to band-gap radiation. For ionizing radiation below atomic displacement thresholds the primary effect on the semiconductor is generation of electron-hole pairs.

The basic photoelectric spectroscopy method, discussed earlier, reveals only centers which produce a free charge carrier when they change their charge state through the absorption of a photon (and perhaps also a phonon). Therefore, the fundamental technique is restricted in its utility to studying levels in the lower half of the band gap for p-type crystals and in the upper half of the band gap for n-type crystals. However, this restriction can be removed by shining band-gap light ($h_\nu > E_g$) onto the crystal.[45,46] This technique is based on the fact that only neutral impurity atoms

can be excited by light and only such atoms contribute to the photoconductivity.[47] For example, consider an n-type semiconductor in which the donor impurity is in excess ($N_D > N_A$). Since the compensating acceptor impurities are completely ionized they do not contribute to the photoconductivity signal and therefore their chemical nature cannot be identified. However, supplementary illumination with band-gap light enables a full analysis of impurities, both major and compensating, to be performed.

In this dissertation, photoelectric spectroscopy augmented with band-gap photoexcitation was utilized to investigate the behavior of extrinsic silicon detectors. Our technique also provides, in addition to the benefits mentioned above, some basic information on the coupling mechanisms between lattice-band and impurity-band carriers as well as an experimental environment potentially related to operational conditions in space environments.

IV-2 Experimental Data On Si:As Material

Si:As detectors were illuminated simultaneously with white light (intrinsic) and IR wavelengths (extrinsic) using several intensities of white light. The resulting spectral photoconductive response curves are illustrated in Figures IV-5 to IV-14 at a temperature of 7 K and a bias field of 105 V/cm.

Figure IV-5 is the spectral response curve without white light illumination. Figure IV-7 now includes the additional white light illumination for a low intensity level of 1 $\mu W/cm^2$ defined by curve 1 in Figure I-4. The photoconductive response now begins to show some structure and gives the appearance that the carrier concentrations within the energy levels under investigation are uniformly distributed with a slight decrease in signal magnitude. Increasing the white light intensity to

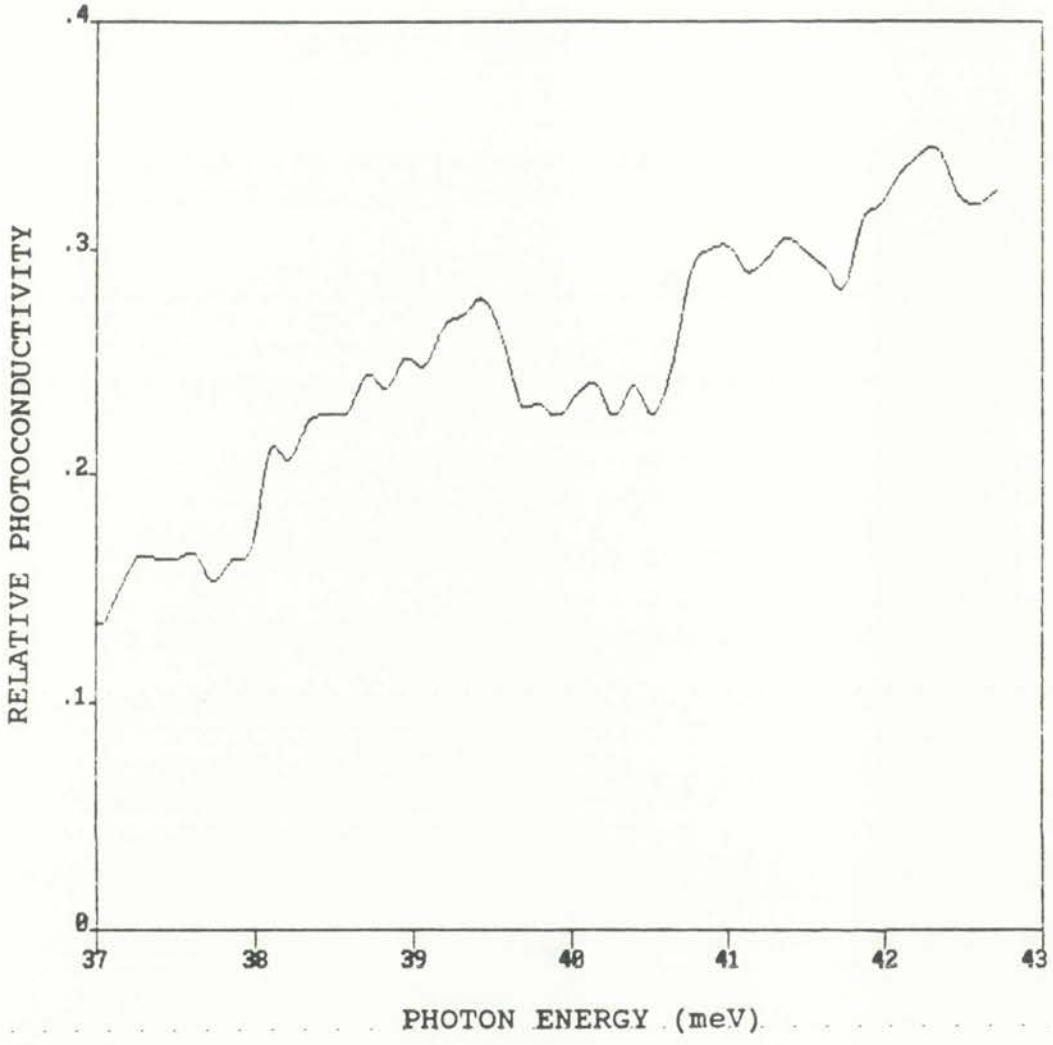

Figure IV-5. **Si:As detector relative photoconductivity response with only IR illumination. Temperature = 7 K, Bias = 105 V/cm.**

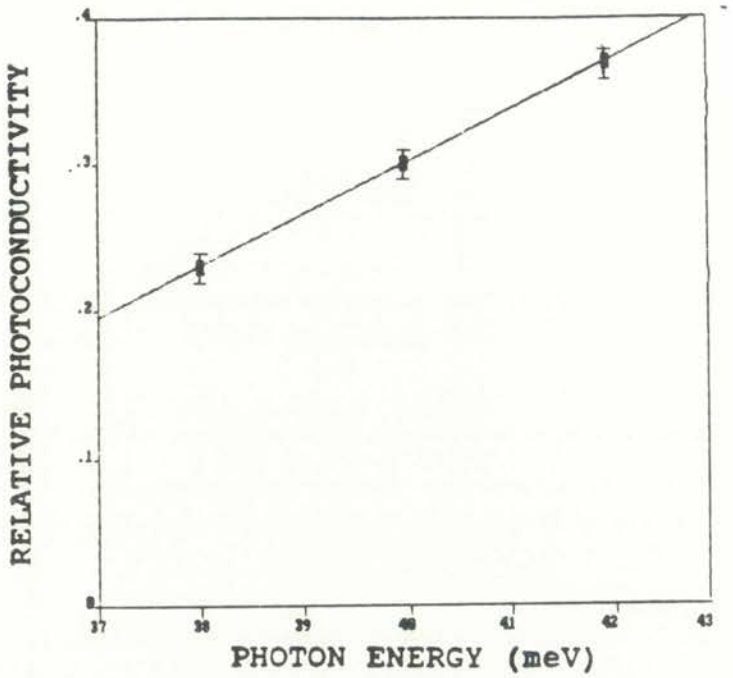

FIGURE IV-6a

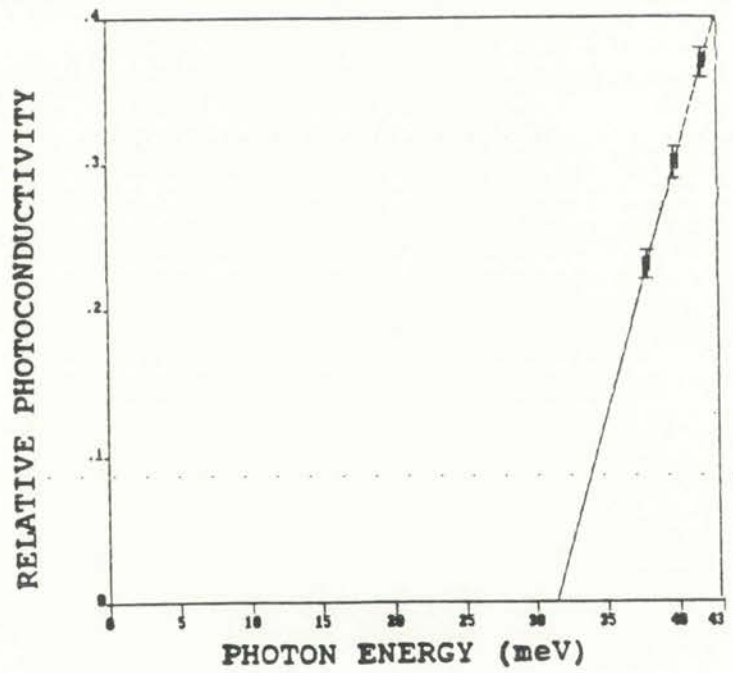

FIGURE IV-6b

Figure IV-6. a. A straight line fit determined by the method of least squares to the average values for the integral of the photoconductive response in Figure IV-5 across three equidistant areas (**37-39, 39-41,** and **41-43** *meV*).
b. Extrapolation of Figure IV-6a to determine x-axis intersection.

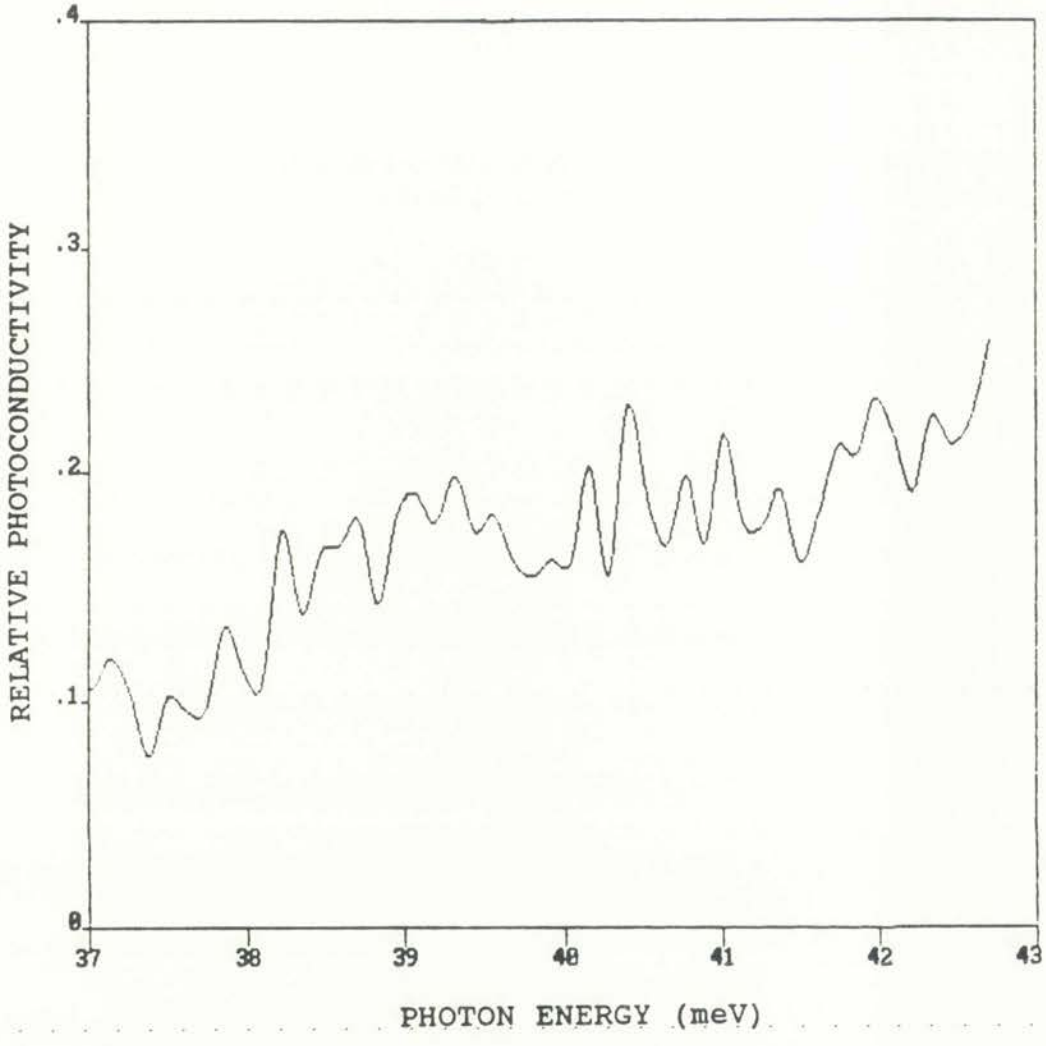

Figure IV-7. **Si:As detector relative photoconductivity response with both IR and white light illumination. White light intensity = lowest (curve 1, Figure I-4), Temperature = 7 K, Bias = 105 V/cm.**

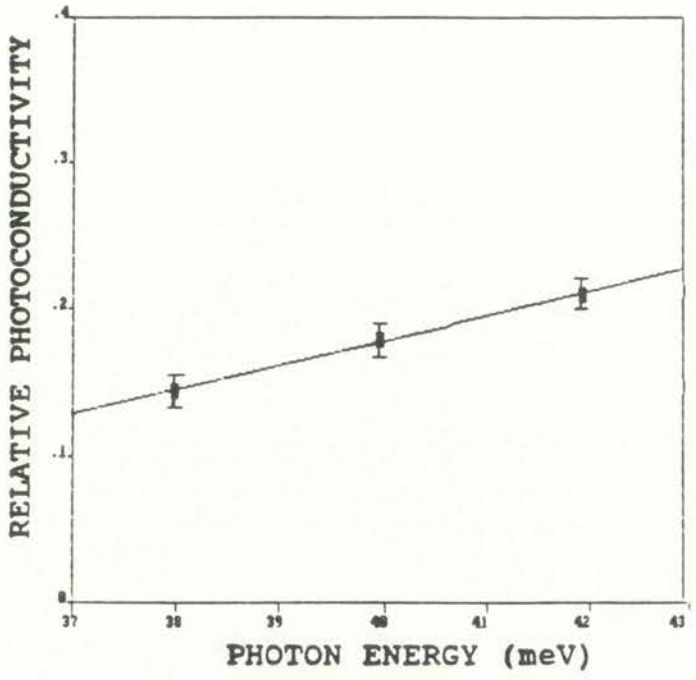

FIGURE IV-8a

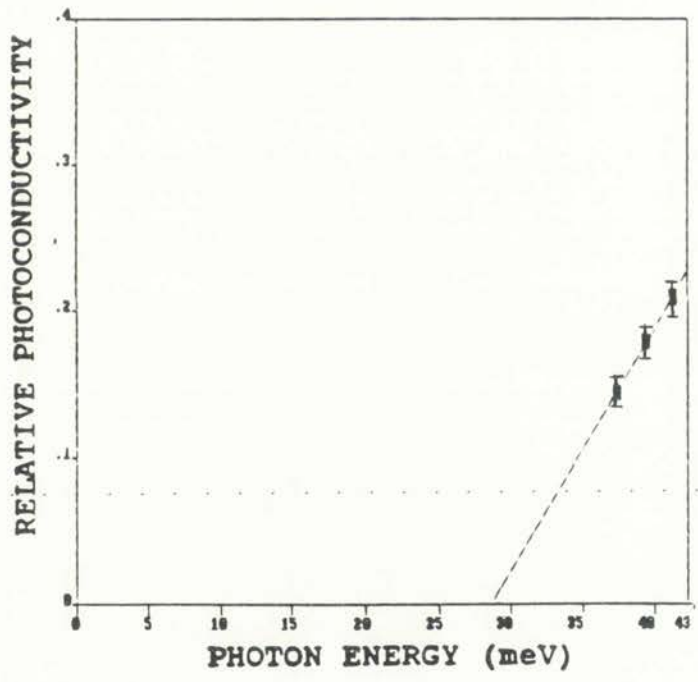

FIGURE IV-8b

Figure IV-8. a. **A straight line fit determined by the method of least squares to the average values for the integral of the photoconductive response in Figure IV-7 across three equidistant areas (37-39, 39-41, and 41-43** meV**).**
b. Extrapolation of Figure IV-8a to determine x-axis intersection.

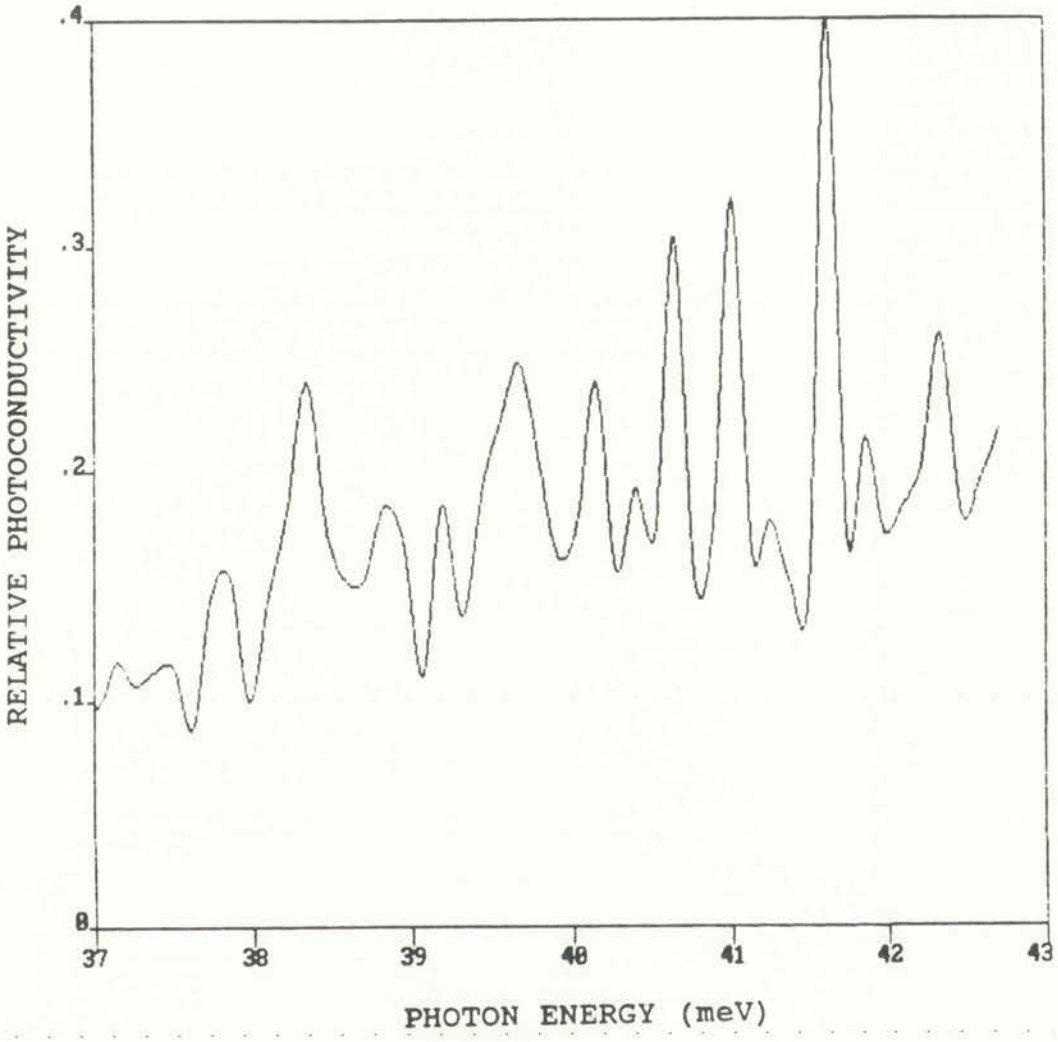

Figure IV-9. **Si:As detector relative photoconductivity response with both IR and white light illumination. White light intensity = medium (curve 2, Figure I-4), Temperature = 7 K, Bias = 105 V/cm.**

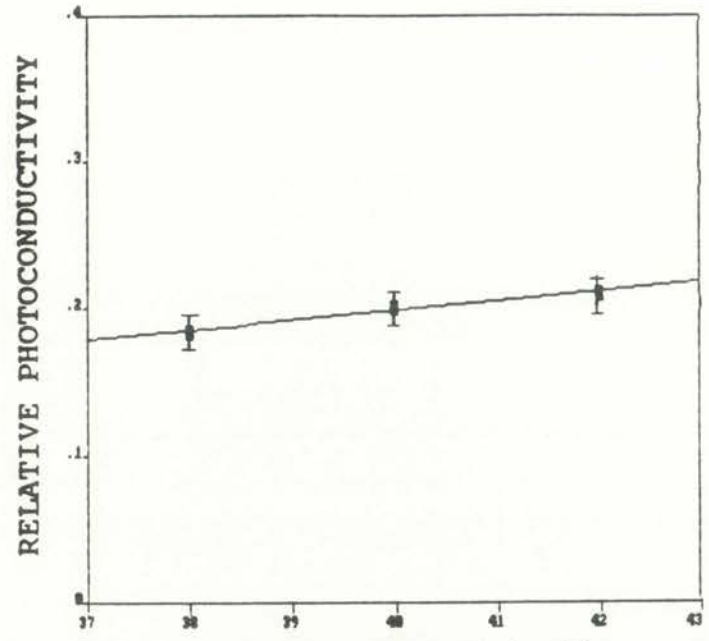

FIGURE IV-10a

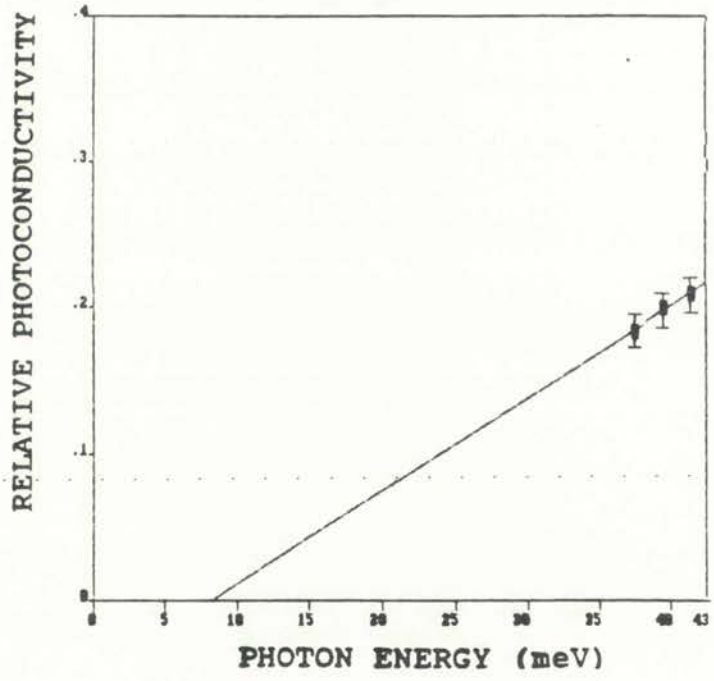

FIGURE IV-10b

Figure IV-10. a. A straight line fit determined by the method of least squares to the average values for the integral of the photoconductive response in Figure IV-9 across three equidistant areas (**37-39**, **39-41**, and **41-43** *meV*).
b. Extrapolation of Figure IV-10a to determine x-axis intersection.

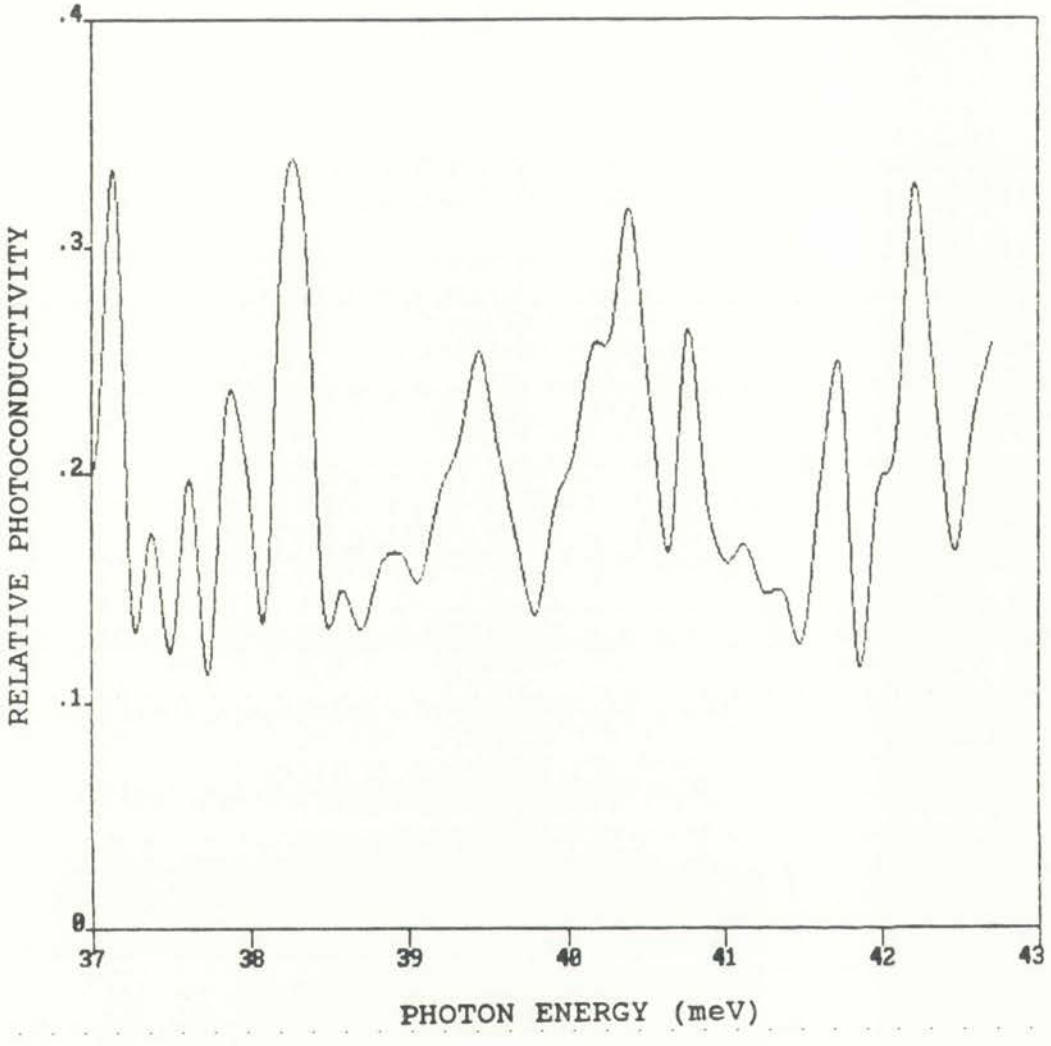

Figure IV-11. **Si:As detector relative photoconductivity response with both IR and white light illumination. White light intensity = high (curve 3, Figure I-4), Temperature = 7 K, Bias = 105 V/cm.**

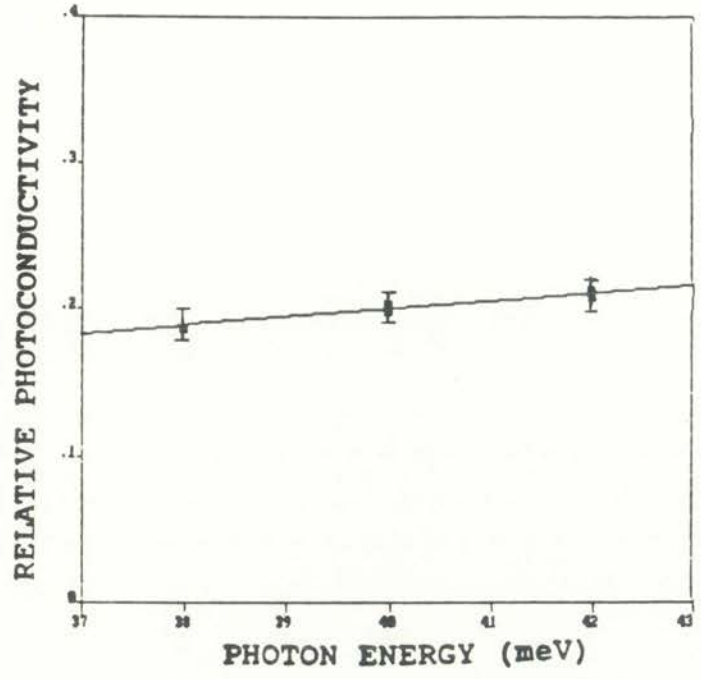

FIGURE IV-12a

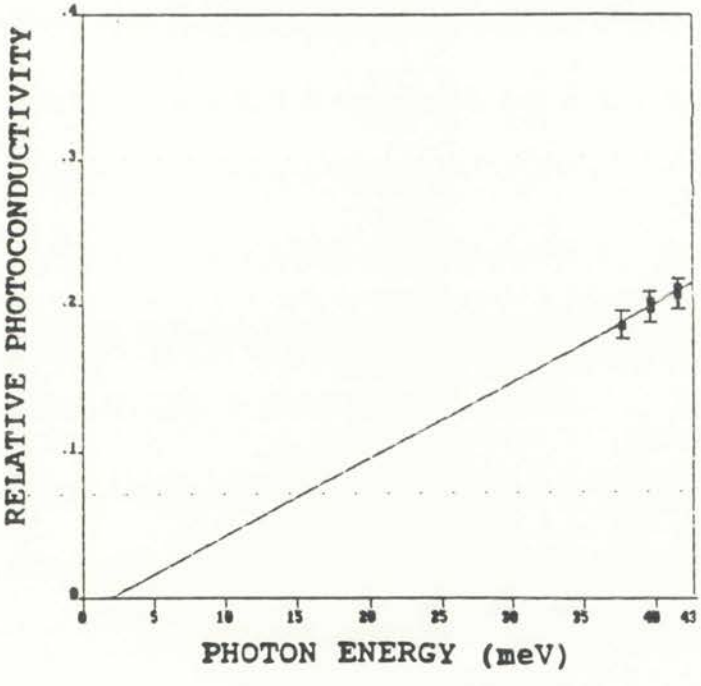

FIGURE IV-12b

Figure IV-12. a. A straight line fit determined by the method of least squares to the average values for the integral of the photoconductive response in Figure IV-11 across three equidistant areas (37-39, 39-41, and 41-43 *meV*).
b. Extrapolation of Figure IV-12a to determine x-axis intersection.

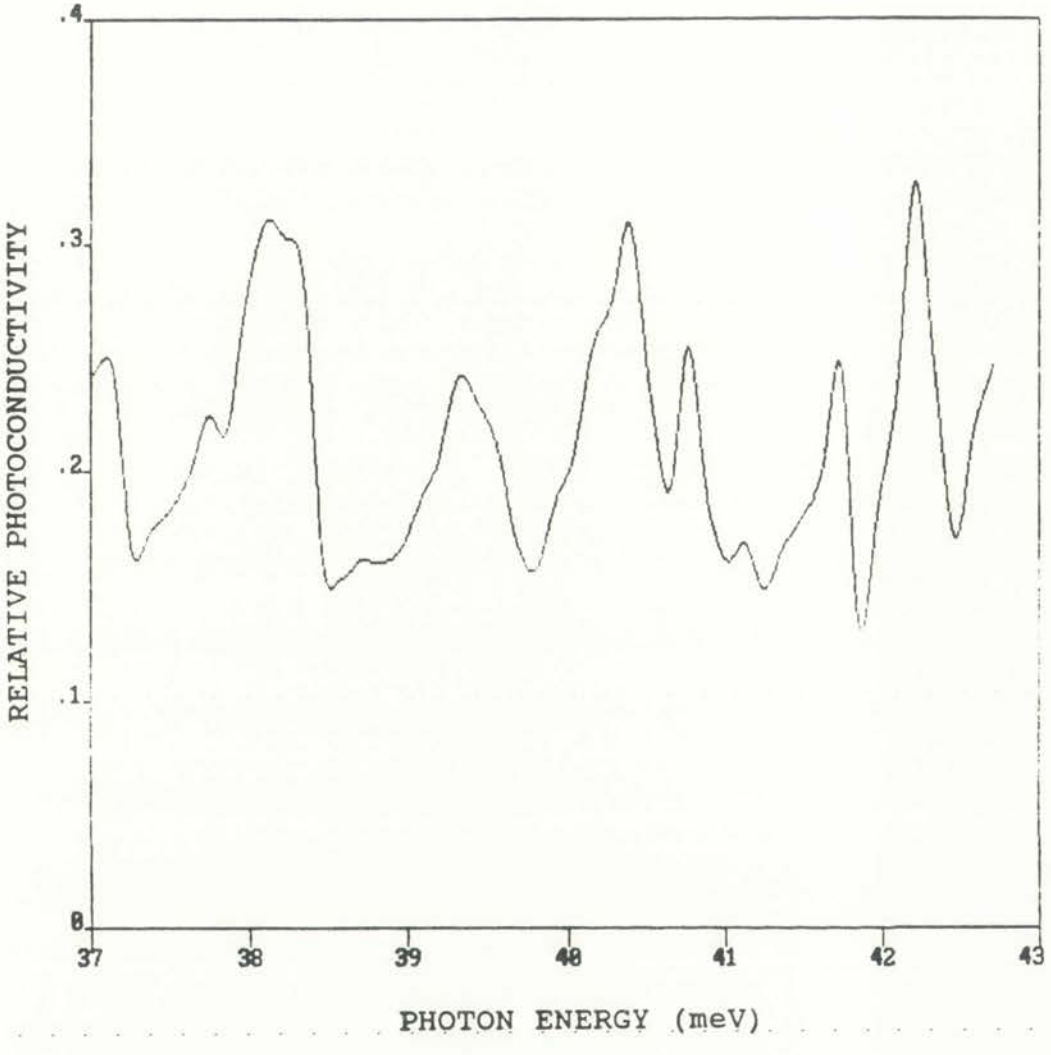

Figure IV-13. **Si:As detector relative photoconductivity response with both IR and white light illumination. White light intensity = maximum (above curve 3, Figure I-4, with sample temperature remaining constant). Temperature = 7 K, Bias = 105 V/cm.**

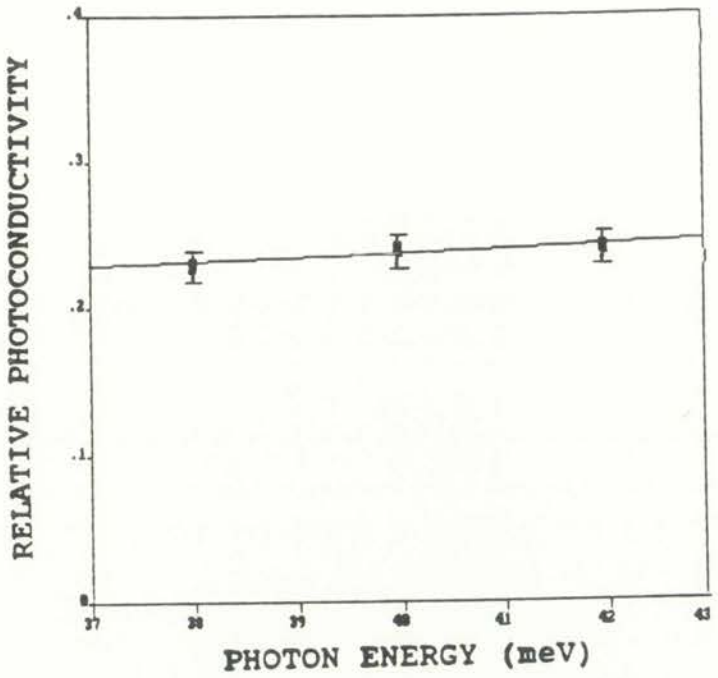

FIGURE IV-14a

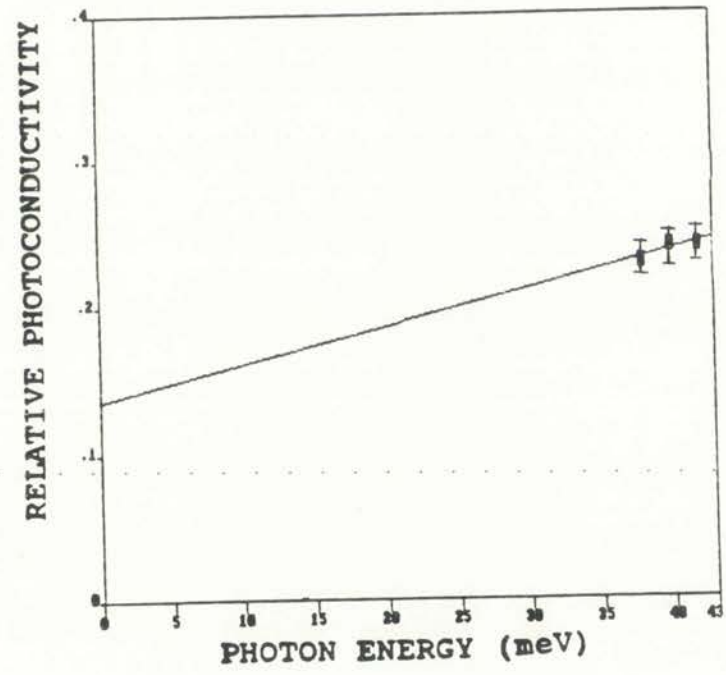

FIGURE IV-14b

Figure IV-14. a. A straight line fit determined by the method of least squares to the average values for the integral of the photoconductive response in Figure IV-13 across three equidistant areas (37-39, 39-41, and 41-43 *meV*).
b. Extrapolation of Figure IV-14a to determine x-axis intersection.

3 $\mu W/cm^2$ (the level defined by curve 2 in Figure I-4) generated more electron-hole pairs within the silicon material. The resulting photoconductive response is shown in Figure IV-9. The spectral response becomes very structured with a distinct narrowing and increased magnitude of the photoconductive lines. This behavior was seen by others[47–49] and was expected to occur when white light intensity was sufficient to generate enough electron-hole pairs to neutralize the shallow ionized impurities. This neutralization of the ionized impurities was the mechanism responsible for narrowing the observed lines.[47]

For the most intense white light illumination of 6 $\mu W/cm^2$, defined by curve 3 in Figure I-4, the resulting photoconductive response is illustrated in Figure IV-11. This response is characterized by photoconductive signals whose peaks approach a limiting signal magnitude across the entire region of interest. In addition, asymmetric broadening towards the low energy side is apparent for the peaks situated near 37, 38, 39, and 40 meV. Additional measurements were performed in order to investigate relative photoconductive changes for white light intensities above the levels of Figure IV-11 while insuring that no sample temperature changes occurred. Figure IV-13 illustrates the fact that additional electron-hole pair generation failed to increase the photoconductive signals above the previously established limit. However, asymmetric broadening is quite evident in the photoconductive response curve. This supports the idea that only a finite number of carriers proportional to the neutral centers are available to contribute to the photoconductive response. Therefore, under band-gap excitation a certain number of electron-hole pairs will be involved in the neutralization of the ionized centers under extrinsic illumination. The remaining electron-hole pairs are involved in such processes as charge transfer and scattering resulting in an asymmetric broadening of the response curves. Further investigation into this phenomena is suggested as a future activity. A better un-

derstanding of this phenomena could provide well defined points for calibration purposes. These calibrated points could then be utilized for confirming infrared detector signals which occur during simultaneous exposure to ionizing radiation environments in space environments.

Comparing Figures IV-8 and IV-11 for photoconductive peaks which become valleys and vice-versa shows two definable occurrences around 41 and 42 meV. It is not understood why minority impurities give peaks of the opposite sign to those of majority impurities in both Si and Ge. Bykova[47] suggests that an increase in the rate of carrier recombination occurs when a minority impurity is ionized by infrared absorption and hence a negative photoconductivity peak is observed. He also suggested that a potential contributing mechanism was the neutralization of charged impurities which results in a significant decrease in ionized impurity scattering. The mobility would then be very sensitive to ionization of the impurities by the photoconductive process which in turn would reduce mobility and hence decrease the photoconductive signal. However, the competition between recombination and mobility effects may be very complex and could give rise to a number of possible mechanisms that lead to differing signs of the signal for majority and minority impurities. In other studies with ultra-pure germanium, band-gap light created a substantial population of neutral minority centers. It was speculated that these centers then generated free minority carriers when they absorbed a photon and a phonon of appropriate energies thus producing a change in the conductivity of the sample.[45] However, the fact that these explanations are incomplete is indicated by the results of other experiments with silicon which have shown spectra containing only positive lines.[45]

The most readily observable features in the spectral photoconductivity data of

Figures IV-7 to IV-13 are the increased peaks at the lower energy levels and the asymmetric broadening. This broadening of the lower edges of the sharp lines arising from isolated neutral impurity centers has been observed for the spectra of both donors and acceptors in Si, Ge, GaAs, and GeSb by a number of researchers.[46–57] The observed broadening has been attributed to a variety of effects; Stark broadening, donor-acceptor pairs, van der Waals forces, and Breit-Wigner-Fano resonant interference between localized states and a continuum.

IV-3 H^--Like Centers

In the above it was suggested that an explanation for the observed anomalous structural changes such as narrowing, asymmetric broadening, reversal and/or disappearance of photoconductive signals could be the result of an extra electron (hole) which is captured by a neutral group-V (group-III) impurity. A model for this center can utilize the results obtained in atomic physics by Bethe and Salpeter,[60] for the H^--like center which forms when a neutral hydrogen atom captures another electron of opposite spin. As a result of the repulsive potential created by the first electron, the binding energy of the second electron turns out to be small compared to the hydrogen ionization energy. These shallow impurities are designated as D^o (group-V) and A^o (group-III) for their "neutral" or un-ionized state. The capture of an extra electron by a neutral donor D^o results in the formation of a D^- center, whereas the capture of an extra hole by an acceptor A^o results in an A^+ center. The ionized state for a D^o center is D^+ and for an A^o center is A^-. The presence of D^- or A^+ centers, as suggested in the above, will be shown to dramatically influence various phenomena such as impurity conduction, scattering, and recombination of free carriers at low temperatures ($kT < E_i$). Indeed a better understanding of the effects associated with H^--like centers as a function of neutral and charged impurity concentration could provide the insight required for understanding problems

associated with semiconductor materials in an ionizing radiation environment, such as space.

The most likely explanation for the occurrence of spectral broadening in our experimental data of Figures IV-7 to IV-13 is that the broadening and the shifting of peaks occurs via charge transfer states (D^-, D^+)[58,59] below the isolated donor (acceptor) excitation energies. The stability of the charge-transfer state relies heavily on the Coulomb attraction between the D^+ and the D^- centers. These charge transfer states could properly be described as excitons[59] in the Mott Hubbard gap between the D^- and D^+ single particle energy bands which are enhanced by band-gap illumination. This donor (acceptor)-pair picture has been shown to work well for transitions to the lowest excited states for densities below $1{\cdot}10^{17} cm^{-3}$ in doped silicon.[56,59]

For D^-, D^+, A^+, A^- and neutral impurity centers to measurably affect either photoconductivity or absorption measurements, appreciable wavefunction overlap is required for effective charge migration through the lattice to occur. Absorption studies[55] on silicon samples doped with $2{\cdot}10^{16} cm^{-3}$ phosphorus atoms at 6 K show a growth in relative strength of the $1s(A_1)$-$3p_o$ line with increasing donor concentration. An increase in the transition probability for this spectral line is associated with formation of molecular orbitals resulting from wavefunction overlap. Norton[61] has calculated that the radius of a wavefunction, as estimated from the effective mass approximation, is $2{\cdot}10^{-6}$ cm, for a binding energy of 3 meV. Thus, the concentration at which banding of D^- states can occur is on the order of $6{\cdot}10^{13} cm^{-3}$ for doped silicon.

In the above, it was suggested that asymmetric broadening was associated with charge-state transfer among H^--like centers. Therefore, conditions which enhance

charge transfer between D^-, D^+, A^+, A^- and neutral impurity centers should exhibit a relative increase in the $1s(A_1)$-$3p_o$ peak as previously observed from Figure IV-5 for extrinsic illumination only where no distinct peak centered around at 38.3 meV (the $1s(A_1)$-$3p_o$ transition) could be seen. However, in Figure IV-11 when band-gap illumination is added a significant peak appears at 38.3 meV. Thus, direct evidence is provided which demonstrates the existence of coupling mechanisms between the conduction-band and impurity-band conductivity processes which requires the presence of H^--like centers.

Experimental proof that D^- states are involved with the photoconductivity process during band-gap illumination could be determined by extrapolating the photoconductivity response into the energy regime of 1-10 meV as predicted by Norton.[61] In order to perform a linear extrapolation of the data, the photoconductive response was first integrated across the experimental energy region from 37 to 43 meV. The average value and the associated error bar for each of three regions (37-39, 39-41, and 41-43 meV) were then plotted and a line was fitted to the plotted values. However, depending on the fit of the line, substantial variations could occur in the extrapolated regions. Therefore, a nonsubjective method for fitting straight lines which reflected some desirable statistical properties was required. The statistical method of least squares was utilized for yielding the linear equation of the line which best fit the data. This line was next plotted and extrapolated until x-axis intersection occurred. This approach of averaging equidistant areas and plotting the values to insure linearity is "self-verifying". If we attempted a straight line fit to all data taken, a single valley or peak could dramatically influence the slope of the line. However, by first averaging the data in each of these equidistant regions, the fact that each value can then be shown to lie on a straight line insures that no one region was responsible for determining the slope of the line. Therefore, this

serves as a "self-verification" that the straight line utilized in the extrapolation was an accurate representation of the experimental data throughout each of the three regions.

The area under the extrapolated curve was indicative of the ionization energies which contributed to the photoconductive signal. One would expect to see areas under the extrapolated photoconductive response between 1 and 10 meV according to Norton.[61] Figures IV-6(a,b), IV-8(a,b), IV-10(a,b), IV-12(a,b) and IV-14(a,b) graphically illustrate this procedure for the Si:As material. The uppermost curve is the average photoconductive response over the energy regime investigated (37-43 meV). The bottom curve in each figure is the extrapolated curve towards lower energies.

Examination of the straight lines reveals progressively decreasing slopes as the intensity of the white light was increased. Figure IV-5 is the photoconductive response with only extrinsic illumination. Figure IV-6(a,b) verifies that only shallow impurities with ionization energies greater than 30 meV contribute to the signal response of Figure IV-5. Figures IV-7, IV-9 and IV-11 are the photoconductive response with both extrinsic illumination and supplementary white light illumination progressively increasing in intensity. The photoconductive response becomes more structured with observable photoconductive peaks arising throughout the experimental energy regime. Correspondingly the linear extrapolations for the average values of the response curves in Figures IV-8b, IV-10b, IV-12b and IV-14b indicate increased contributions from carriers with energies below 15 meV.

The curves discussed above demonstrate significant changes in the photoconductivity spectra resulting from simultaneous extrinsic and white light illumination can be attributed to participation of carriers from energy levels of the same magnitude

associated with $D^-(A^+)$ centers. One curve, Figure IV-14b intersects the x-axis in the negative region, unlike the others. The most probable explanation is that $\pm 10\%$ uncertainty in the data for the 37-43 meV region would be significantly magnified upon extrapolation to the lower energies. However, if this data was not in error, one likely explanation is the theory of Anderson negative-U systems which accounts for structural distortions of negative energy within the lattice.[70]

IV-4 Additional Spectral Experimental Data

In order to verify these results for other impurities, we performed the same experiments on silicon detectors doped with bismuth at a concentration of $4 \cdot 10^{16} cm^{-3}$ and containing compensating impurities, mainly boron, at a concentration of $6 \cdot 10^{13} cm^{-3}$. For these experiments measurements were performed both at 8 K ($kT < E_i$) and at 16 K ($kT > E_i$) where thermal ionization becomes a factor. For the higher temperature ($kT > E_i$) at 16 K the concentration of H^--like centers is small due to thermal remission. Therefore, these conditions allows us to determine the impact of thermally induced transitions on the spectral changes.

Figure IV-15 shows the photoconductivity spectrum we measured for the Si:Bi detector at 16 K without white light illumination. Figure IV-17 shows the spectral response with additional white light illumination with intensity corresponding to curve 3 of Figure I-4. Relatively little change occurs besides an increase in the peak at 41 meV. However, cooling the detector to 8 K and repeating these measurements yielded the results in Figures IV-19 and IV-21. For these conditions ($kT < E_i$) significant concentrations of H^--like centers can exist for participation in charge transfer phenomena. Figure IV-19 shows an increased response around 39 meV without additional white light. With additional white light illumination, significant increases in the peak at 41 and 38 meV can be seen in Figure IV-21. The 38.3 meV

peak is the $1s(A_1)$-$3p_o$ transition. This transition was previously used to verify wavefunction overlap sufficient for impurity-band conduction processes to occur.[55] Our results thus provided additional proof for the existence of mechanisms requiring the presence of H^--like centers to effectively couple energy between the conduction band and impurity bands. Figures IV-16b, 18b, 20b and 22b, show the average photoconductive response for our data extrapolated towards lower energies. The only curve which indicated participation of 1-10 meV carriers was our data plotted in Figure IV-22b, for Si:Bi at 8 K under extrinsic and white light illumination. This agrees with the previous results for Si:As.

The above results should also hold true for p-type material and intrinsic radiation in general. Therefore, measurements were performed on Si:Al material to examine these issues and the results are shown in Figures IV-23 to IV-27. The Si:Al detectors were at 7 K (below thermal ionization threshold) and biased at 100 V/cm. Figure IV-23 is the photoconductive response with only extrinsic radiation. Figure IV-25 is the photoconductive response when white light is added. The photoconductive response associated with lower energy levels increased in magnitude as the Si:As and Si:Bi samples had. In addition, the response magnitude was found to reach a limiting signal magnitude with additional white light intensity.

In order to investigate long-lived increases in photoconductivity, we exposed the Si:Al material to ^{60}Co irradiation. This source of radiation can create displacement defects in silicon in addition to creating electron hole pairs analogous to white light exposure. Our Si:Al detectors were exposed to a 100,000 rad total dose over a 120 min period, while at 7 K. Photoconductive measurements were then performed 30 min after irradiation without additional white light exposure. Our results are plotted in Figure IV-27 which shows an increased photoconductive response whose

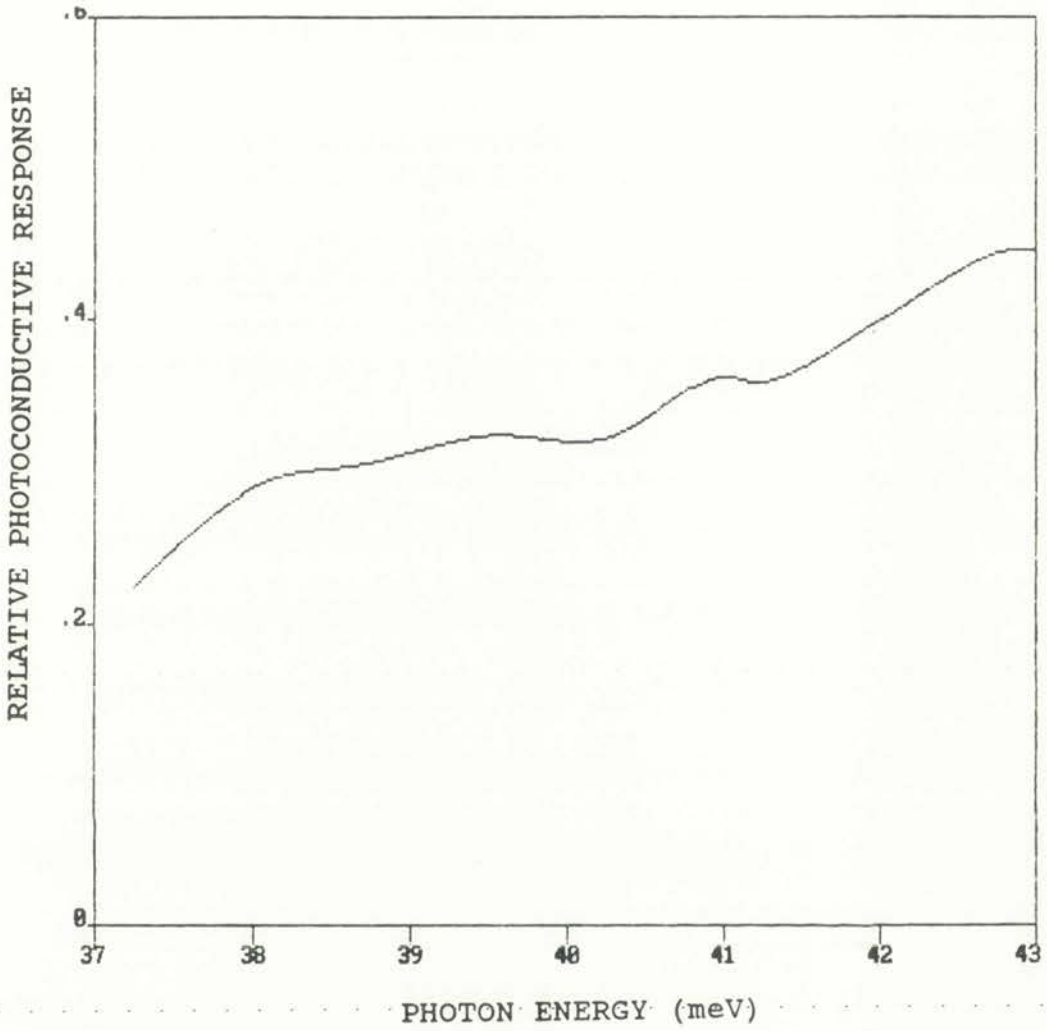

Figure IV-15. **Si:Bi detector relative photoconductivity response with only IR illumination. Temperature = 16 K, Bias = 100 V/cm.**

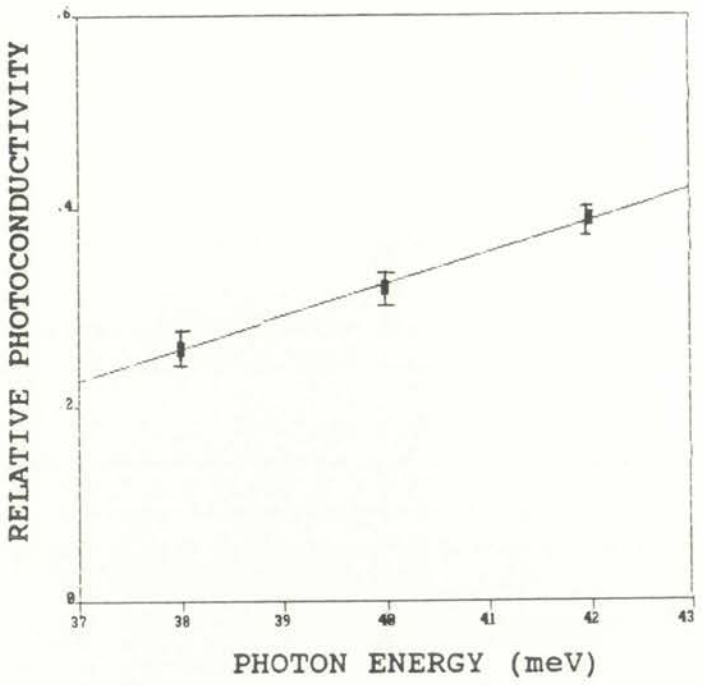

FIGURE IV-16a

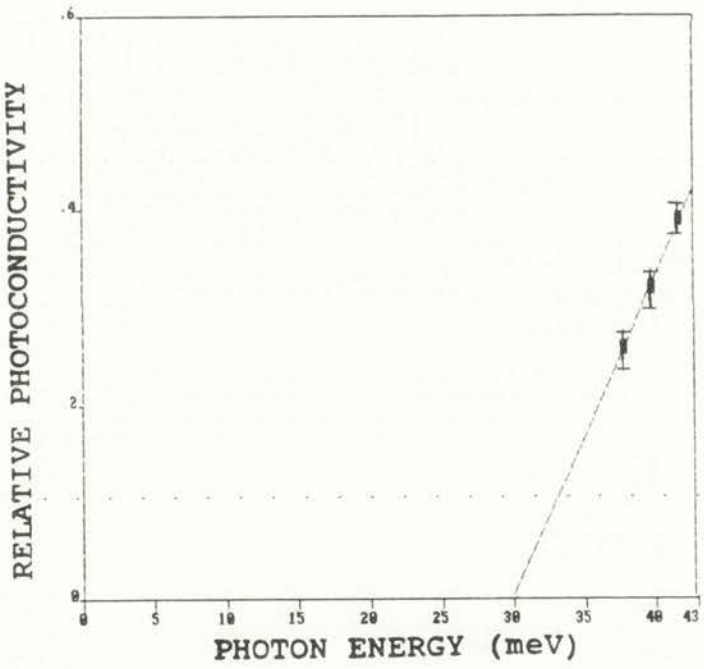

FIGURE IV-16b

Figure IV-16. **a. A straight line fit determined by the method of least squares to the average values for the integral of the photoconductive response in Figure IV-15 across three equidistant areas (37-39, 39-41, and 41-43 *meV*).**
b. Extrapolation of Figure IV-16a to determine x-axis intersection.

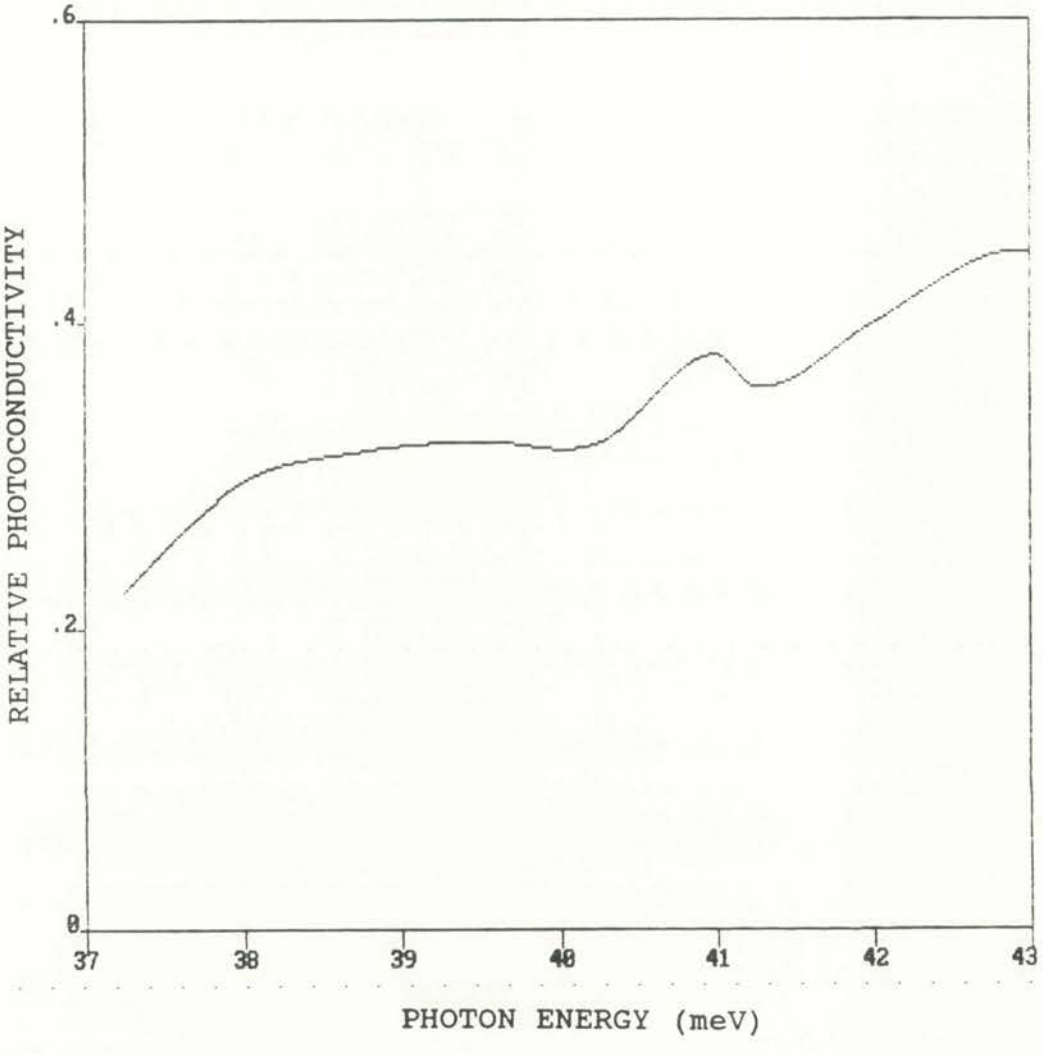

Figure IV-17. **Si:Bi detector relative photoconductivity response with IR and white light illumination. White light intensity = high (curve 3, Figure I-4), Temperature = 16 K, Bias = 100 V/cm.**

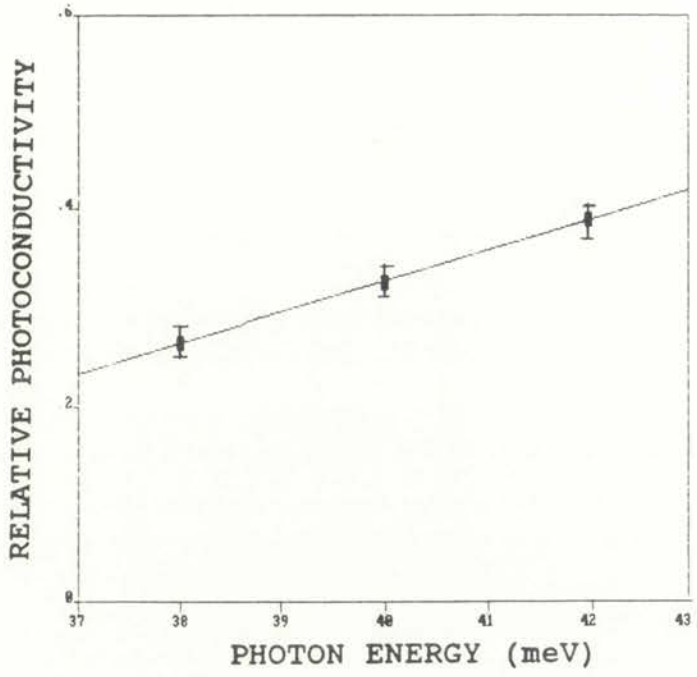

FIGURE IV-18a

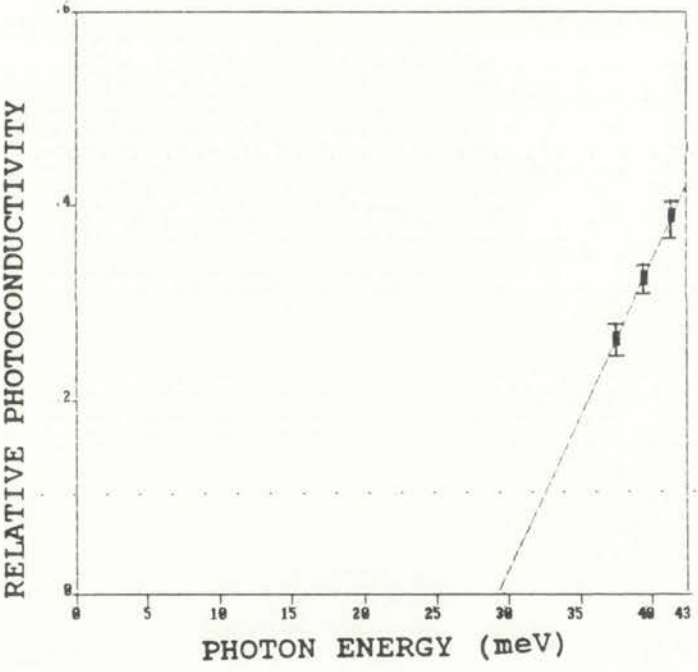

FIGURE IV-18b

Figure IV-18. a. **A straight line fit determined by the method of least squares to the average values for the integral of the photoconductive response in Figure IV-17 across three equidistant areas (37-39, 39-41, and 41-43** *meV*).
b. **Extrapolation of Figure IV-18a to determine x-axis intersection.**

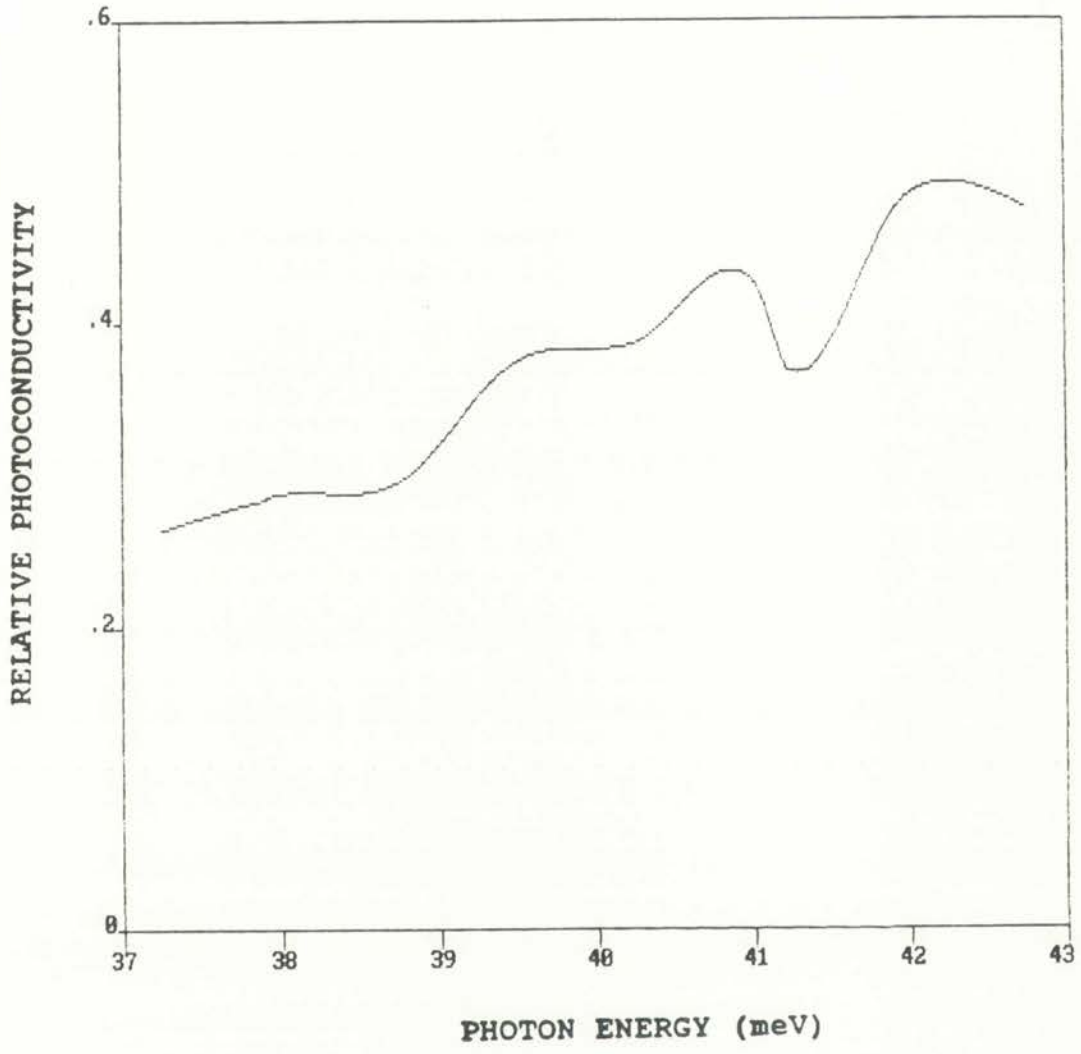

Figure IV-19. **Si:Bi detector relative photoconductivity response with only IR illumination. Temperature = 8 K, Bias = 100 V/cm.**

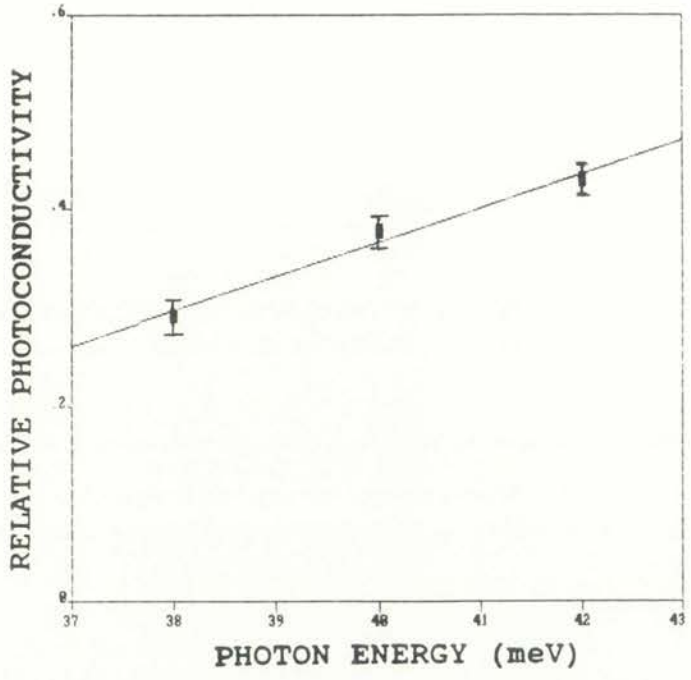

FIGURE IV-20a

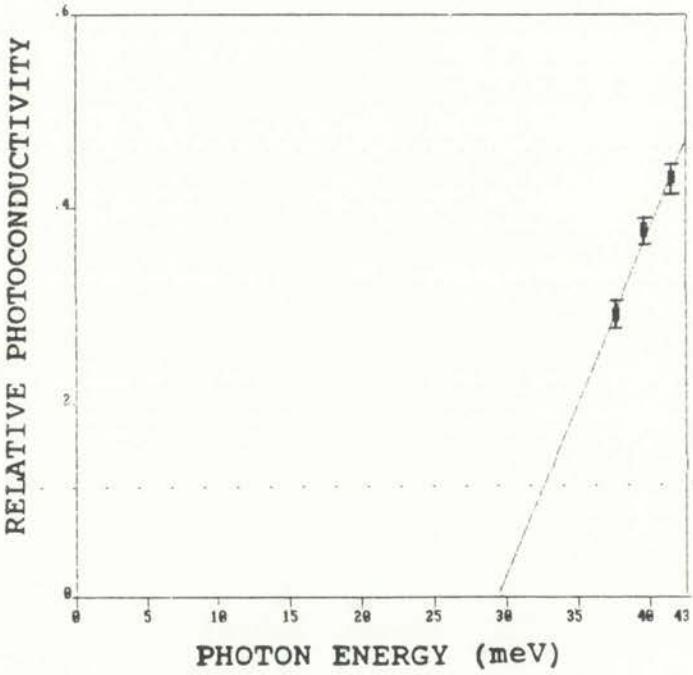

FIGURE IV-20b

Figure IV-20. a. A straight line fit determined by the method of least squares to the average values for the integral of the photoconductive response in Figure IV-19 across three equidistant areas (37-39, 39-41, and 41-43 *meV*).
b. Extrapolation of Figure IV-20a to determine x-axis intersection.

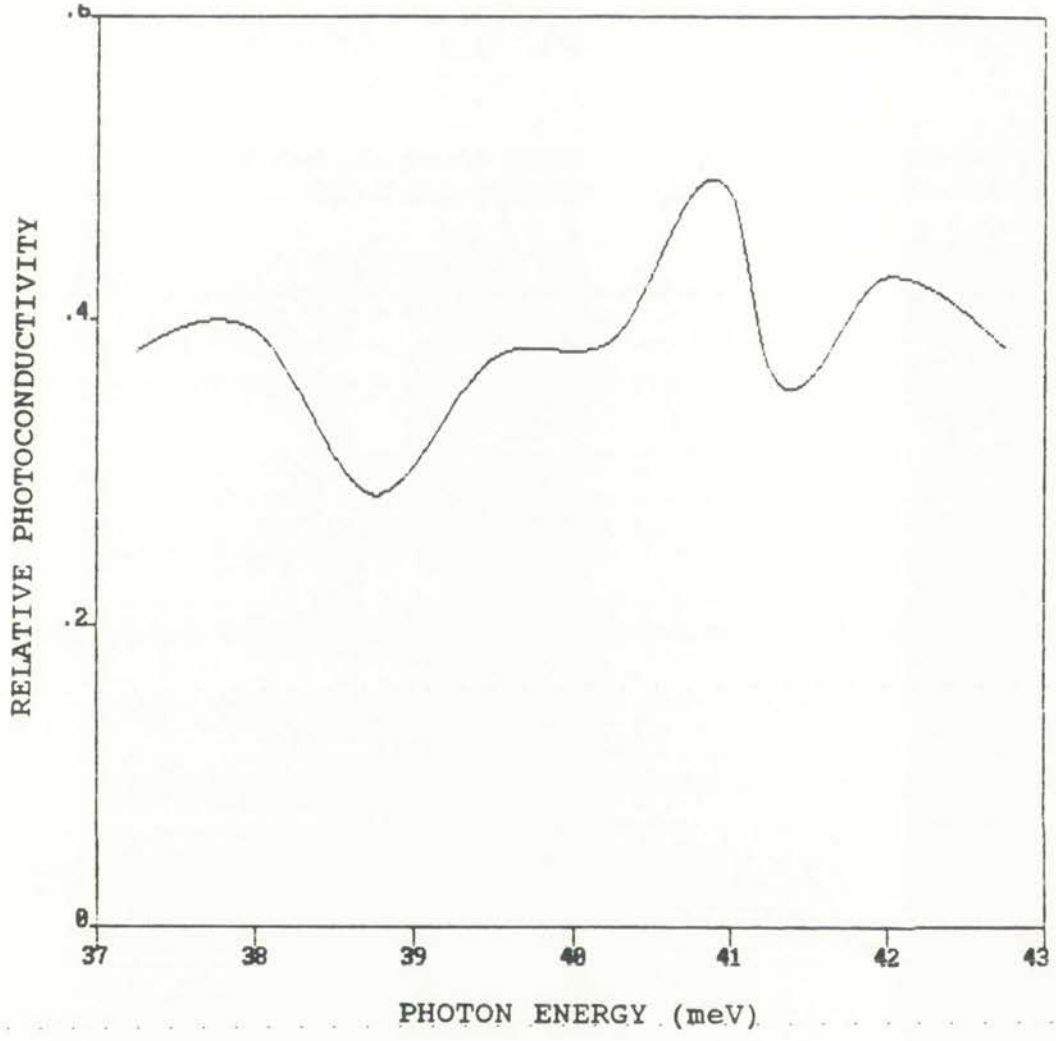

Figure IV-21. **Si:Bi detector relative photoconductivity response with both IR and white light illumination. White light intensity = high (curve 3, Figure I-4), Temperature = 8 K, Bias = 100 V/cm.**

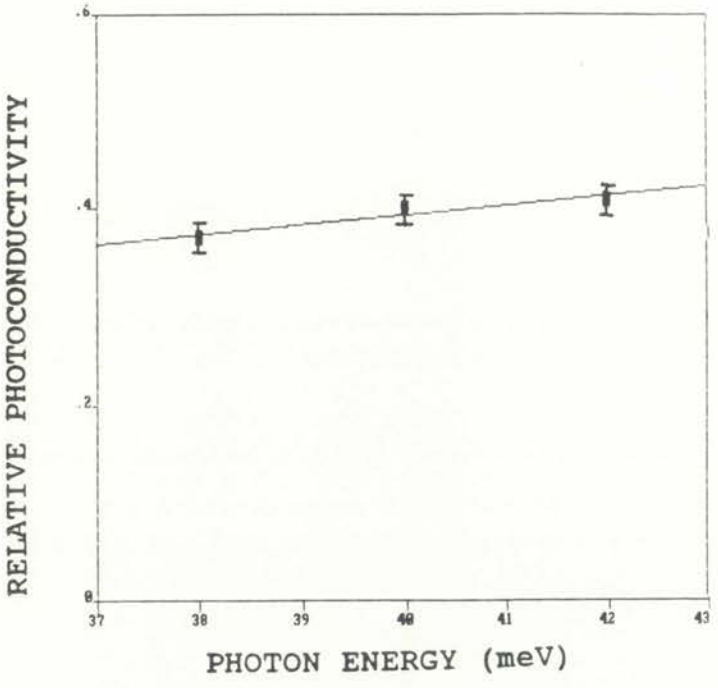

FIGURE IV-22a

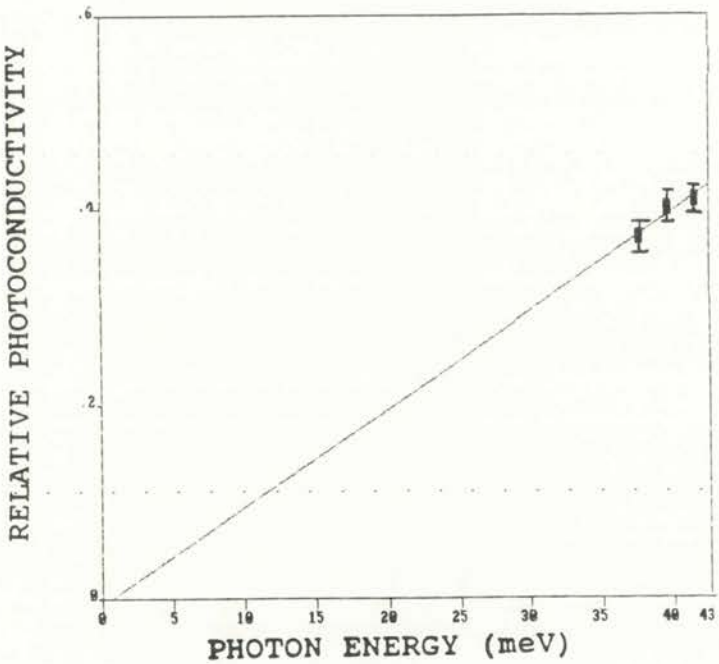

FIGURE IV-22b

Figure IV-22. a. **A straight line fit determined by the method of least squares to the average values for the integral of the photoconductive response in Figure IV-21 across three equidistant areas (37-39, 39-41, and 41-43** meV**).**
b. Extrapolation of Figure IV-22a to determine x-axis intersection.

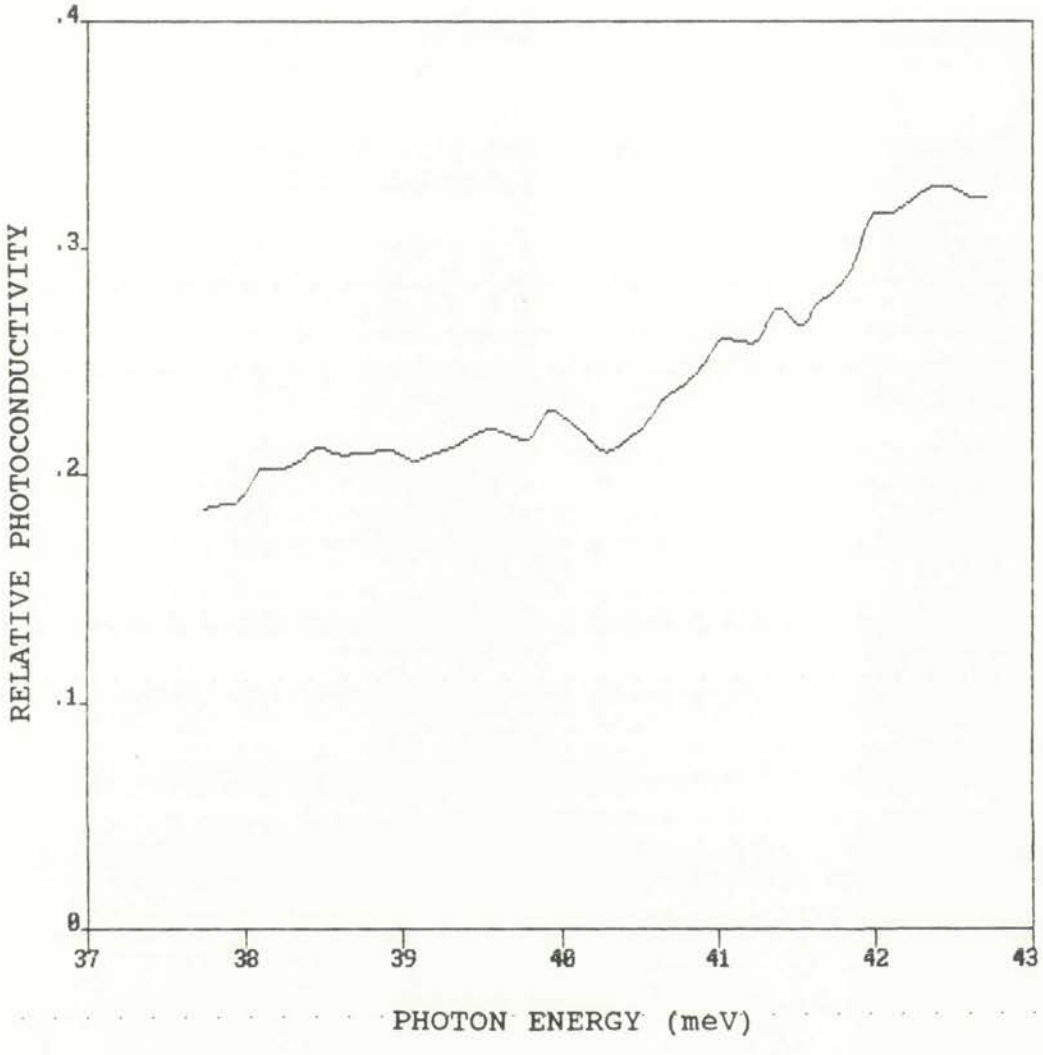

Figure IV-23. **Si:Al detector relative photoconductivity response with only IR illumination. Temperature = 7 K, Bias = 100 V/cm.**

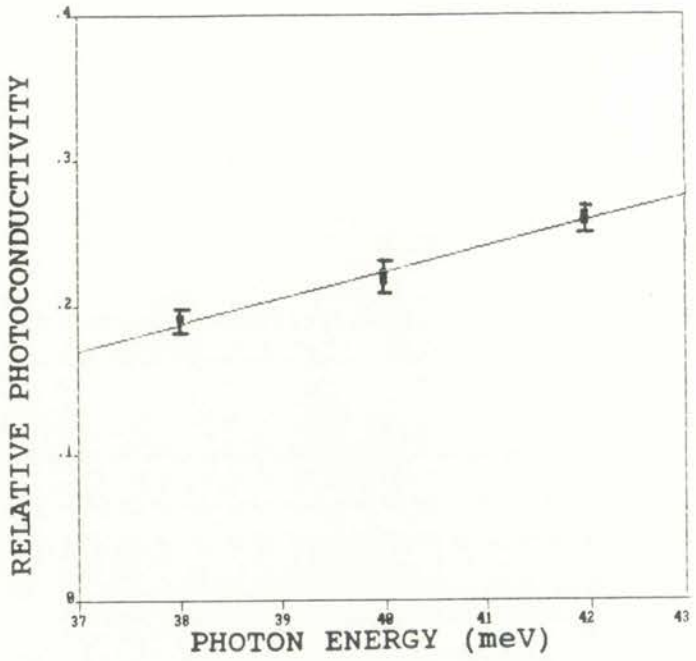

FIGURE IV-24a

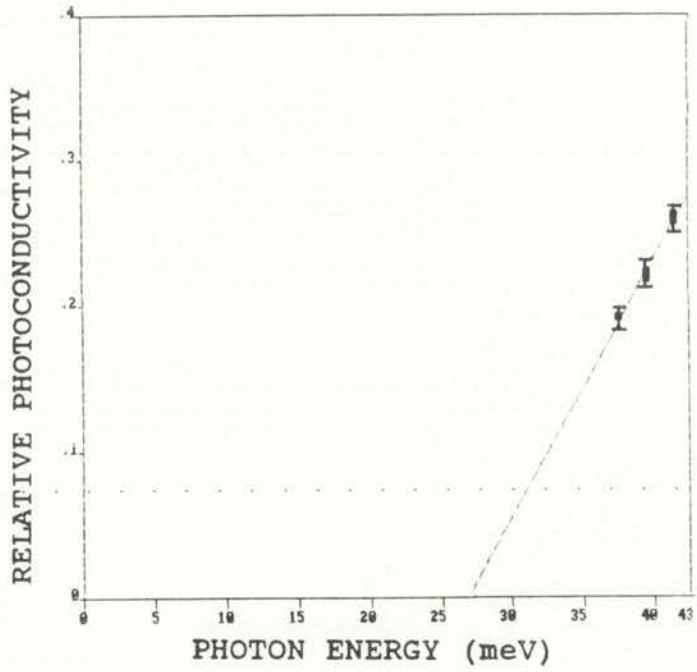

FIGURE IV-24b

Figure IV-24. a. **A straight line fit determined by the method of least squares to the average values for the integral of the photoconductive response in Figure IV-23 across three equidistant areas (37-39, 39-41, and 41-43 *meV*).**
b. Extrapolation of Figure IV-24a to determine x-axis intersection.

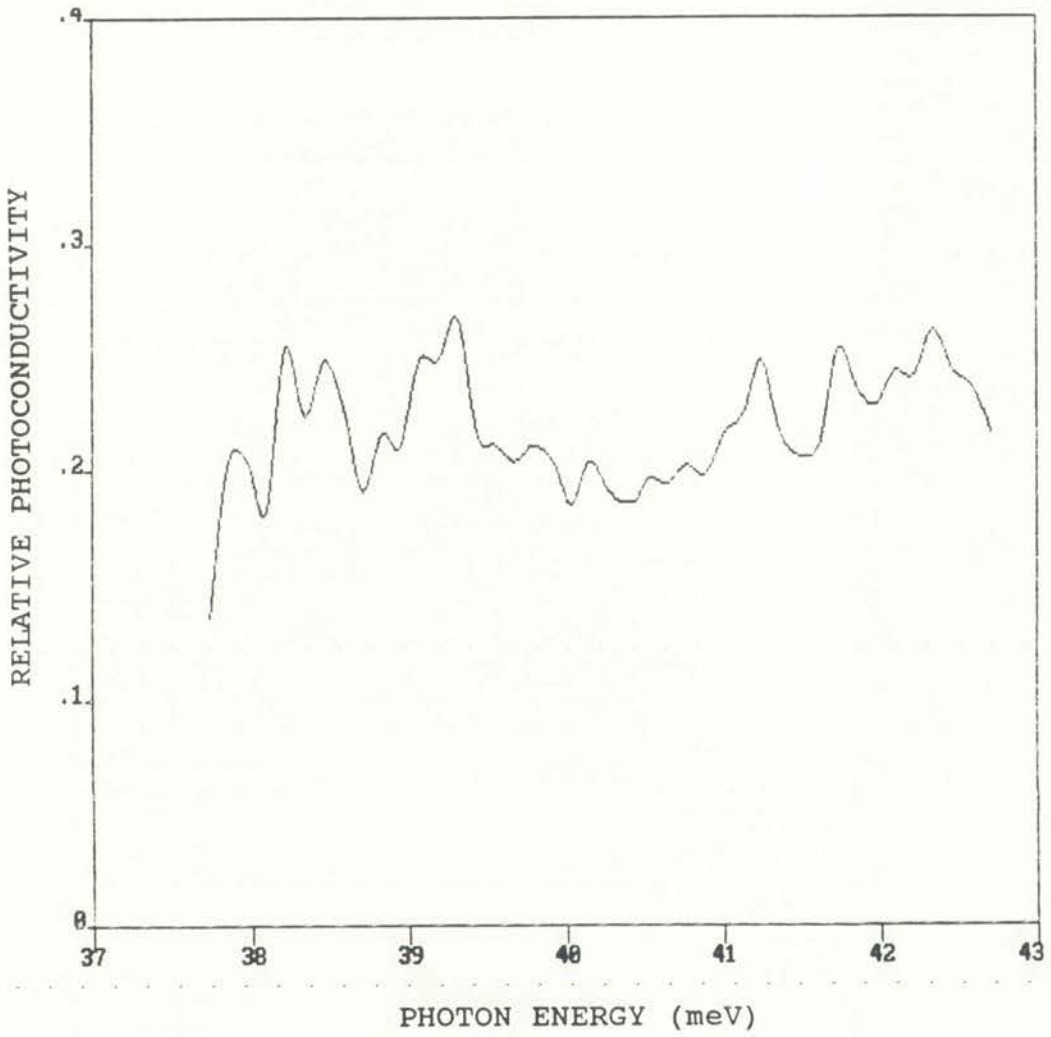

Figure IV-25. **Si:Al detector relative photoconductivity response with both IR and white light illumination. White light intensity = high (curve 3, Figure I-4), Temperature = 8 K, Bias = 100 V/cm.**

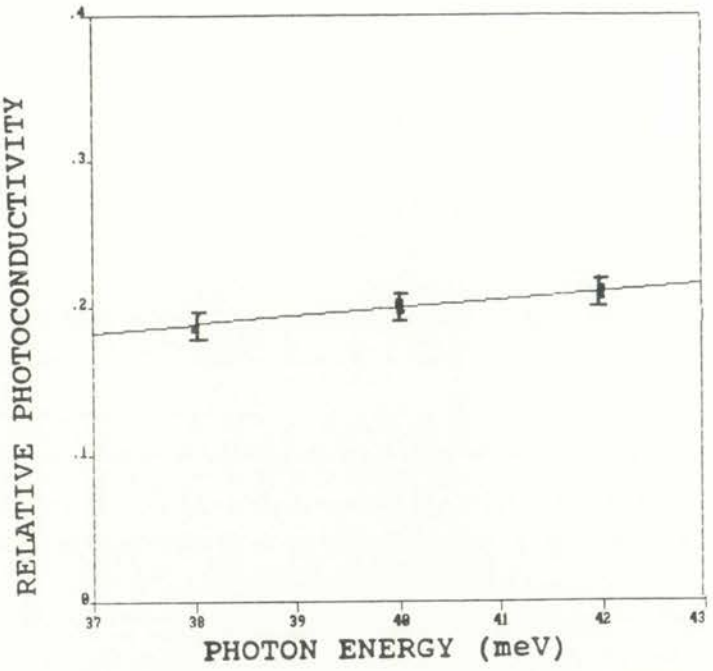

FIGURE IV-26a

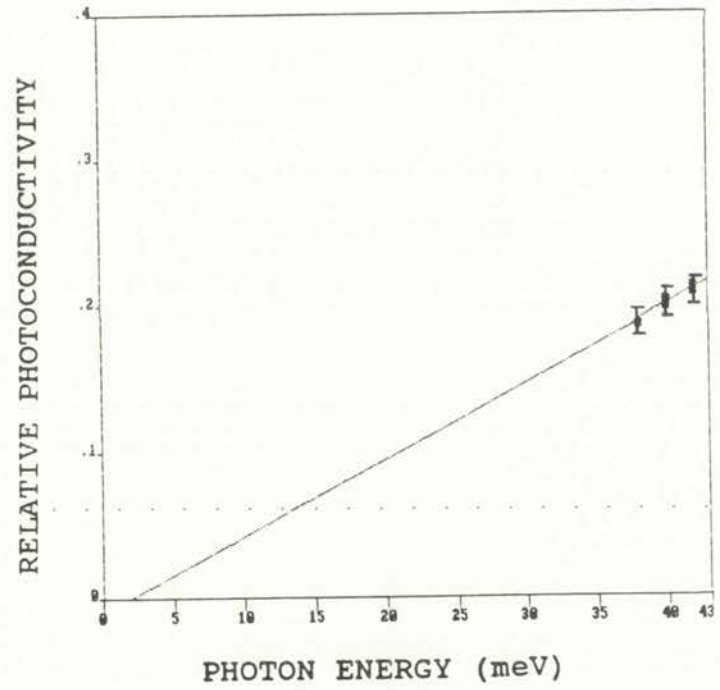

FIGURE IV-26b

Figure IV-26. **a. A straight line fit determined by the method of least squares to the average values for the integral of the photoconductive response in Figure IV-29 across three equidistant areas (37-39, 39-41, and 41-43 *meV*).**
b. Extrapolation of Figure IV-26a to determine x-axis intersection.

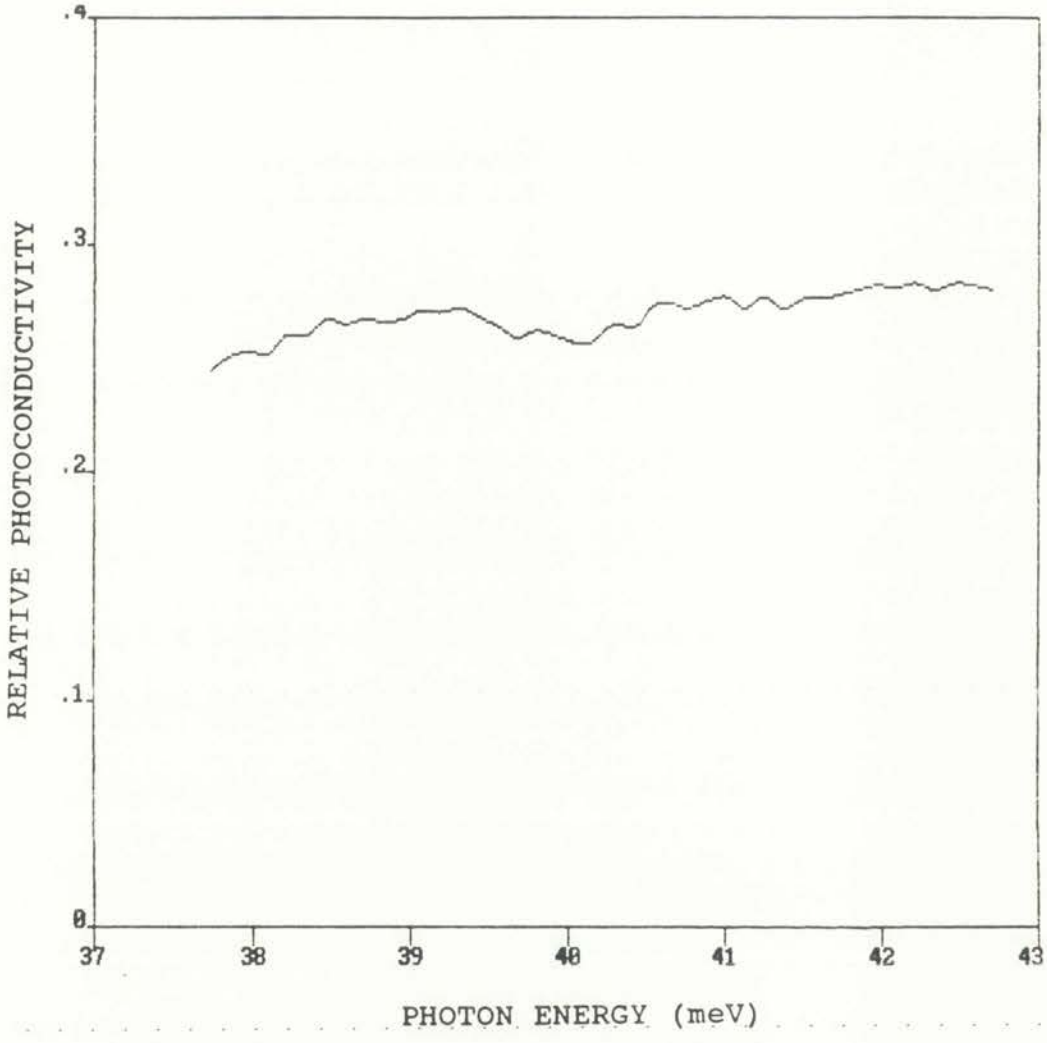

Figure IV-27. **Si:Al detector relative photoconductivity response with only IR illumination 30 min after exposure to 100 K rad ^{60}Co irradiation. Temperature = 8 K, Bias = 100 V/cm.**

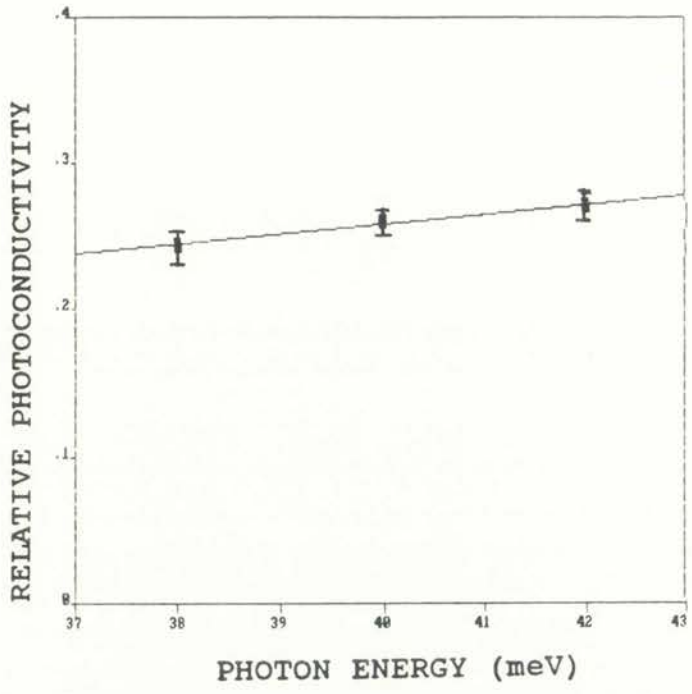

FIGURE IV-28a

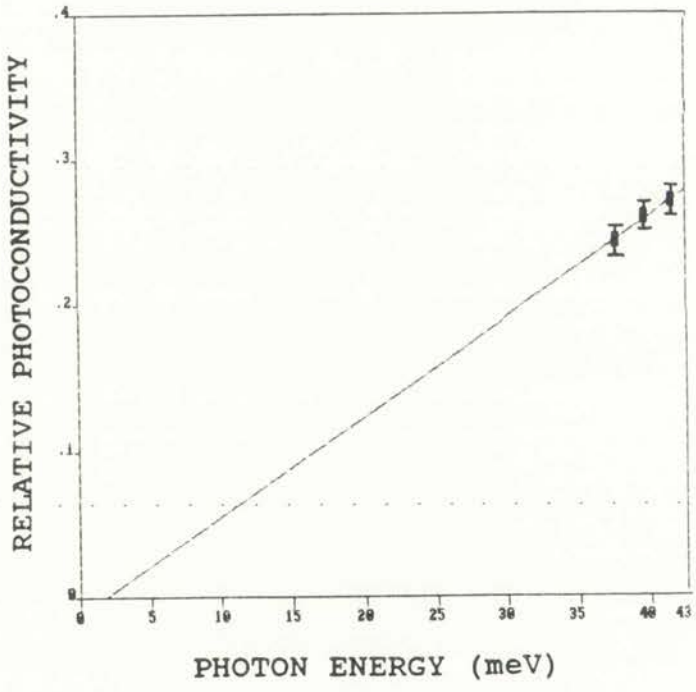

FIGURE IV-28b

Figure IV-28. a. **A straight line fit determined by the method of least squares to the average values for the integral of the photoconductive response in Figure IV-31 across three equidistant areas (37-39, 39-41, and 41-43** *meV*).

b. **Extrapolation of Figure IV-28a to determine x-axis intersection.**

magnitude approached the limiting values previously achieved under white light illumination in Figure IV-25. In addition, the average photoconductive response extrapolated towards lower energies for our data indicates that significant concentrations of long-lived carriers in the 1-10 meV energy regime resulting from the ^{60}Co irradiation can impact the photoconductivity response. However, additional measurements with white light were unable to be performed due to a dewar leak resulting in a loss of cryogen.

Qualitatively our results described above agree with previous findings in which only 10-rad dose levels resulted in enhanced responsivity.[71] The authors of the previous study ruled out responsivity changes due to displacement damage in the silicon detectors by energetic electrons resulting from the ^{60}Co radiation. These speculations were based on the predicted radiation-induced defects being several orders of magnitude less than the known shallow impurity concentrations. Therefore, it was suggested that the observed responsivity enhancement involved changes in the charge state of the impurities during irradiation.

Our results presented in the above indicate that extra electron (hole) localization in a system of neutral and charged centers in semiconductors could manifest itself via photoconductivity changes in both magnitude and temporal behavior. These extra electrons (holes) have the potential to occur in several forms: isolated H^- (A^+) centers and impurity molecular complexes of type H^--H^+ (A^+-A^-) or possibly H_2^-(A_2^-).[63]

The core separations of the complexes are governed by the neutral impurity concentration N^o. Therefore, an increase of N^o leads to an increase of the fraction of the various other complexes which could form via hopping mechanisms. The range of binding energies of the extra electron lies inside the Hubbard gap and

extends from 0.05 to 0.5 E_o, where E_o is the ionization energy for a shallow neutral impurity.[63]

IV-5 Discussion of Spectral Experimental Data

The experimental data presented in the above demonstrated that simultaneously illuminating doped silicon detectors with band-gap and extrinsic radiation significantly affected the impurity-band conductivity. The data further suggested that coupling mechanisms between the conduction-band and impurity-band processes involved H^--like centers. In the following, an analysis of the probability that band-gap illumination could effectively couple with shallow neutral impurity centers will be performed. This analysis will illustrate the need for coupling mechanisms to exist if significant photoconductivity changes occur.

When an impurity is introduced into a semiconductor, the resulting potential can produce a variety of effects such as scattering and conductivity changes. If a potential associated with the impurity is sufficiently large it has the capability to bind one or more electrons in localized states. These states may contribute significantly to the scattering of carriers as discussed in Chapter III. In addition, a localized electron which inhabits an energy level in the forbidden gap characteristic of the impurity presents an ionization cross section to the photons characteristic of the impurity potential. Because the impurity potential also influences the cross section presented to electrons in the conduction band, the properties associated with photoionization and scattering cross sections are not independent of one another.[71] In the following, photoionization cross sections of extrinsic silicon for both band-gap and extrinsic illumination conditions will be derived.

Following the presentation by Ridley[71,72] a photoionization cross section for shal-

low impurities in silicon will be presented. The photoionization cross section σ_ν, as defined by Ridley is

$$\sigma_\nu = \frac{16\ \pi^2\ a_o^2 \alpha_o}{\eta_r} \left(\frac{R}{\hbar\nu}\right) \frac{|\hat{a}\ \cdot\ \vec{P}\ |^2}{2\ m} N(E_k)\ V \qquad \text{(IV-4)}$$

$$\vec{P} = \langle\ T|\vec{p}|C\rangle \qquad \text{(IV-5)}$$

where a_o is the Bohr radius, α_o the fine-structure constant, η_r the refractive index, R the Rydberg energy, $\hbar\nu$ the phonon energy, $\hat{a}$ the unit polarization vector, m the free-electron mass, $N(E_k)$ the number of conduction-band states per unit energy per unit volume, V the volume of the crystal, and P the momentum matrix element between the trap state T and conduction state C. This expression does not include a local-field correction, nor does it include the effect of phonon coupling. However, according to Ridley neither of these are important in the present context since the calculation is being limited to donor-like centers. Equation IV-5 now becomes

$$p = \frac{m}{m^*}\ h\ k\langle\ T|C\rangle \qquad \text{(IV-6)}$$

where m^* is the effective mass. Therefore, the photoionization cross section as defined by Equation IV-4 can be rewritten as

$$\sigma_\nu = \frac{16\ \pi^2\ a_o^2 \alpha_o}{3\ \eta_r} \left(\frac{R}{\hbar\nu}\right) \frac{m}{m^*}\ E_k\ N(E_k)\ V\ \ |\langle\ T|C\rangle\ |^2 \qquad \text{(IV-7)}$$

or

$$\sigma_\nu = \sigma_o\ G(\hbar\nu) \qquad \text{(IV-8)}$$

where

$$\sigma_o = \frac{16\ \pi^2\ a_o^2 \alpha_o}{3\ \eta_r}\ \frac{m}{m^*} \tag{IV-9}$$

and

$$G(\hbar\nu) = \left(\frac{R}{\hbar\nu}\right) E_k\ N(E_k)\ V\ \ |\langle\ T|C\rangle\ |^2 \tag{IV-10}$$

Figure IV-29b, plots Equation IV-7 for the photoionization cross-section of a hydrogenic donor. Utilizing Ridley's plot in Figure IV-29a shows that the photon must have 1.5 to 2 times the donor ionization energy to have a high probability of ionization. One can next determine the photoionization cross-section from Figure IV-29b to be $1{\cdot}10^{-20} cm^2$.

By calculating the photoionization cross-section for intrinsic silicon one can compare the effect on photoconductivity from band-gap excitation compared to the contribution from excitation of shallow impurities. In the following the photoionization cross section calculation for band-to-band excitation will be presented in a manner which numerically agrees with first-principles derivations[71,72] but is conceptually simpler.

Assume an intrinsic silicon sample which is illuminated with white light with an illuminated area of 1 cm^2 and a thickness of $5{\cdot}10^{-5} cm$. Silicon has $5.2 \cdot 10^{22} atoms/cm^3$. Extrapolating a $1/e$ absorption depth from Figure IV-30 of $2{\cdot}10^{-4} cm^{-1}$, implies that $2.6{\cdot}10^{18}$ silicon atoms are affected. Since each of the four valence electrons have the same probability for photoionization, this implies that altogether $1.04{\cdot}10^{19}$ electrons could potentially be ionized. Therefore, the photoionization cross section for band-to-band excitation at 500 nm is

Figure IV-29a

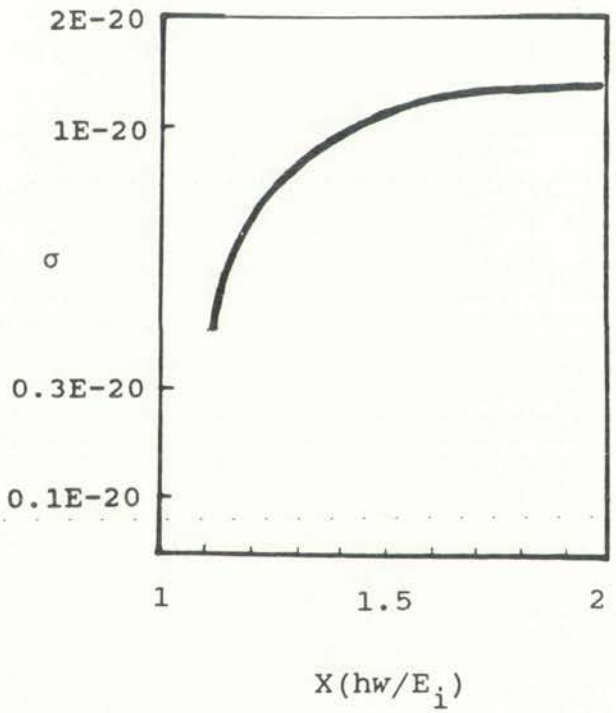

Figure IV-29b

Figure IV-29. a. Photoionization of a shallow hydrogenic center.
b. Photoionization cross section (σ) for the shallow hydrogenic center in Figure IV-29a with an activation energy (E_i) for ionization.

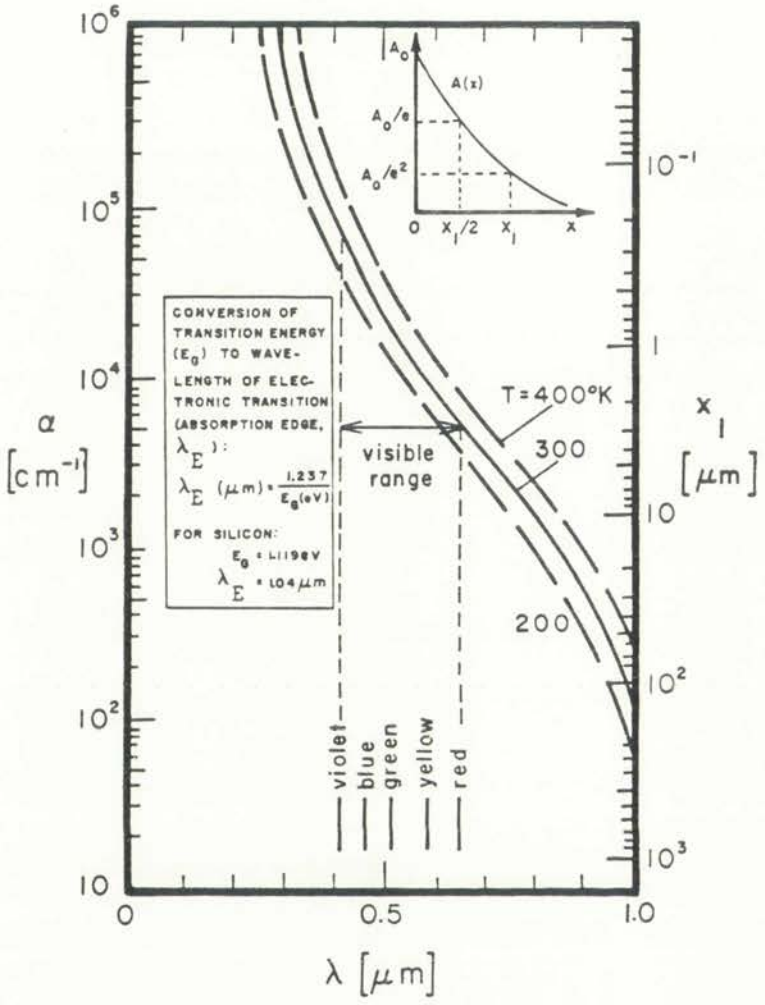

Figure IV-30. **The absorption coefficient (α) and penetration depth (x_1) versus wavelength (λ) for silicon.**

$$\sigma_{bb} = (4 \cdot 2.6 \cdot 10^{18})^{-1} = 9.6 \cdot 10^{-20}\ cm^2 \qquad \text{(IV-11)}$$

Utilizing the cross section calculations enables one to determine the relative importance of the shallow impurity-band carriers versus band-to-band excitations in their contribution to the photoconductive response. In the above, the photoionization cross-section was found to be $1{\cdot}10^{-20}cm^2$ for the impurity band versus $9.6{\cdot}10^{-20}cm^2$ for the band-to-band. Multiplying the impurity-band cross section by its $5{\cdot}10^{16}atoms/cm^3$ and the band-to-band cross section by $5{\cdot}10^{22}atoms/cm^3$ enables one to determine the relative contributions to photoconductivity process by white light. Therefore, only one electron from the impurity band versus $1{\cdot}10^7$ electrons from the silicon valance band will contribute to the photoconductivity signal as a result of white light illumination.

When one considers the dramatic enhancement of the photoconductive response from shallow impurities in the spectral experimental data it becomes obvious that energy coupling between the majority carriers and the impurity band occurs. In the following chapter, temporal photoconductive data will be used to investigate selected energy levels, their lifetimes, and increased photoconductive responses associated with these levels.

CHAPTER V

TEMPORAL EXPERIMENTAL DATA AND DISCUSSION

When electrons (holes) are injected into the conduction band (valence band) from neutral donors (acceptors) many will become trapped in nonequilibrium Hubbard band states as previously discussed. This trapped charge must be transferred to positively charged (negatively charged) donor (acceptor) sites in order to recombine. For N-type material there are at least two methods by which this transfer can occur: by excitation to the conduction band followed by transport to the recombination site, or by hopping within the upper Hubbard band to the recombination center. Because the activation energies are different for these two mechanisms one could potentially differentiate between the two processes. The resulting time constant for recombination should also vary in relation to the time it takes for the electrons to reach recombination centers. Therefore, one would expect that temporal photoconductive data could provide useful information.

In the following, our photoconductive data as a function of time will be presented for various conditions. The photoconductivity response of the materials we studied possessed a variety of transient effects. These transient effects will be discussed and equations for rise and fall times will be considered. Finally, photoconductivity effects we observed involving intrinsic and extrinsic illumination will be analyzed in terms of the developed model. This will provide the additional insight necessary for determining the existence and potential impact of energy coupling mechanisms between the conduction- and impurity-band carriers.

V-1 Transient Photoconductive Model

The literature on photoconductivity abounds with attempts to describe experimentally observed growth and decay of photoconductivity signals in terms of

simple monomolecular or bimolecular recombination processes.[1-3,73] In most cases, particularly if trapping processes are important, such analyses are only gross approximations and sometimes represent little more than curve fitting. With this caveat in mind, a model commonly used in the analysis of impurity photoconductivity in n-type semiconductors will first be presented as the starting point from which to analyze the temporal data.[1,10,73]

Consider an n-type semiconductor with a concentration of shallow donor states N_D and a concentration of trapping states N_T as illustrated in Figure V-1. The generic term N_T represents a variety of shallow trapping mechanisms such as acceptor states or ionized neutral donor states. In the establishment of an equilibrium, electrons from shallow donor levels migrate to the trapping levels. For this simple model, a square pulse of illumination by light with energy $h\nu > E_T$ and $h\nu < E_g$ will produce a characteristic photoconductive response, illustrated in Figure V-2.

For these simplest of cases, the electron trap can be in one of two states: (1) N^o its neutral state prior to trapping an electron, and (2) N_T^- when it has trapped an electron. Since the thermal recombination rate at the electron trapping center depends on the electron density n and the density of trapping centers, its recombination rate is given by

$$r = v_{th}\ \sigma_n^o\ n\ (N_T - N_D + n) \qquad \text{(V-1)}$$

where σ_n^o is the thermal capture cross section, v_{th} is the thermal velocity, N_T is the trap concentration, and N_D is the donor concentration. For dark conditions in equilibrium, this recombination rate is equal to a thermal generation rate which depends on N_T and is

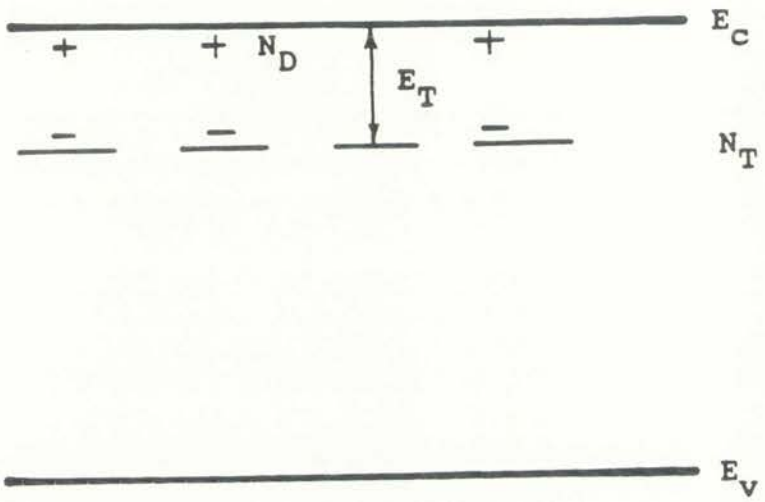

Figure V-1. N-type extrinsic silicon detector with shallow donor levels of concentration N_d and shallow electron traps of density N_T with energy E_T below the conduction band.

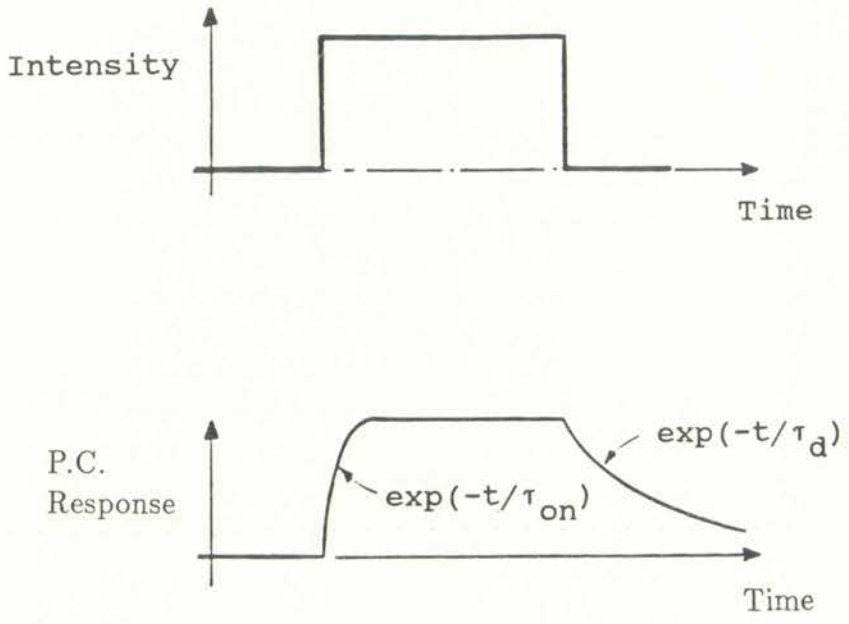

Figure V-2. **Extrinsic photoconductivity transients produced by a square pulse of illumination. Typically, the turn-on transient is shorter than the turn-off transient as illustrated.**

$$g = v_{th}\ \sigma_n^o\ n_1\ (N_D - n) \tag{V-2}$$

where n_1 is the electron density in the conduction band if the Fermi level is at the level of the traps. When the temperature is low, such that n is small and the value of N_t^- is approximately equal to that of N_D, the equilibrium condition $r = g$ gives

$$n_1 = \frac{N_c\ N_T}{N_D}\ e^{-(\triangle E_T/kT)} \tag{V-3}$$

and

$$n_0 \approx \frac{n_1\ N_D}{N_T - N_D} \tag{V-4}$$

where N_c is the effective density of states at the conduction-band edge, E_T is the energy level of the trap with respect to the conduction-band edge, and n_o is the electron density in the conduction band at thermal equilibrium.

Consider a photon flux passing through the material of I photons $cm^{-2}s^{-1}$. If σ_i is the photoionization cross section for the capture of a photon by an electron at the electron trap level with transfer to the conduction band for unity quantum efficiency, the generation rate produced by photons is

$$g_\nu = \sigma_i\ (N_D - n)\ I \tag{V-5}$$

From Equations V-1 to V-5

$$\frac{dn}{dt} = \sigma_i\ (N_D - n)\ I + v_{th}\ \sigma_n^o\ n_1\ (N_D - n) - v_{th}\ \sigma_n^o\ n\ (N_T - N_D + n). \qquad \text{(V-6)}$$

Considering that $n = n_o + \triangle n$, $\triangle(N_T) = -\triangle n$, and $N_{TO}^- + n_o = N_T^- + n$, we obtain

$$\frac{d(\triangle n)}{dt} = \sigma_i\ N_{T0}^-\ I - v_{th}\ \sigma_n^o \left[\frac{\sigma_i I}{v_{th}\ \sigma_n^o} + n_0 + \triangle n + n_1 + (N_T - N_{T0}^-)\right]. \qquad \text{(V-7)}$$

Equations of this form have been discussed extensively by Ryvkin.[73] For illumination levels such that $\triangle n << N_{TO}^-$, then from Equation V-7, the application of a square wave of light with intensity I, results in a simple exponential rise

$$\triangle n_i \ = \ \triangle n_{ss}\ (1 - e^{-t/\tau_{on}}) \qquad \text{(V-8)}$$

where $\triangle n_{ss}$ is the steady state concentration and

$$\tau_{on} \ = \ \frac{1}{v_{th}\ \sigma_n^0\ (n_1 + N_T^0 + n_0)}. \qquad \text{(V-9)}$$

For the turn-off transient t_d the decay is

$$\triangle n_d \ = \ \triangle n_{ss}\ e^{-t/\tau_d} \qquad \text{(V-10)}$$

where

$$\tau_d \ = \ \frac{1}{v_{th}\ \sigma_n^0\ (n_1 + N_T^0 + n_0)} \qquad \text{(V-11)}$$

From Equations V-7 and V-10 it is seen that the turn-on transient τ_{on} is faster than the turn-off transient τ_d. This characteristic is common for most conditions. However, the following experimental data will illustrate an important set of conditions under which the turn-off transient is faster than the turn-on transient.

V-2 Temporal Photoconductivity Data

The data which will be presented in this section are representative of the temporal photoconductive responses obtained for the various extrinsic silicon materials discussed in Chapter IV. Figures V-3 to V-5 and V-6 to V-9 are for the Si:Al and Si:Bi detectors respectively, which were discussed in the previous chapter. Figures V-3 for Si:Al and V-6 for Si:Bi both have response curves which are predicted by the standard transient photoconductivity model discussed in the above. In both cases the decay time is longer than the rise time as expected when illuminated by a square wave pulse of IR light at 39 meV with a duration of 100 ms. For Si:Al (Figure V-3) the rise time is approximately 50 ms with a decay time of 75 ms. For Si:Bi (Figure V-6) the rise time is approximately 25 ms with a 50-ms decay time.

Our photoconductive response transients of Figures V-3 and V-6, which exhibit decay times greater than the rise times, are typical for most of those reported in the literature. For example, Haynes and Hornbeck[74] found that the response transients for shallow traps in n-type silicon were characterized by rapid rise times with longer decay times. Their decay times of approximately 45 ms were similar to our decay times in the above when only extrinsic illumination was utilized. When our detectors were illuminated with intrinsic radiation, however, the model begins to fail for extrinsic silicon photoconductors at temperatures below 15 K ($kT < E_i$) where thermal ionization becomes negligible.

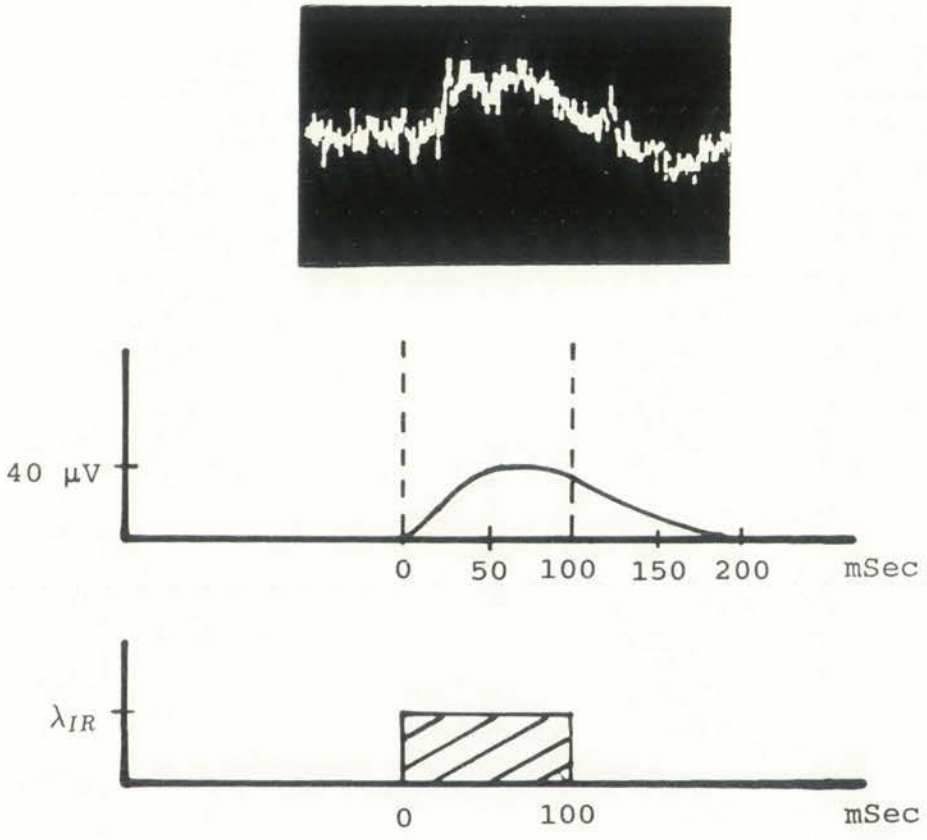

Figure V-3. **Si:Al detector illuminated with a 100 ms IR (39 meV) square pulse. The photoconductivity response is shown in the oscilloscope picture and a schematic for clarity. Temperature = 8 K, Bias = 100 V/cm.**

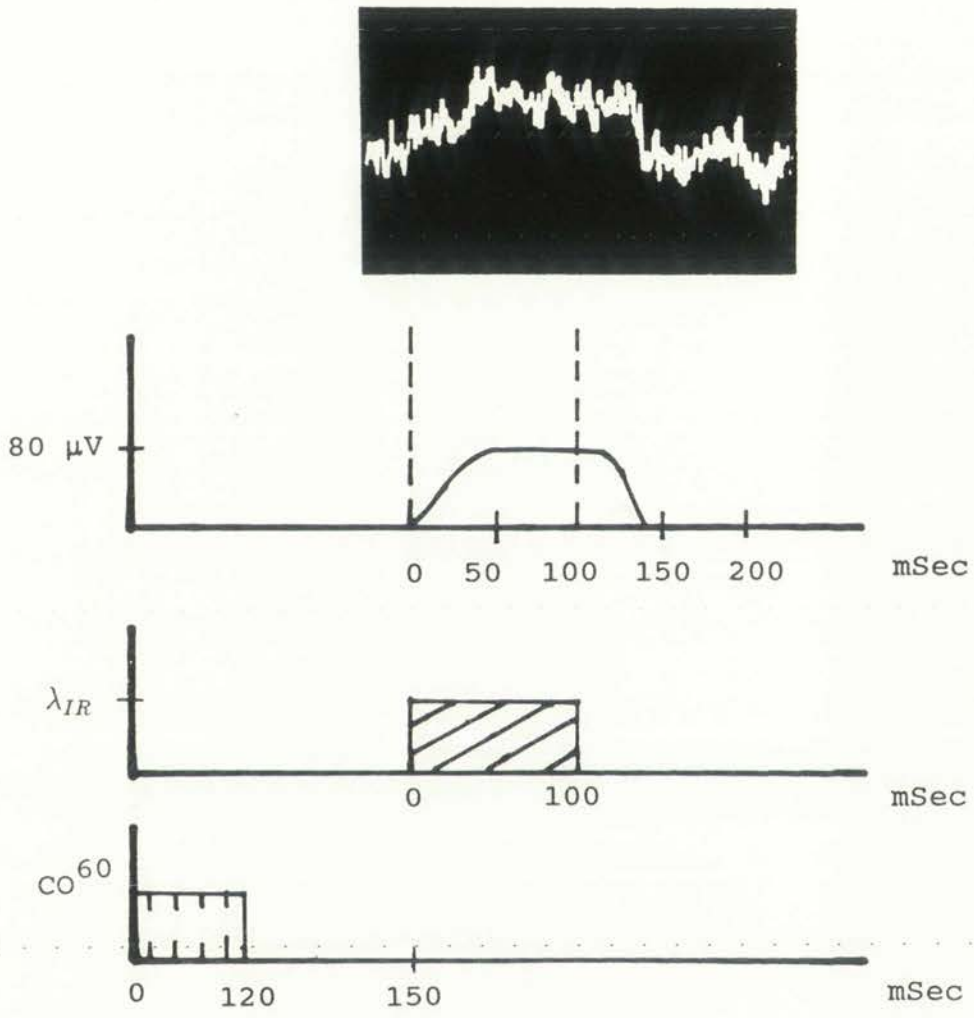

Figure V-4. **Si:Al detector illuminated with a 100 *ms* IR (39 *meV*) square pulse 30 *min* after a 100,000-rad ^{60}Co exposure within 120 *min*. The photoconductivity response is shown in the oscilloscope picture and schematic for clarity. Temperature = 8 *K*, Bias = 100 *V/cm*.**

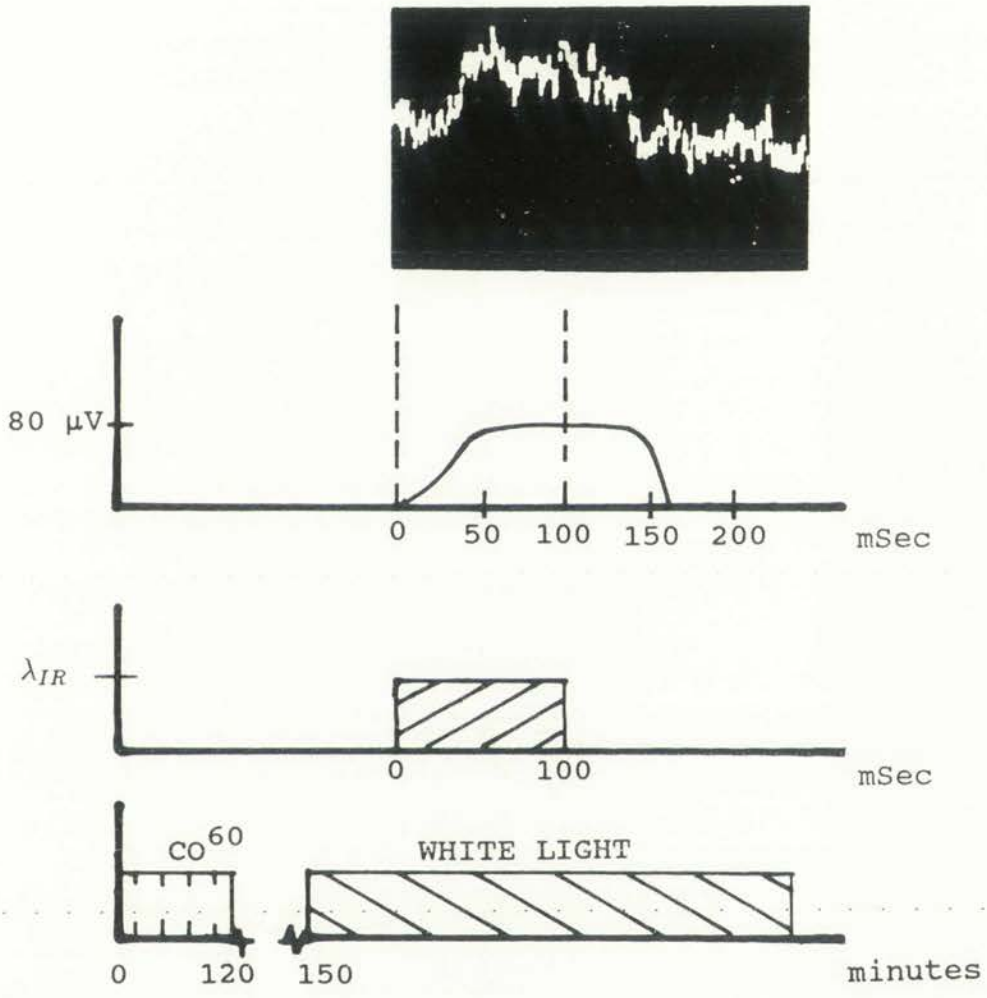

Figure V-5. **Si:Al detector illuminated simultaneously with a 100 *ms* IR (39 *meV*) square pulse and continuous white light 30 *min* after a 100,000-rad ^{60}Co exposure over a 120-*min* period. The photoconductivity response is shown in the oscilloscope picture and the schematic for clarity. Temperature = 8 *K*, Bias = 100 *V/cm*.**

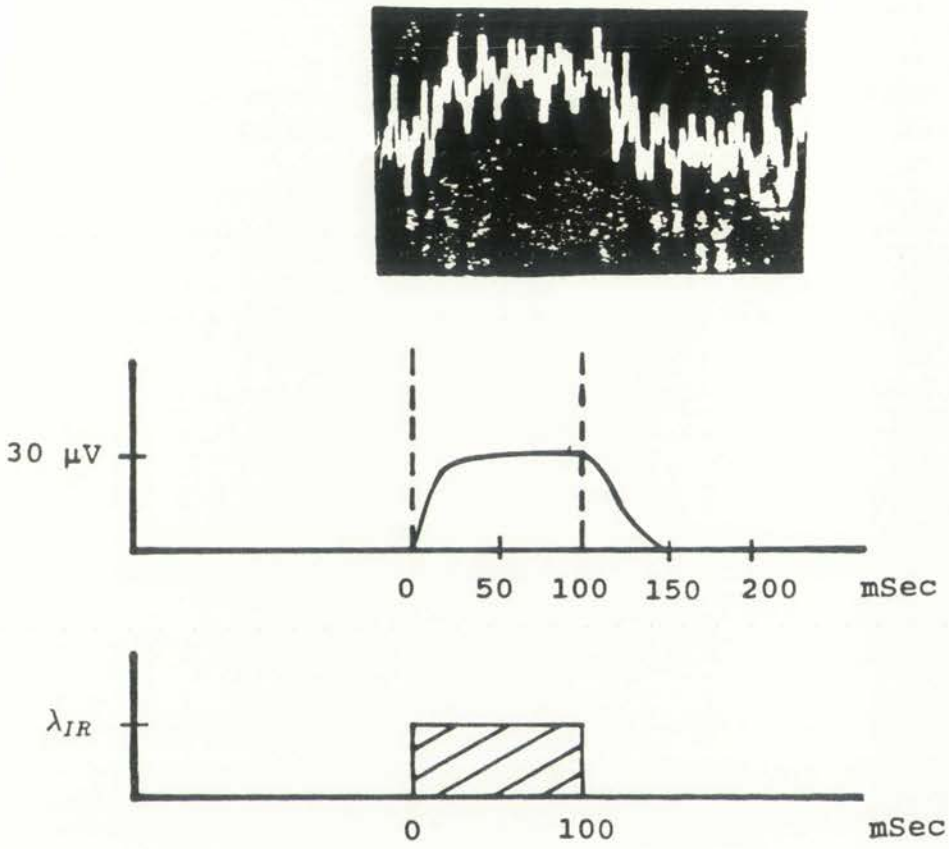

Figure V-6. **Si:Bi detector illuminated with a 100 ms IR (39 meV) square pulse. The photoconductivity response is shown in the oscilloscope picture and the schematic for clarity. Temperature = 8 K, Bias = 100 V/cm.**

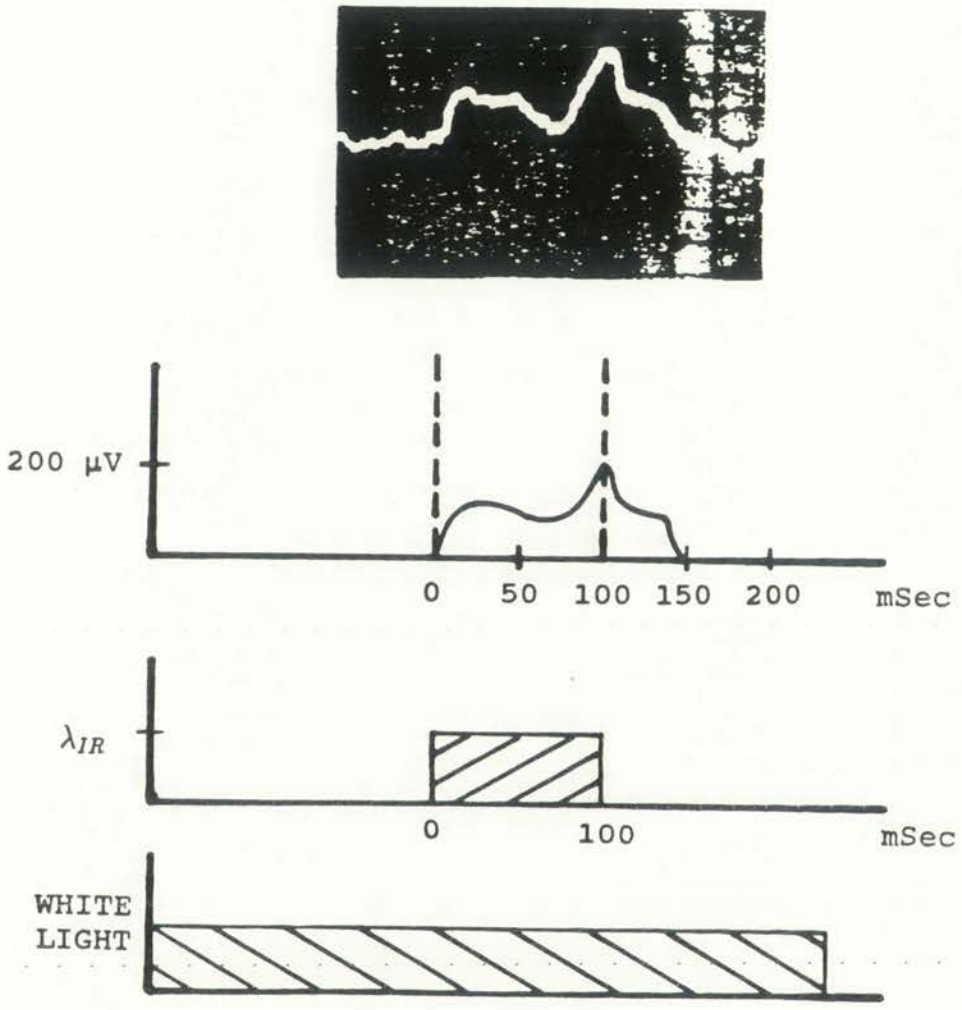

Figure V-7. **Si:Bi detector illuminated simultaneously by a 100 ms IR (39 meV) square pulse and continuous white light. The photoconductivity response is shown in the oscilloscope picture and the schematic for clarity. Tempera ture = 8 K, Bias = 100 V/cm.**

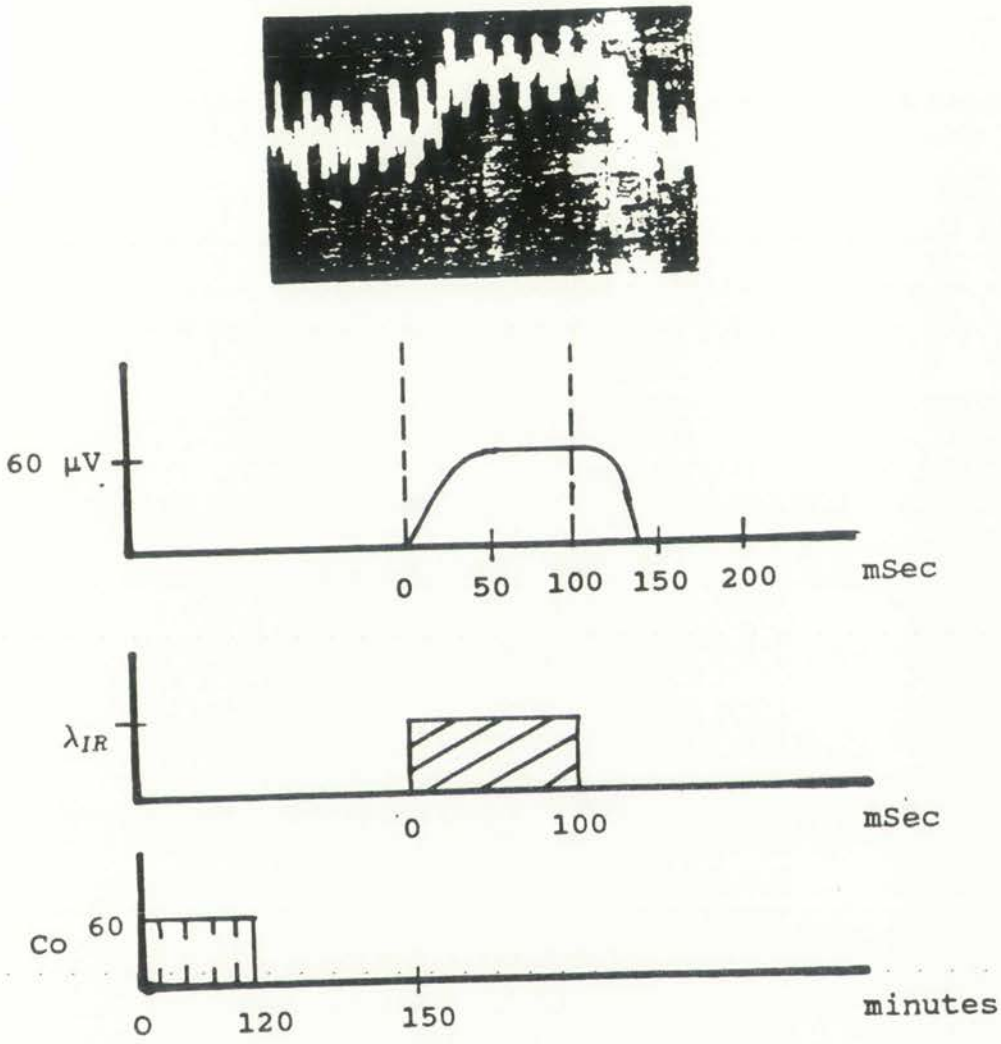

Figure V-8. **Si:Bi detector illuminated with a 100 ms IR (39 meV) square pulse 30 min after a 100,000-rad ^{60}Co exposure over a period of 120 min. The photoconductivity response is shown in the oscilloscope picture and the schematic for clarity. Temperature = 8 K, Bias = 100 V/cm.**

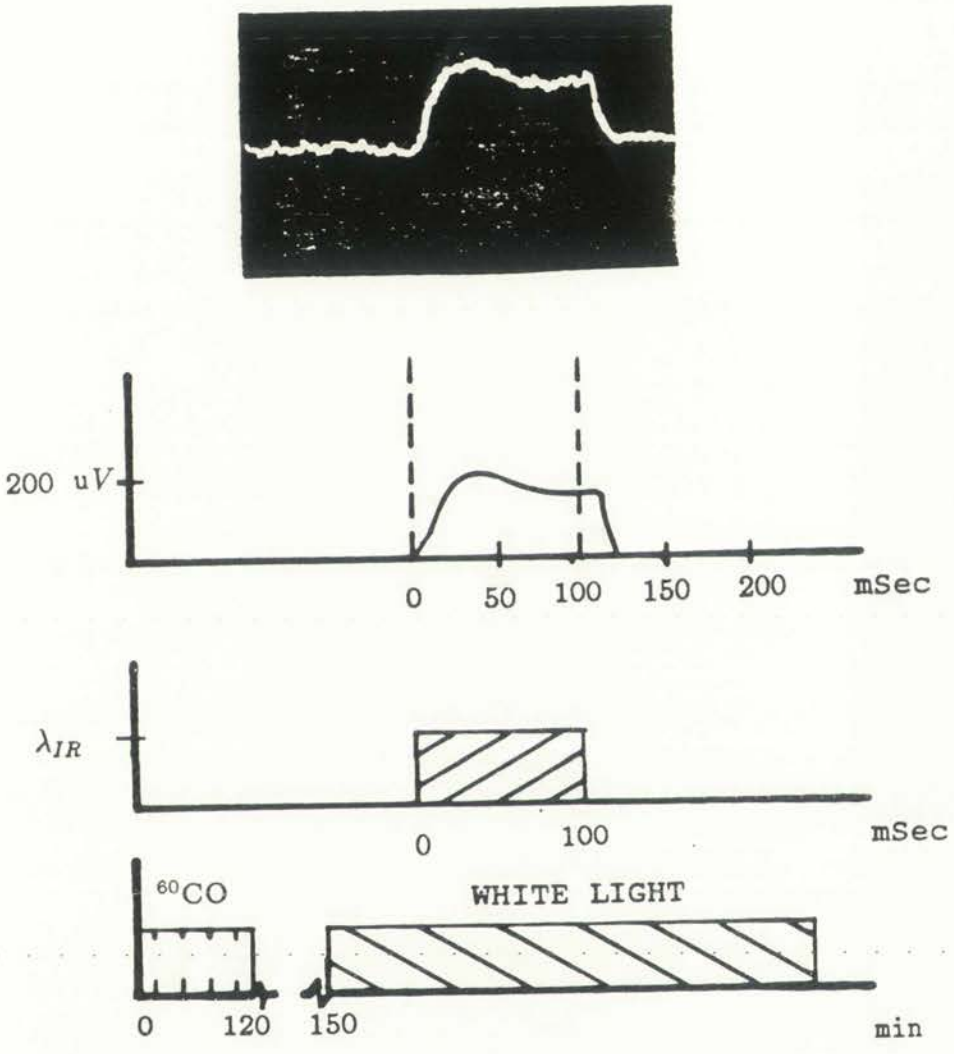

Figure V-9. **Si:Bi detector illuminated simultaneously with a 100 ms IR (39 meV) square pulse and continuous white light 30 min after a 100,000-rad ^{60}Co exposure over a 120-min period. The photoconductivity response is shown in the oscilloscope picture and the schematic for clarity. Temperature = 8 K, Bias = 100 V/cm.**

Examination of Figures V-3 to V-5 for Si:Al reveals several important points. First, the rise time remained relatively unaffected when the sample is illuminated with intrinsic radiation from either a white light or ^{60}Co source. However, Figure V-4, which we took 30 *min* after irradiation with a ^{60}Co source (100 *K*-rad total dose), reveals a photoconductive response which was both greater in relative magnitude as well as longer-lived. The signal magnitude increased by a factor of two and the long-lived response was 25% longer than the 100 *ms* IR pulse. The resulting decay time was now only 15 *ms* as opposed to 75 *ms* previously. Next, the detector was illuminated continuously with a white light intensity defined by curve 3, Figure I-4. Our measured response resulting from the 100-*ms* IR pulse is shown in Figure V-5. Once again a long-lived response, approximately 40 *ms* in duration, and a shortened decay time of 14 *ms* were observed along with an increase in signal magnitude for our data.

Referring to Figures V-6 to V-9 for the Si:Bi samples, we also observed the same general phenomena for n-type material; enhanced signal response magnitude, a long-lived component and a shortened decay time. For Si:Bi the decay time decreased from an initial 50 *ms* to around 7 *ms*. Figure V-6 is our photoconductive response following a 100 *ms* IR square-wave infrared pulse. The signal response peaked around 20 μV on the oscilloscope with a corresponding decay time of 50 *ms*. When white light was added the magnitude of the response curve increased by a factor of ten, to around 200 μV as seen in Figure V-7. In addition the long-lived component of our response curve maintains its illuminated levels for a period equivalent to 45% of the IR pulse after the IR pulse ends. The rapid decay curve is approximately 7 *ms* in duration. The interesting behavor exhibited in Figure V-7 was not an artifact but was repeatable under white light illumination. However, experimental constraints prevented further investigations necessary to understand

the responsible mechanisms.

Following the above measurements, our Si:Bi detector was exposed to 100,000 rads of ^{60}Co irradiation over a period of 120 min with a constant temperature of 8 K. The photoconductive response to a 100 ms IR (39 meV) square-wave pulse 30 min after irradiation is shown in Figure V-8. Our signal magnitude increased by a factor of two for the same conditions prior to irradiation. In addition, the previously observed long-lived response with a rapid decay became evident as it also had during white light illumination.

Our final set of measurements, which immediately followed the ones of Figure V-8, involved simultaneous illumination with white light during the 100 ms IR pulse (39 meV). The resulting curve, shown in Figure V-9, shows a factor of ten increase in signal magnitude and a rapid decay component compared to the rise time in comparison to pre-irradiation conditions without white light (Figure V-6). When Figure V-9 is compared to the same illumination conditions before ^{60}Co exposure (Figure V-6), qualitatively our resulting response curves are similar. Both show signal magnitude increases of approximately ten times compared to non-band-gap illumination conditions with rapid decay components following the IR pulse.

Therefore, following an examination of our temporal data we must conclude that mechanisms which couple energy between carriers in the conduction band and the impurity band do exist as previously suggested by our spectral response curves in Chapter IV. In the above, our temporal data demonstrated that significant changes both in magnitude, duration, and decay times of the photoconductive response associated with shallow impurities occur with the addition of intrinsic radiation at very low temperatures. The fact that little change was experienced in the rise curved indicate that there are no significant changes in the density of empty traps available

for the majority carriers to become trapped in the beginning of the excitation phase.[1]

Schulman and Honig[75] examined intrinsic oscillatory photoconductivity in silicon at 4 K nearly 20 years ago. Qualitatively, their photoconductivity response curves resembled our curves in Figures V-4 to V-5 and V-7 to V-9 in that they exhibited a very rapid decay time compared to the rise time. They speculated that a photoconductivity mechanism existed whereby a large generation rate of low-energy excitons and their capture by impurities results in a decrease of electron mobility. It was further speculated that the impurity-exciton complex responsible could be an experimentally established neutral donor-exciton complex.[78] Gershenzon[62] investigated H^--like impurity centers via photoconductivity spectra as a function of temperature for Si:P with a concentration of $9 \cdot 10^{16}$ atoms/cm^3. He demonstrated significant D^- population exist for temperatures below $15K$. The photoconductive peaks for his data shifted from 5 to 15 meV as sample temperatures increased from 2 to 9 K. Our spectral photoconductivity response curves in Chapter IV showed increased photoconductivity towards the lower energies as well as asymmetric broadening towards the energy regime of increased carriers for Gershenzon's data. Therefore, the next logical question is the potential impact that H^--like states could have on the transitions from ground to excited states in the measurable area of interest from 37 to 43 meV as studied by others.

In order to examine the above question, Capizzi[59,76] performed absorption studies on Si:P samples at 10 K. For concentrations in the $1 \cdot 10^{16} cm^{-3}$ range, absorption lines originating from ground state transitions to excited states broadened considerably as the concentration was increased. Indeed, at these levels, the $1s$-$2p_o$ transition even begins to reveal some structure. The authors attributed these changes in line shape to the formation of hydrogenic impurity molecules, with transitions between

homeopolar levels (H^-, H^+) and to the ionic (H^--H^+ type). This same phenomenon was subsequently observed in Ge:As by other groups.[64] It now becomes apparent that H^--like centers are definitely involved in the increased photoconductivity response from the addition of band-gap radiation for temperatures below thermal ionization as previously speculated.

In addition to an increased photoconductivity response following intrinsic illumination, rapid decay times on the order of 0.1 to 10 ms were typical values for the our data. Norton[77] provided experimental evidence to support the existence of a band of impurity states associated with negatively charged donors in silicon and germanium for temperatures below 10 K. The silicon samples were doped with $8.5 \cdot 10^{15} cm^{-3}$ phosphorus donors and about $3 \cdot 10^{12}$ acceptors. A direct evaluation of the decay time as a function of temperature indicated electron recombination occurred in 20 to 500 μs.

Others have looked at recombination times for the capture of a hole by a neutral donor.[61] It was suggested that the recombination of an electron with a hole captured by a neutral donor occurs via the same process as the decay of a free exciton, except that a shorter decay time is expected.[44] This is due to the impurity providing better coupling to the lattice for emission of the necessary energetic phonon associated with the indirect band gap. The associated decay time is therefore expected to be on the order of the 2.6 microsecond decay time of a free exciton in silicon.[44] In addition, a Shockley-Read type of process leading to recombination of the captured hole with an electron on a donor via capture of a radiation induced electron by the $(D^o)+$ state has also been suggested which would have equally fast recombination times.[44] From the above, it appears reasonable to assume that the rapid decay times for our experimental results are intimately associated with H^--like centers and/or

complexes as well as the neutral impurity concentrations (D^o, A^o). In order to evaluate these assumptions a model for photoconductivity associated with H^--like centers for n-type silicon will be utilized in the following section.

V-3 Photoconductivity From Negative Donor Ions

The following discussion is based on a model formulated by Norton[61] and synopsizes his essential points relative to H^--like centers and observed rapid decay times. In order to model the photoconductivity associated with the photoionization of D^- states in silicon, one needs to determine the parameters which control the density of D^- states (donor impurities with an extra bound electron). Norton calculated the density of D^- states from the requirement of detailed balance, together with a knowledge of the generation and recombination parameters. The parameters which Norton considered and diagrammed are illustrated in Figure V-10. From Figure V-10, one observes the generation of electrons by excitation from neutral donor states G^o and from negative donor traps G^-. Recombination can occur at excited states of positively charged donors D^+, and electrons will be trapped at neutral donors D^o to form D^- states. Lastly, recombination can occur as the result of direct neutralization of a close pair of oppositely charged donors D^-, resulting in two neutral donors. The densities of states can be in one of three configurations: the neutral donor state, N_d^o, in which case Norton does not distinguish excited states; the positively charged donors, N_d^+; and the negative donors, N_d^-. Therefore, one can write:

$$N_d = N_d^0 + N_d^- + N_d^+. \tag{V-12}$$

At low temperatures there will be N_a compensated donors, so

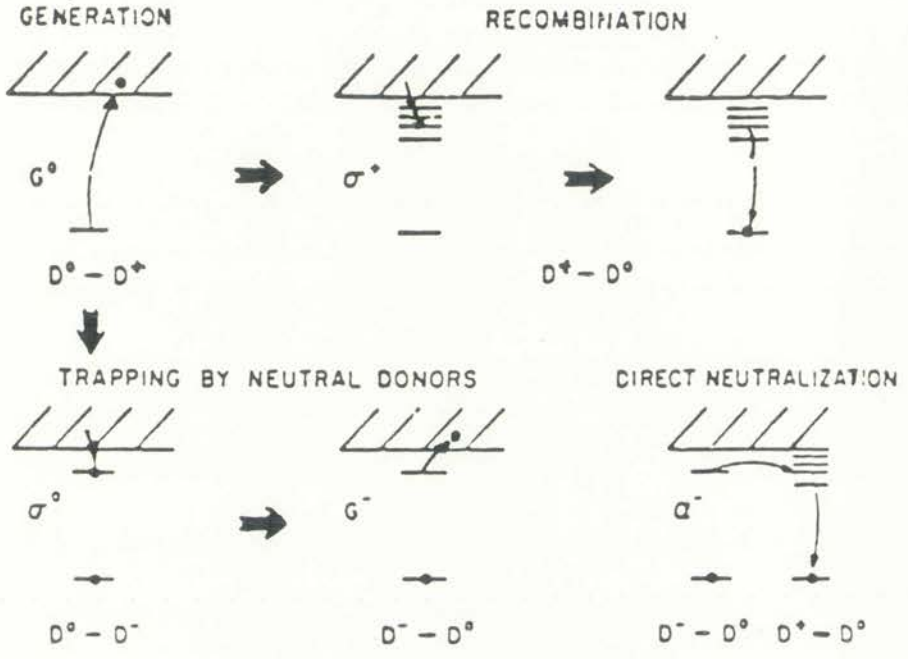

Figure V-10. Generation, recombination, trapping, and direct neutralization mechanisms are illustrated for the effect each has on the charge state of the donor impurity. The parameters associated with each mechanism are shown, along with the transition made by the electron in each case.

$$N_d^+ = N_a + N_d^- + n \tag{V-13}$$

where n is usually smaller than N_a or N_d^- and therefore is ignored. Thus, one obtains

$$N_d^0 = N_d - 2N_d^- + N_a. \tag{V-14}$$

In steady state, the net rate of change of the concentration in each charge state will be zero. Hence,

$$\frac{dN_d^-}{dt} = n < v > \alpha^0 \; N_d^0 - (G^- + B^-) \; N_d = 0 \tag{V-15}$$

$$\frac{dN_d^0}{dt} = n < v > (\alpha^+ \; N_d^+ - \alpha^0 \; N_d^0) + (G^- + B^-) \; N_d^- - G^0 \; N_d^0 = 0 \tag{V-16}$$

where $< v >$ is the average velocity of the electrons, α^o and α^+ are the capture cross sections for electrons at neutral and positively ionized donors, respectively, and G and G^o are the optical generation probabilities for D^- and D^o states, respectively. The term B^- accounts for thermal ionization of the D^- center which cannot be excluded above 2 K. Thermal ionization of the D^o centers however, is negligible below 15 K. Solving these equations for $N_d = 4 \cdot 10^{16} \; cm^{-3}$ and $N_a = 5 \cdot 10^{12} cm^{-3}$, Norton found for a bias of 100 V/cm approximately $1 \cdot 10^{15} cm^{-3}$ D^- centers. These concentrations and bias conditions were almost identical to those used in our experiments and therefore serve as representative values which might be expected.

When the extra bound electron at the neutral donor is captured by a donor which is missing an electron, direct neutralization can occur. This extra electron has the capability to migrate from one donor to another via impurity-band conduction mechanisms previously discussed. Earlier, it was pointed out that this condition is easily obtained for concentrations as low as $1 \cdot 10^{16} cm^{-3}$ at temperatures below 10 K. Norton presents an argument whereby the migration of D^- states can occur in very lightly doped material on the order of $1 \cdot 10^{13} cm^{-3}$. Thus, he rationalizes that direct neutralization cannot be neglected and calculates the impact of direct neutralization on the concentrations of D^- centers. Norton concluded that for the above mentioned concentrations and field bias, direct neutralization of neutral centers control the carrier lifetime. This conclusion corresponds with the previously discussed information on scattering mechanisms in Chapter III. For the examples utilized in Chapter III, Sclar's neutral impurity scattering theory which includes the effect of a bound electron state suggested that neutral impurity scattering was the limiting factor for mobility.

The totality of the results presented above strongly suggest that H^--like centers do indeed have a profound impact on the photoconductive response. Based on these results the following scenario for describing enhanced photoconductivity and long-lived responses with rapid decay times can be postulated.

Illuminating the extrinsic silicon detectors at temperature levels where thermal ionization is negligible results in a continuous repopulation of the neutral donor centers. Applying a single 100 ms square pulse of IR light depopulates these centers, in turn destroying the H^--like centers and complexes. This nonequilibrium state continues throughout the 100 ms time period. Because significant wavefunction overlap exists for charge transfer, impurity-band conduction occurs in conjunction

with the normal conduction-band mechanisms. However, transport via hopping in the impurity band is a much slower transport process than the conduction-band mechanisms. Therefore, one would expect to observe a longer lived component from impurity-band conduction processes which result in a significant photoconductive signal after the IR light is turned off.

Once the IR light is turned off this nonequilibrium system continues to excite carriers into the conduction band via coupling mechanisms which are intimately involved with H-like centers. The resulting long-lived signal is a mixture of impurity-band carriers and conduction-band carriers for a short period after the IR light is turned off. Shutting the IR light off allows the system to reach equilibrium very quickly. This occurs through repopulation of the neutral centers via band-gap light and the associated H^--like centers and complexes which develop on the rapidly increasing neutral donor population. This process is characterized by an initial long-lived response followed a short time later by this cascading effect permitting rapid recombination to occur. Hence, the hallmark of D^- center involvement in transient behavior is a long-lived response followed by a decay time which is faster than the rise time, in agreement with our experimental data.

CHAPTER VI

SUMMARY

In this dissertation we have investigated and discussed a variety of effects on photoconductivity under conditions where the photoexcitation was either extrinsic (from sub-band-gap IR photons) or combined extrinsic and intrinsic (the latter from above-band-gap white light photons). Our results showed clearly that the presence of steady intrinsic excitation had significant effects on both the spectral and temporal characteristics of extrinsic excitation processes in the devices we studied.

Modeling based on the simplest considerations indicates that impurity-band and lattice-band transport should be essentially noninteracting under the conditions of our experiments, fundamentally because of the significant difference between the mean lattice-band carrier energy ($3/2\ kT \approx 1meV$) and the impurity-level ionization energy ($\approx 40\ meV$). However, in contrast to this expectation, we have clearly demonstrated strong interactions in all cases studied. These results make it clear for the first time that important energy transfer mechanisms exist between impurity-band and lattice-band carriers whether or not temperatures are sufficiently low that thermal ionization can contribute to photoconductivity processes.

Our experiments and conclusions, which are unique relative to the previous literature, represent an important connection between two previous areas of activity. The first of these involved studies devoted to proving the existence of $D^-(A^+)$ centers and determining their ionization energies. For these studies, samples were illuminated only with very long-wavelength extrinsic radiation (1-15 meV) at temperatures where thermal ionization was insignificant. The second area of prior activity utilized the sensitivity of photoconductivity techniques to study ultrapure semiconductor materials, principally germanium and silicon. In these studies, higher

experimental temperatures were required ($T > 15K$ for silicon) to enhance phonon coupling and promote transitions of carriers into the conduction band via thermal ionization. The uniqueness of our studies lies in the use of moderately heavily-doped samples as opposed to relatively pure materials, the use of temperatures both below and above the threshold for significant thermal ionization, and the application of combined extrinsic and intrinsic illumination.

The totality of our spectral and temporal experimental results strongly suggests that H^--like centers are involved in the observed photoconductive response for temperatures where thermal ionization is considered negligible. The ability for a neutral impurity atom (i.e. un-ionized Group III or Group V atom) to bind an extra electron (hole) analogous to a hydrogen atom was shown to significantly impact the photoconductivity. The resulting photoconductivity signals both increased in relative magnitude and broadened asymmetrically towards lower energy. In addition, long-lived photoconductivity responses with increased decay times were observed. It was speculated that the extra electron (hole) localization in a system of neutral and charged centers could occur in various forms such as H^--like centers, impurity molecule complexes of type H^--H+, or possibly H_2^-, depending on the conditions. However, although we were able to modulate the total concentration of H^--like centers using both band-gap illumination and ^{60}Co irradiation, the complexity of the situation did not allow us to catalog the complexes involved or determine their relative contributions.

In this final section, we wish to point out that the contributions of this work have important implications for the current generation of advanced infrared detection devices known as Blocked-impurity-Band (BIB) detectors. These devices employ a specialized device structure (unfortunately not available to us) which al-

lows the collected charge from carriers moving in an impurity band to be separated, in principle, from the charge from carriers moving in the conduction and/or valence bands. Owing to this feature, it has been proposed that certain BIB infrared detectors can have the property of Intrinsic Event Discrimination (IED) whereby the effects from transient intrinsic excitation (from a cosmic ray particle or a nuclear event, for example) can be separated from the desired signal from extrinsic radiation (from an infrared-emitting target, for example).

As we have discussed previously, at the low temperatures of 7-10 K (which are typical of our experiments as well as of BIB detector operation) carriers with energies on the order of $kT \approx 1meV$ have negligible probability of interacting with single carriers bound with much higher energies ($\approx 40\ meV$) to shallow impurities or their associated impurity bands. However, the unexpectedly strong extrinsic-intrinsic interaction that has been demonstrated in our experiments owing to the important effect of D^- formation represents a significant potential difficulty for the intended operation of the IED concept.

The current theoretical understanding of the D^- centers is unfortunately sufficiently rudimentary that there is no understanding of the generality of the effect and its potential sensitivity to the local electronic structure of the impurity/host system. There thus can be no clear answer at the present time as to whether impurities other than those studied in this work might show less tendency for D^- formation and thus greater likelihood of successful demonstration of the IED concept. However, the work we have completed has defined an important limiting mechanism for the IED concept which was not understood previously. Furthermore, our work represents an important starting point for future studies which will be significant in determining the ultimate viability of this potentially attractive concept.

It is suggested that these future studies focus on two principal areas. The first of these would involve a comprehensive dynamic computer model simulation of the carrier concentrations, level occupancies, and transport mechanisms for both the lattice band and impurity band. The best approach here would be a highly physical simulation where the carrier population is handled as an ensemble of identified individual carriers whose fate depends on Monte Carlo options that come into play at each time step. The simulation program could be developed from the starting point where there is no energy transfer between lattice-band and impurity-band populations, subsequently permitting various physical mechanisms to be incorporated and studied as desired. The development of such a simulation program and its application to the problem we have studied experimentally would undoubtedly lead to important contributions to the detailed understanding of the physical mechanisms involved.

An appropriate second area for further studies would be to conduct more-sophisticated experiments which would have the capability of resolving the lattice-band and impurity-band transport phenomena in real time. In this context, it would be useful to have available fast pulsed sources of both extrinsic and intrinsic excitation. The former could be realized with a pulsed infrared laser system using appropriate downconversion, and the latter could be realized with a pulsed visible laser system or a pulsed electron beam. The electron beam has the advantage that it can easily penetrate a light-tight thin metal window at energies well below lattice-damage thresholds, thus making it possible to introduce essentially only intrinsic excitation in a closed Dewar system with very low infrared background. With adequate sensitivity and temporal resolution, it should be possible, based on the coupling mechanisms we have identified, to observe both impurity-band and lattice-band responses following pulsed intrinsic excitation. Resolving these two processes

is based on the fact that the photoconductive response of lattice-band carriers will be significantly faster than the response of impurity-band carriers which is determined by various hopping mechanisms. In addition to providing an independent verification of the lattice-band to impurity-band energy transfer mechanisms we have identified in this work, the proposed future activity could provide a framework with which to investigate the viability of the Intrinsic Event Discrimination concept for various temperatures, materials, and doping regimes.

REFERENCES

1. R.H. Bube, Photoconductivity of Solids (John Wiley and Sons, New York, 1960).

2. A. R. Rose, Concepts in Photoconductivity and Allied Problems (John Wiley and Sons, New York 1963).

3. P.R. Bratt, "Impurity Germanium and Silicon Infrared Detectors, in Semiconductors and Semimetals, Vol.12, (Academic Press, New York, 1977).

4. T.M. Lifshits and F.Y. Nad, "Photoconductivity in Germanium Impurity Ionization Energy", Sov. Phys.-Dokl., Vol.10, No.6, p.532, 1965.

5. T.M. Lifshits, et al, Sov. Phys. Semicon., "Temperature Dependence of Photothermal Ionization and the Probability of Hole Trapping by Excited States of Hydrogen-like Acceptors", Vol.2, No.6, p.652, 1968.

6. Ch.M. Kogan and B.I. Sedunov, "Photothermal Ionization of an Impurity Center in a Crystal", Sov. Phys. Sol. St. Vol.8, No.8, p.1898, 1967.

7. S.M. Kogan and T.M. Lifshits, "Photoelectric Spectroscopy - A New Method of Analysis of Impurities", Phys. Stat. Sol.(a) p.11, 1977.

8. A. Onton, et al, "Spectroscopic Investigation of GroupIII Acceptor States in Silicon", Phys. Rev. Vol.163, No.3, p.686, 1967.

9. J.S. Blakemore, "Solid State Physics" (W.B. Saunders Co., Philadelphia, 1969).

10. A.G. Milne, "Deep Impurities in Semiconductors" (John Wiley & Sons, Inc., New York, 1973).

11. O. Madelung, "Introduction to Solid-State Theory" (Springer-Verlag, New York, 1978).

12. R.A. Smith, "Semiconductors" (Cambridge University Press, Great Britain, 1978).

13. W. Kohn, "Solid State Physics", edited by F. Seitz and D. Turnbull (Academic Press, New York, 1957).

14. H.F. Wolf, "Semiconductors" (Wiley-Interscience, New York, 1971).

15. B.I. Shklovskii and A.L. Efros, "Electronic Properties of Doped Semiconductors" (Springer-Verlag, New York, 1984).

16. D. Long, "Scattering of Conduction Electrons by Lattice Vibrations", Phys. Rev. Vol.120, p.2024, 1960.

17. P. Norton, et al, "Impurity and Lattice Scattering Parameters Determined from Hall and Mobility Analysis in N-type Silicon", Phys. Rev. B, Vol.8, p.5632, 1973.

18. C. Herring and E. Vogt, "Transport and Deformation Potential Theory for Many Valley Semiconductors with Anisotropic Scattering", Phys. Rev. Vol.101, p.944, 1956.

19. H. Brooks, "Theory of the Electrical Properties of Germanium and Silicon", in Adv. in Electronics and Electron Physics, Edited by L. Marton, Vol.7, p.85 (Academic Press, New York, 1955).

20. C. Herring, "Transport Properties of a Many Valley Semiconductor," Bell Syst. Tech. J., Vol.36, p.237, 1955.

21. A.G. Samoilvich, et al, "The anisotropy of Electron Scattering by Ionized Impurities and Acoustic Phonons," Sov. Phys. Sol. St., Vol.3, p.2385, 1962.

22. D. Long and J. Meyers, "Ionized-Impurity Scattering Mobility of Electrons in Silicon," Phys. Rev. Vol.115, p.1107, 1959.

23. D. Long, " Ionized Impurity Scattering Mobility of Electrons in Silicon," Phys. Rev., Vol.129, p.2464., 1963.

24. S.S. Li and W.R. Thurber, "The Dopant Density and Temperature Dependence of Electron Mobility and Resistivity in N-type Silicon", Sol. St. Elect., Vol.20, p.609, 1977.

25. C. Erginsoy, "Neutral Impurity Scattering in Semiconductor," Phys. Rev. Vol.79, p.1013, 1950.

26. N. Sclar, "Neutral Impurity Scattering in Semiconductors", Phys. Rev., Vol.104, p.1559, 1956.

27. T.C. McGill and R. Baron, "Neutral Impurity Scattering in Semiconductors", Vol.11, No.12, p.5208, 1975.

28. G.F. Neumark, "Concentration and Temperature Dependence of Impurity-to-band Activation Energies," Phys. Rev. B5, p.408, 1972.

29. N.F. Mott, "On the Transition to Metallic Conduction in Semiconductors", Can. J. Phys., Vol.34, p.1356, 1956.

30. E.M. Conwell, "Impurity Band Conduction in Germanium and Silicon", Phys. Rev., Vol.103, p.51, 1956.

31. H. Fritzsche, "Resistivity and Hall Coefficient of Antimony-doped Germanium at Low Temperatures", J. Phys. Chem. Solids, Vol.6, p.69, 1958.

32. J. Hubbard, "Electron Correlation in Narrow Energy Bands.", Proc. R. Soc. A., Vol.276, p.238, 1963.

33. J. Hubbard, "Electron Correlations in Narrow Energy Bands. II. The Degenerate Case.", Proc. R. Soc. A., Vol.277, p.237, 1964.

34. J. Hubbard, "Electron Correlations in Narrow Energy Bands. III. An Improved Solution.", Proc. R. Soc. A., Vol.281, p.401, 1964.

35. N.F. Mott, "Conduction in Non-crystalline Systems," Phil. Mag., Vol.26, p.1015, 1972.

36. N.F. Mott, "Metal-insulator Transition in Doped Silicon", Phil. Mag. B., Vol.47, No.6, p.577, 1983.

37. B. Massarani, et al, "Hopping Conductivity Changes with the Concentration of Compensating Centers," Phys. Rev. B, Vol.15, No.4, p.2224, 1977.

38. A. Miller and E. Abrahams, "Impurity Conduction at Low Concentrations", Phys. Rev., Vol.120, No.3, p.745, 1960.

39. B.I. Shklovskii and A.L. Efros, "Structure of Impurity Bands in Lightly Doped Semiconductors", Sov. Phys. Semicond., Vol.14, No.5, p.487, 1980.

40. F.T. Morin, and J.P. Maita, "Electrical Properties of Silicon Containing Arsenic and Boron," Phys. Rev. Vol.96, p.28, 1954.

41. A.H. Kalma and C.J. Fischer, "Neutron Damage Mechanisms in Silicon at 10 K", IEEE Trans. Nuc. Sci., Vol.NS-24, p.2158, 1977.

42. M.D. Petroff, J.C. Pickel, and M.P. Curry, "Low-level Radiation Effects in Extrinsic Infrared Detectors", IEEE Trans. Nuc. Sci., Vol.NS-26, p.4840, 1979.

43. R.L. Williams, "Response Characteristics of Extrinsic Photoconductors," J. Appl. Phys., Vol.40, p.184, 1969.

44. A.F. Milton and M.M. Blouke, "Sweepout and Dielectric Relaxation in Compensated Extrinsic Photoconductors,: Phys. Rev. B, Vol.3, No.12, p.4312,.

45. E.E. Haller, W.L. Hansen, and F.S. Goulding, "Physics of Ultra-Pure Germanium", Advances In Physics, Vol.30, No.1, p.93, 1981.

46. T.M. Lifshits, et al, "Photoelectric Spectroscopy of Impurities in Semiconductors", Soviet Phys.-J. Exper. Theor. Phys. Letters Vol.7, p.2076, 1968.

47. E.M. Bykova, T.M. Lifshits, and V.I. Sidorov, "Photoelectric Spectroscopy as a Means for Complete Qualitative Analysis of Residual Impurities in a Semiconductor", Sov. Phys. Semicond., Vol.7, No.5, p.986, 1973.

48. Skolnick, L.Eaves, and R.A. Stradling, "Far Infrared Photoconductivity from Majority and Minority Impurities in High Purity Si and Ge", Solid State Communications, Vol.15, p.1403, 1974.

49. S.N. Artemenko, "Influence of an Electrically Inactive Impurity on the Width of Photothermal Ionization Lines of a Different Shallow Impurity", Sov. Phys. Semicond., Vol.8, No.11, p.1405 1975.

50. R. Newman, "Concentration Effects on the Line Spectra of Bound Holes in Silicon," Phys. Rev. Vol.103, p.103, 1956.

51. R.A. Stradling and L. Eaves, Proc. 4th Intl. Symp. GaAs, U. Colo. 1972, p.65, ed. C. Hilsum, Institute of Physics, London, 1973.

52. G.E. Stillman, C.M. Wolfe, and J.O. Dimmock, Proc. 3rd Intl. Conf. Photoconductivity, Stanford, 1969, p.169 Edited by E.M. Pell, Pergamon, New York, 1971.

53. V.N. Aleksandrova and E.M. Gershenson, "Spectroscopic Evidence for the Interaction between Shallow Hydrogenic Donors in GaAs, InP, and CdTe,: Sov. Phys. - JETP Vol.43, p.305, 1976.

54. K.K. Bajaj, et al., Phys. C, Vol.8, p.530, 1975.

55. P.Townsend, "Infrared absorption in Phosphorus Doped Silicon and the D Band", J. Phys. C:Solid State Phys., Vol.11, p.1481 1978.

56. G.A. Thomas, M. Capizzi, and F. DeRosa, "Optical Measurements of the Approach to the Anderson Transition", Phil. Mag. B, Vol. 42, No.6, p.913 1980.

57. S. Narita and M.Kobayashi, "Far-infra-red Investigations of Impurity Bands in Semiconductors", Phil. Mag. B, Vol.42, No.6, p.895 1980.

58. R.N. Bhatt and T.M. Rice, "Clustering in the Approach to the Metal-insulator Transition", Phil. Mag. B, Vol.42, p.895 1980.

59. M. Capizzi, et al., "Observation of a Donor Exciton Band in Si licon", Sol. State Comm., Vol.31, p.611 1979.

60. H.A. Bethe and E.E. Salpeter, Quantum Mechanics of One and Two Electron Atoms (Springer Berlin, Berlin, 1957).

61. Norton, "Photoconductivity from Shallow Negative Donor Ions in Silicon: A New Far-infrared Detector", J. Appl. Phy. Vol.47, No.1, p.308 1976.

62. N.A. Gemma, et al., "Localized and Delocalized Characters in Optical Spectra of Interacting Donors in Semiconductors", J. Phys. Soc Jpn. Vol.51, p.1207, 1982.

63. E.M. Gershenzon, et al, "H -like Impurity Centers and Molecular Complexes Created by Them in Semiconductors," Sov. Phys. Uspekhi Vol.23, p.684, 1980.

64. M.Y. Kobayashi, et al., "Far-infrared Absorption Spectra of Impurity Band in n-type Germanium," J. Phys. Soc. Jpn. Vol.47, p.138, 1979.

65. M.Y. Kobayashi, et al., "Far-infrared observation of D -band in n-type Germanium," J. Phys. Soc. Jpn. Vol.51, p.844, 1982.

66. A. Natori and H.Kamimura, "Optical Absorption Spectrum of a D Center in Strong Magnetic Fields", Phys. Soc. Jpn. Vol.47, p.1550, 1979.

67. W. Shockley and W.T. Read, Jr., "Statistics of the Recombinations of Holes and Electrons," Phys. Rev., Vol.87, p.835, 1952.

68. J.P. McKelvey, Solid State and Semiconductor Physics, Robert E. Krieger PuB. Co., Malabar, Florida, 1984.

69. P.Norton, " Formation of the Upper Hubbard Band from Negative-donor-ion states in Silicon," Phys. Rev. Letters, Vol.37, p.164 1976.

70. G.A. Baraff, E.O. Kane, and M. Schluter, "Theory of the Silicon Vacancy: An Anderson Negative-U System", Inst. Phys. Conf. Ser. No.59, p.19 1980.

71. B.K. Ridley, "The Photoionization Cross Section of Deep-level Impurities in Semiconductors", J. Phys. C: Solid St. Phys., Vol.13, p.2015, 1980.

72. M.A. Amato and B.K. Ridley, "A Comparison of Simple Theoretical Models for the Photoionization of Impurities in Semiconductors", J. Phys. C: Solid St. Phys., Vol.13, p.2027, 1980.

73. S.M. Ryvkin, Photoelectric Effects in Semiconductors (Consultants Bureau, New York, 1964).

74. J.R. Haynes and J.A. Hornbeck, "Trapping of Minority Carriers in Silicon. II. N-type Silicon", Phys. Rev., Vol.100, No.2, p.606, 1955.

75. H. Schulman and A. Honig, "Intrinsic Oscillatory Photoconductivity in Silicon", in Proceedings of the Third Int. Conf. on Photoconductivity, Edited by E.M. Pell, (Pergamon Press, New York, 1969).

76. G.A. Thomas, et.al, "Optical Study of Interacting Donors in Semiconductors", Phys. Rev. B, Vol.23, No.10, p.5472, 1981.

77. P. Norton, "Electron Lifetime and Transport in the Upper Hubbard Band of Impurity-doped Semiconductors", Phys. Conf. Ser. No.43, p.993, 1979.

78. J.R. Haynes, "Experimental Proof of the Existence of a New Electronic Complex in Silicon," Phys. Rev. Letters, Vol.4, p.361, 1960.

79 M.D. Petroff, J.C. Pickel and M.P. Curry, "Low-level Radiation Effects in Extrinsic Infrared Detectors," IEEE Trans. Nuc. Sci. NS22 No.6, p.4840, 1979.